Model-based predictive control of a battery energy storage for fast frequency control in distribution grids using load flow analysis

Modellprädiktive Regelung eines Batteriespeichers zur Frequenzstabilisierung in einem Verteilnetzabschnitt mittels Lastflussanalyse

Master Thesis

submitted in partial fulfilment of the requirements for the degree of
Master of Engineering
at the department Life Sciences of

Hamburg University of Applied Sciences (HAW Hamburg)

In cooperation with
Fraunhofer Institute for Silicon Technology (ISIT)

Supervisors:
1. Dr.-Ing. Gerwald Lichtenberg (HAW Hamburg)
2. Dr.-Ing. Georg Pangalos (Fraunhofer ISIT)

Sascha Nadja Ringlstetter
Matriculation number: [redacted]
Hamburg, 31. August 2017

Hereby I declare that I produced the present work myself only with the help of the indicated aids and sources.

Hamburg, 31. August 2017 Sascha Nadja Ringlstetter

Contents

1 Introduction

This thesis proposes a model-based predictive control algorithm for a Li-ion based Battery Energy Storage System (BESS) using load flow computations. It should be examined if such a controller can show improved performance in stabilising the frequency in a distribution grid compared to current load frequency control services. A continuous control algorithm was developed in Matlab environment combining different concepts that are described in the following. A simulation study was conducted for evaluating the controller behaviour and for comparing it with other operating modes.

Deviations of the system frequency from its set point value in electric networks result from imbalances between generated and consumed energy. Such can be sudden changes in demand power that are compensated by conventional generation units with rotating masses. In real networks, frequency deviations are tackled by primary and secondary Load Frequency Control (LFC) units. They react to measured frequency deviations by proportionally injecting or absorbing active power into or from the grid.
The proposed battery control algorithm is based on active power measurements at strategic points of the electricity grid, which are assumed to be obtained faster than frequency measurements. Based on the observed changes in system loads, future frequency deviations are predicted in short-term range. This allows the computation of a battery signal that efficiently reduces the expected frequency deviation.
With the motivation of increasing the speed of the control algorithm, load flow analysis techniques were applied for calculating line and transformer losses in the power grid. A simplified model of the distribution grid was used for determining the active and reactive power losses, required active and reactive power of connected generators, as well as voltage magnitudes and angles at all buses of a steady-state operated electric network. The grid structure was assumed to be similar to an island grid, with one coupling point to the transmission grid that is represented by a synchronous generator. The prediction of future frequency deviation was based on a dynamic model of a conventional reheat-steam turbine. A BESS connected to the power system was modelled for partly compensating small load changes and thus helping to reduce future frequency deviations. The optimal sequence of active power provided by the battery storage should be determined with a downhill simplex optimisation algorithm.

In the following document, chapters 2 and 3 comprise introductions into the underlying theoretical concepts of network analysis and model-based predictive control. The models applied in the proposes controller structure are explained in chapter 4. Chapter 5 presents the approach, results and analysis of the simulation study. Finally, chapter 6 summarises the main conclusions drawn and gives some proposals for future work.

2 Electric distribution grids

This chapter will give an overview of the theoretical background and modelling concepts for electric distribution networks that were applied in the proposed battery controller. They include static network calculation, dynamic modelling of expected frequency deviations, and an introduction to applications of large scale Li-ion based battery storages in electrical networks.

2.1 Electric transmission and distribution networks

Electricity is transported and distributed from generating sources to customers at different voltage levels. Lines of various different nominal voltages exist for both transmission and distribution grids, also within single countries. Electricity lines can be classified by their voltage level as low voltage (< 1 kV), medium voltage (1 kV to 36 kV) and high voltage (> 36 kV), [1]. Grids are defined as connections of lines with similar voltages and common control regulations. Power grids are characterised by their purpose, share of generation and consumption, structure, management and operation. Table 1 illustrates the variety of different voltage levels used in the distribution grids of some European countries. Transmission grids are usually operated at higher levels, for example 110 kV, $132 - 150$ kV, 220 kV, 300-330 kV, $380 - 400$ kV, 750 kV, and sometimes with DC. The difference between the two grid types will be explained throughout this section.

Country/Voltage level	Medium voltage	High voltage
Germany	10, 15, 20, 30	110
United Kingdom	11, 30	132
Spain	11, 15, 20, 30	45, 66, 110, 132
Denmark	-	60
France	20	-
Czech Republic	3, 5, 6, 22, 35	110

Table 1: Voltage levels in some European distribution grids, [1]. All values in kV.

2.1.1 Transmission grids

The purpose of transmission grids (also: bulk power system) is to transport large amounts of energy from generation plants over significant distances to load centres. Such grids are usually meshed and operated at high or very-high voltage level, [2, p.34]. Generation capacities of connected power plants are usually in the range of several hundred MW, such as conventional power plants or large wind farms. Most transmission line cables are three-core based. In accrodance with the meshed structure, the direction of energy flow in large parts of transmission grids changes frequently. National transmission grids may

comprise several connected control areas. They are operated by Transmission System Operators (TSOs).
In Germany, these are "TransnetBW GmbH", "TenneT TSO GmbH", "Amprion GmbH" and "50Hertz Transmission GmbH".
The regulations for the Continental European synchronously operated electricity transmission grid are issued by "ENTSO-E", the European Network of Transmission System Operators for Electricity. It is an international association of European TSOs and the European Commissions reference body, [3]. Before 2009, the institution was named "UCTE", Union for the Co-ordination of Transmission of Electricity. The main task of this association comprising 43 TSOs from 36 European countries is to coordinate the operation and development of the synchronised connected European electricity transmission grid. The Continental European synchronously operated electricity transmission grid has a peak and off-peak design load of 300 GW and 150 GW, respectively, [4]. An interesting and detailed online map of the European transmission grid can be found in [5]. The monitoring and real-time analysis systems of several European TSO's is conducted by the technical coordination centre for Central West Europe "Coreso".

2.1.2 Distribution grids

Via substations, the transmission grids are coupled to distribution grids. Within those, electric energy is transmitted to local networks with residential customers or other end users such as industry, institutions, or small and medium enterprises (SMEs), [3]. Distribution grids can be high, medium or low voltage-based, or a combination of several different voltage levels, as the name relates mainly to the grid functionality. While in medium and high voltage distribution grids commonly three-core lines are used, in low voltage grids often four-wire cables are applied, [2, p.34f]. The grids are operated by Distribution System Operators (DSOs).
Historically, the energy flow in the often radial networks is mono directional, which means only from the coupling point in the direction of consumers. However, increasing share of distributed (often renewable) electricity sources can lead to multi-directional, time-variant flow of electric energy.

2.2 Single line AC load flow analysis

Load flow (power flow) calculation is a well-established method for analysing large power systems, [6, p. 4-7]. It is used for determining the operating characteristics of an electric network under steady-state conditions. The system states are basically computed by solving a set of non linear, continuously differentiable equations. Over the last decades, the convergence and usability of the algorithm could be enhanced by including the Newton-Raphson method, sparse matrix programming, and numerical integration techniques. A load flow analysis can form the base for further analyses of transmission or distribution networks, such as unit commitment, security assessment, optimal system operation, fault or stability analyses. The following sections will present the basic principle of the single

line load flow analysis of AC electric networks. Single line means means that the three phases of a natural system are represented by one single phase in its model.

2.2.1 Principle

In load flow calculation, the power network is modelled as a set of buses (nodes), which are connected through transmission lines. All network elements are represented by simplified algebraic models that are comprised of equivalent inductance, capacitance and resistance, [6, p.7f][7, p.5f]. Such lumped-circuit models exist, for example, for connecting lines and cables, transformers (on nominal and off-nominal tap ratio, in-phase and phase-shifting), and shunt elements. Loads and generators are modelled as constant sources or sinks of active and reactive power.

The whole system is assumed to be in steady-state or quasi steady state operation, the latter meaning that it can be regarded as steady state with sufficient accuracy. Hence, dynamic phenomena, such as electro-magnetic transients or small load changes are neglected. The system frequency and all voltages are assumed to be constant within one load flow analysis [6][7]. The operating state of the system can be fully described by specifying the following variables at each bus k in the system [7].

- V_k - voltage magnitude
- θ_k - voltage phase angle
- P_k - net active power (algebraic sum of generation and consumption)
- Q_k - net reactive power

This corresponds to knowing the complex voltages and complex powers (active and reactive) absorbed or generated at all buses, leading to the complex power flows and losses along the connecting lines [6]. Usually, all variables are expressed in p.u. (per unit) values with respect to a system base.
The following three basic types of buses are defined. At each of these, two variables are given beforehand and two unknowns have to be determined, [6, p.17][7, p.31f].

1. $V\theta$ **slack bus** (swing/reference bus): a selected voltage-controlled bus, whose voltage phase angle is used as reference for the whole system. Its active and reactive power injection will balance the system's generations, loads and losses. Usually one (or multiple) generating station responsible for Load Frequency Control (LFC) is specified as slack bus.

2. PQ **nonvoltage-controlled bus** (load bus): bus at which total injected power $P_k + jQ_k$ is given. Buses of this type usually corresponds to consumers and form the majority of buses in the system.

3. PV **voltage-controlled bus**: bus with fixed voltage magnitude and active power injection. They can represent a synchronous generator with voltage control or synchronous compensators injecting reactive power at substations.

2.2.2 Algorithm

This section presents the basic steps of load flow computation. In the nodal method, one nonlinear algebraic equation can be formulated for each bus of the system, based on Kirchhoff's Current Law. The equation for one node (bus)

$$I_k = \sum_{m \in K} Y_{km} E_m \tag{2.1}$$

$$= \sum_{m \in K} (G_{km} + jB_{km})(V_m e^{j\theta m}), \tag{2.2}$$

comprises the net current I_k of the respective node and complex voltages $E_k = V_k e^{j\theta k}$ of all adjacent nodes as variables (K : set of buses adjacent to k including k). Currents and voltages are linked through line admittances $Y_{km} = (G_{km} + jB_{km})$, [7, p.27ff][6, p.12ff][2, p.808ff]. The single equations are combined with the help of the system admittance matrix Y to

$$I = Y \cdot E. \tag{2.3}$$

With complex net power injection at each bus k : $S_k = P_k + jQ_k = E_k I_k*$, the active and reactive power components can be calculated as

$$P_k = V_k \sum_{m \ell K} V_m (G_{km} \cos\theta_{km} + B_{km} \sin\theta_{km}), \tag{2.4}$$

$$Q_k = V_k \sum_{m \ell K} V_m (G_{km} \sin\theta_{km} - B_{km} \cos\theta_{km}), \tag{2.5}$$

and the resulting system of equations is solved iteratively, [7].
In order to reflect operating limits of generators and other network components (lines, transformers etc.), inequality constraints may be formulated. The consideration of such limits can be realized by transforming a bus into a different bus type when a constraint is violated or by incrementally adjusting the bus variables until the constraints are satisfied. For iteratively solving the nonlinear equation system, a Newton-Raphson algorithm is applied using linear approximations based on Taylor series expansion of first order, [6]. In each iteration p, the updated variable

$$x^{p+1} = x^p + \Delta x^p \tag{2.6}$$

$$\approx x^p - \mathbf{J}^{-1}(x^p) f(x^p) \tag{2.7}$$

is computed based the estimate $x^{(p)}$ of the variable x. The Jacobian matrix $\mathbf{J}$ for n functions $f = (f_1(x), f_2(x), ...f_n(x))^T$ with a vector of variables $x = (x_1, x_2, ..., x_n)^T$ is constructed from first-order partial differentials, such as $J_{km} = \frac{\delta f_k}{\delta x_m}$ for $f_k(x_m)$). For the load flow computation, with

$$\mathbf{x} = \begin{pmatrix} \theta \\ \mathbf{V} \end{pmatrix}, \tag{2.8}$$

$$\mathbf{f}(\mathbf{x}) = \begin{pmatrix} \Delta\mathbf{P}(\mathbf{x}) \\ \Delta\mathbf{Q}(\mathbf{x}) \end{pmatrix} \tag{2.9}$$

the Jacobian matrix

$$\mathbf{J} = \begin{pmatrix} \frac{\partial \Delta \mathbf{P}}{\partial \theta} & \frac{\partial \Delta \mathbf{P}}{\partial \mathbf{V}} \\ \frac{\partial \Delta \mathbf{Q}}{\partial \theta} & \frac{\partial \Delta \mathbf{Q}}{\partial \mathbf{V}} \end{pmatrix} \tag{2.10}$$

$$= \begin{pmatrix} \frac{\partial \mathbf{P}}{\partial \theta} & \frac{\partial \mathbf{P}}{\partial \mathbf{V}} \\ \frac{\partial \mathbf{Q}}{\partial \theta} & \frac{\partial \mathbf{Q}}{\partial \mathbf{V}} \end{pmatrix} \tag{2.11}$$

can be formulated, based on (2.4) and (2.5), [6][8]. Hence the system of nonlinear equations

$$\begin{pmatrix} \Delta \mathbf{P}(\theta, \mathbf{V}) \\ \Delta \mathbf{Q}(\theta, \mathbf{V}) \end{pmatrix} = \mathbf{J}(\theta, \mathbf{V}) \begin{pmatrix} \Delta \theta \\ \Delta \mathbf{V} \end{pmatrix} \tag{2.12}$$

can be obtained. In each nodal equation, different variables are known or unknown according to the respective bus types, as defined in section 2.2.1. The main steps of in iterative load flow computation are illustrated as a flow chart in figure 2.1. In this thesis, a Matlab code for basic load flow computation based on Newton Raphson iterative method was used, which had been retrieved from Matlab file exchange, [9]. The computational speed of load flow calculations can be further increased by the so-called decoupling method. In a certain range of θ around zero, the relationships $P - V$ and $Q - \theta$ can be neglected, [10, p.45ff]. This corresponds to setting the following elements of the Jacobian matrix to zero: $\delta P/\delta V$ and $\delta Q/\delta \theta$, leading to

$$\mathbf{J}_{decoupled} = \begin{pmatrix} \frac{\partial \mathbf{P}}{\partial \theta} & 0 \\ 0 & \frac{\partial \mathbf{Q}}{\partial \mathbf{V}} \end{pmatrix}. \tag{2.13}$$

By this, the dimension of the set of equations to be solved is reduced. The admittance matrix characterises the connections of all nodes of the network with each other. Depending on how meshed the network is, this matrix usually shows a high degree of sparsity, allowing the application of special sparse matrix algorithms for storage and solving issues. By this, the computational speed can be further enhanced, [2, p.812].

2.2.3 Test feeder

The aim of test feeders is to provide benchmark systems for comparison and verification of power system analysis methods and programmes, [11]. Such test feeders can have different characteristics, such as being one- or three-phase based, radial or meshed, balanced or unbalanced. Test feeder data contain load data with specification of bus types and variable values (e.g. active and reactive power for PQ-bus). Line data is given in forms of equivalent model data. Further information and operating limits may be given, such as electrical (e.g. type of line: transformer, other) or geospatial data like length of the lines or location of the buses, and minimum/maximum voltage magnitudes, angles, power values. Usually all data is expressed in p.u. values, which enables using test feeders at voltage levels different to the original version, and independently from the original system frequency.

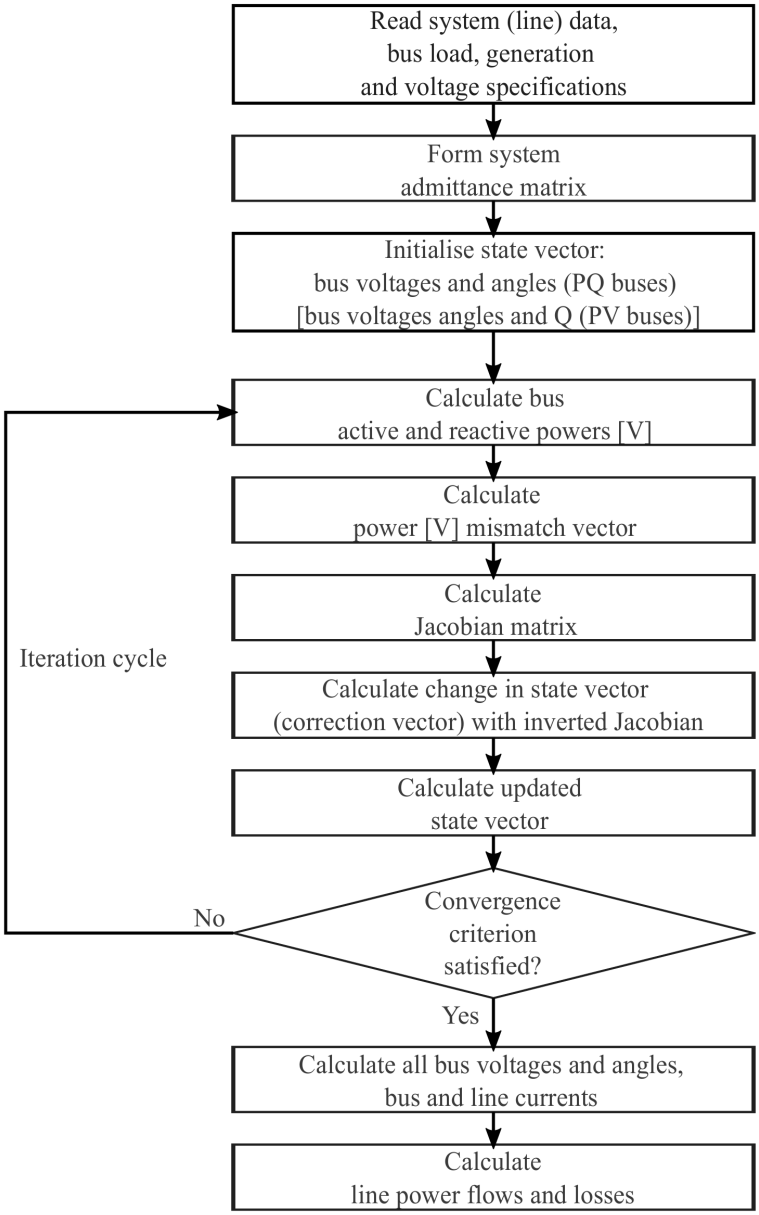

Figure 2.1: Main calculation steps of load flow iterative algorithm based on Newton-Raphson method, after [2, p.1054f][6, p.18][9].

Test feeders have been published by various sources and adapted by the users for their applications, as mentioned in several publications. Some relatively popular three-phase distribution grid test feeders were published by IEEE in 1991, such as a 13-bus on 4.16 kV level and 24.9 kV based 34-bus system, [12][11]. Both were developed as reduced-order models from actual distribution systems (Texas, New Mexico) and are available in Matlab Simulink.
The University of Washington published a single-phase 14-bus test feeder in 1993 that

has been used in several publications, [13]. It is available in IEEE Common Data Format, and represents a simplified portion of a Midwestern American Electric Power System as of 1962.
A set of single-phase test feeders published by the UK Centre for Sustainable Electricity and Distributed Generation (SEDG) in 2005 is representative of UK distribution networks, [14]. The so-called "EHV1" model is a rural network test case on originally 33 kV level including long lines. It is fed from one 132 kV supply point. Due to a sub-sea cable, the test feeder shows voltage problems at the extremities of the system. It also contains a connection to another network. As this test feeder is both recent and representing a network similar to the aimed application of the battery storage, the "EHV1" test feeder was chosen as basis for the network models in this thesis. The feeder's data and the official graphical scheme can be downloaded from [14].

2.2.4 Combining varying system frequency with load flow analysis

Generally, in load flow analysis steady-state conditions are assumed, including a constant system frequency. Though, in literature two different approaches can be found, which aim at combining frequency deviations resulting from load-generation imbalances with classical load flow computations. In section 2.3, some theory on possible origins of frequency deviations can be found.

Extended load flow (direct)
In the first approach, presented by Okamura et.al. in the 70s [15] and used in [8] and [16][17], the deviation of system frequency from a rated frequency $\Delta f = f - f_{nom}$ is directly included in the load flow algorithm. The deviation Δf is incorporated into the Newton-Raphson equations as additional state variable and is iteratively determined during computations. The respective elements of the extended Jacobian matrix

$$\begin{pmatrix} \Delta\mathbf{P}(\theta, \mathbf{V}, \mathbf{\Delta f}) \\ \Delta\mathbf{Q}(\theta, \mathbf{V}, \mathbf{\Delta f}) \end{pmatrix} = \mathbf{J}_{extended}(\theta, \mathbf{V}, \mathbf{\Delta f}) \begin{pmatrix} \Delta\theta \\ \Delta\mathbf{V} \\ \Delta(\Delta f) \end{pmatrix} \tag{2.14}$$

are derived from equations formulating the interaction of generators and frequency response as well as frequency-dependent loads. In order to maintain a solvable set of equations (square matrices), ΔP_{ref} may be introduced as additional variable on the left hand side of the equation, representing the deviation of a generator bus from its reference value, [8].

Stepwise load flow (indirect)
The approach of stepwise load flow is described by Bakken et.al. in [18]. In order to calculate slow power system dynamics of large networks with multiple generators, a sequence of regular stationary AC load flows is combined with computation of frequency deviation from resulting power imbalance, based on droop response.
The inputs to the algorithm are network topology data, information on amount, type and limitations of available generation units. Starting from an initial state of the system, the stepwise power flow is executed recursively for changing loads, under the assumption that

scheduled generation usually is adjusted stepwise at the full change of hour, but demand is in-/ or decreasing linearly (also calculated stepwise, but at higher resolution). The resulting power imbalance is used for calculating the frequency deviation by combined droop settings of all connected generators. Based on the updated generator output powers, the network operating state including all line flows, bus powers and complex voltages, are determined with a static load flow analysis.
Besides the basic algorithm, the publication [18] presents further extensions, such as including distribution of generation among connected units, secondary reserve, cases of generator or load outages, integration of wind power and economic aspects.

2.2.5 Comparison load flow and other electric network modelling approaches

Load flow analysis modelling of power systems is characterised by a high computational speed due to the included steady-state assumptions and significant simplification of the electric network. However, with more detailed methods as described in following, it is possible to describe further aspects of power grids more accurately.

A computationally demanding type, because very detailed, type of network analysis are full electro-magnetic transient models (EMT). Herein, all instantaneous values of (sinusoidal) voltages and currents are determined, [19, p.9]. They can include detailed passive elements-representation of generators, transmission lines and loads. Such models are applied for analysing time-variant dynamic behaviour of electric grids, for example oscillatory behaviour of generators in case of short circuits or switching activities [2, p.851][6, p.245]. Due to the high computational demand, but ability to approximate short-time time-variant transient effects well, EMT models are typically used for off-line computation of small time frames, for example for design and coordination of transmission line insulation and equipment, [20].
Another type of electric network simulations that had been derived from EMT models are so-called dynamic stability simulations (also: RMS simulations). They omit fast electromagnetic transients in order to increase simulation speed. Dynamic stability simulations are based on reduced order generator models and symmetric or unsymmetrical components methods, [19, p.9]. Possible applications are assessment of transient stability, fault ride through, or dynamic behaviour of network components, [20].
Additionally to the single-phase load flow presented and used in this work, power system can be studied using three-phase load flow. The method can be applied if electric grids are not balanced, which means power flows of different magnitudes occur in the phases of the network. This enables the assessment of unbalanced operation and detection of related negative effects on generators and transmission lines [6, p.42f]. Naturally, consideration of differences between phases requires more complex modelling and solving algorithms compared to single-phase load flow, resulting in increased storage and computational requirements.

2.3 Frequency deviation in electric networks

In AC-based electric power networks, a common frequency can be observed throughout the whole system. It is named system frequency (mains frequency) and is a measure of the rotational speed of all generators that are coupled and synchronised with the grid, [21]. Within the ENTSO-E (European Network of Transmission System Operators) and neighbouring synchronized grids, the nominal value of system frequency is 50.0 Hz, [22]. It may be temporally changed to slightly different set point frequencies, for example for correction of the synchronous time.

2.3.1 Origin of frequency deviation, rotating masses

The actual system frequency can deviate from its set point value in case of imbalances between net generated and consumed power. Such deviations are mainly related to active power imbalances. Hence, they occur often at the change of the hour and during morning (sunrise) and evening (sunset) times, when the usually change faster than generation, [23][24]. Intermittent Renewable Energy Sources (RES) may add further variability of active power in the grid, however from the side of generating units. Frequency measurements are published online by many sources, commonly in intervals of seconds.
Physically, deviations in system frequency result from synchronous generators, whose turbine shafts are directly coupled to the grid. In case of disturbances of the demand-generation equilibrium, the additional positive or negative active power can be delivered immediately from the kinetic energy of the rotating masses (turbine shafts). This leads to an increased or decreased rotational speed of the turbine shaft, which directly results in a change of system frequency. For example, a sudden increase in total demand power can be compensated by a rotating mass of a conventional power plant, but at the expense of a higher braking torque acting on the turbine shaft and slowing it down. Thus, the frequency within the electric grid would drop, [2, p.728]. In conventional power plants, additionally to the kinetic energy of rotating masses, the change in requested generation power is compensated by an increased use of primary energy. This is realised with a controller aiming at restoring a constant rotational speed of the turbine shaft. Hence, after an initial frequency drop caused by the withdrawal of kinetic energy from rotating masses, the system frequency will be held at a constant value through primary governor action. The remaining frequency deviation is called quasi-steady state deviation, [21]. Both the governor unit and the turbine controller on which it is acting are characterised by time constants of several seconds, causing delayed reaction. Figure 2.2 schematically illustrate the typical dynamic frequency response caused by primary control action of a conventional generation unit after a step change in load. Real measurements of frequency drops can be assessed with enveloping trumpet curves. By this, the quality of secondary control in the respective control areas can be evaluated, based on trumpet curve parameter values obtained from frequency monitoring over several years, [21].

The relationship between load-generation imbalance and quasi-steady-state frequency deviation is approximately proportional. It is described by the network power frequency

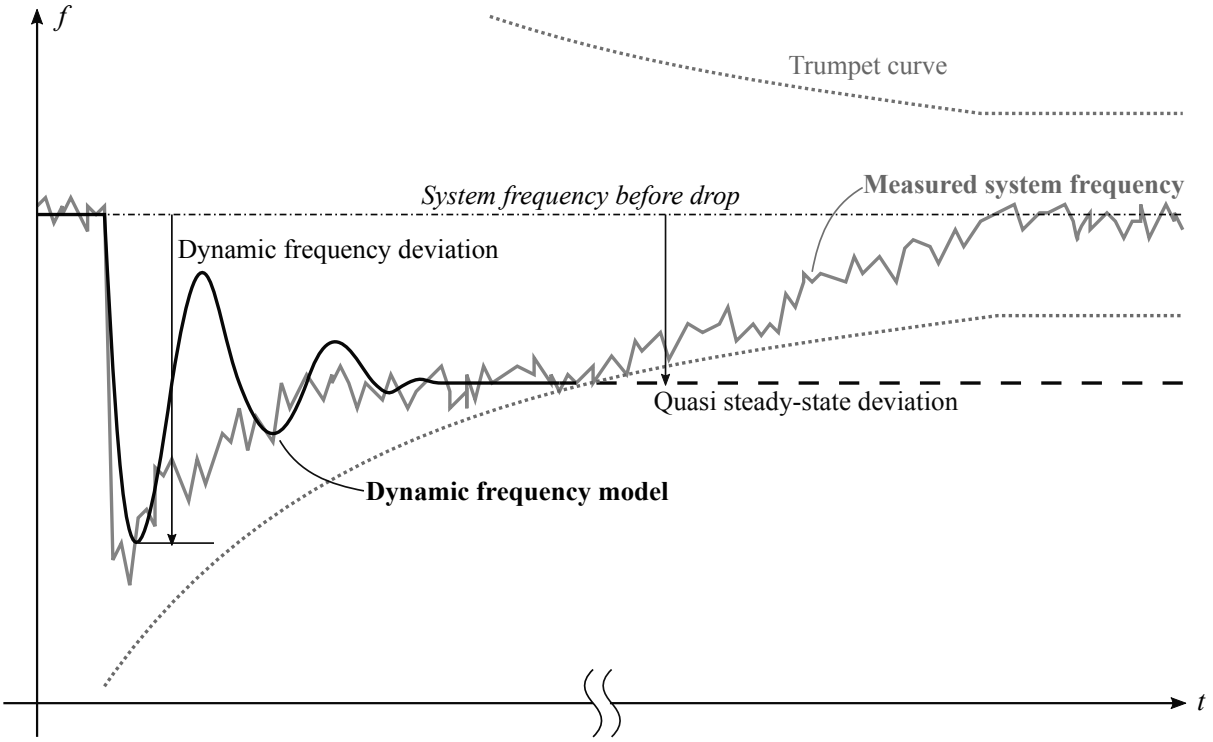

Figure 2.2: Schematic frequency deviation (black), real frequency drop (grey) and trumpet curve (grey dotted). Time not to scale, after [21].

characteristic

$$\lambda = \frac{\Delta P}{\Delta f}, \tag{2.15}$$

in MW/Hz, where ΔP is the step change in power (disturbance) and Δf is the resulting steady-state frequency deviation. Within one control area of the electricity grid, a summarised power frequency characteristic can be determined by combination of the single control areas' characteristics, weighted with contribution coefficients, [21].

The related droop s of a generator is a more popular characteristic, expressed either dimensionless or as percentage. It is the reciprocal of power frequency characteristic λ (2.15), relative to nominal system frequency $f_n = 50$ Hz and rated generator active power P_n

$$s = \frac{\Delta f / f_n}{\Delta P / P_n}. \tag{2.16}$$

The droop corresponds to the slope of a generator characteristic as shown in figure 2.3 for two generators with different droops (under equilibrium conditions). The droop value can be interpreted in two ways: either as variation in system frequency (on the abscissa) when the generator is requested to provide a certain relative change in active power (on ordinate). Or as the variation in (relative) output power, compared to the rated value, in case of a certain frequency deviation in the grid, [21]. Figure 2.3, can be interpreted

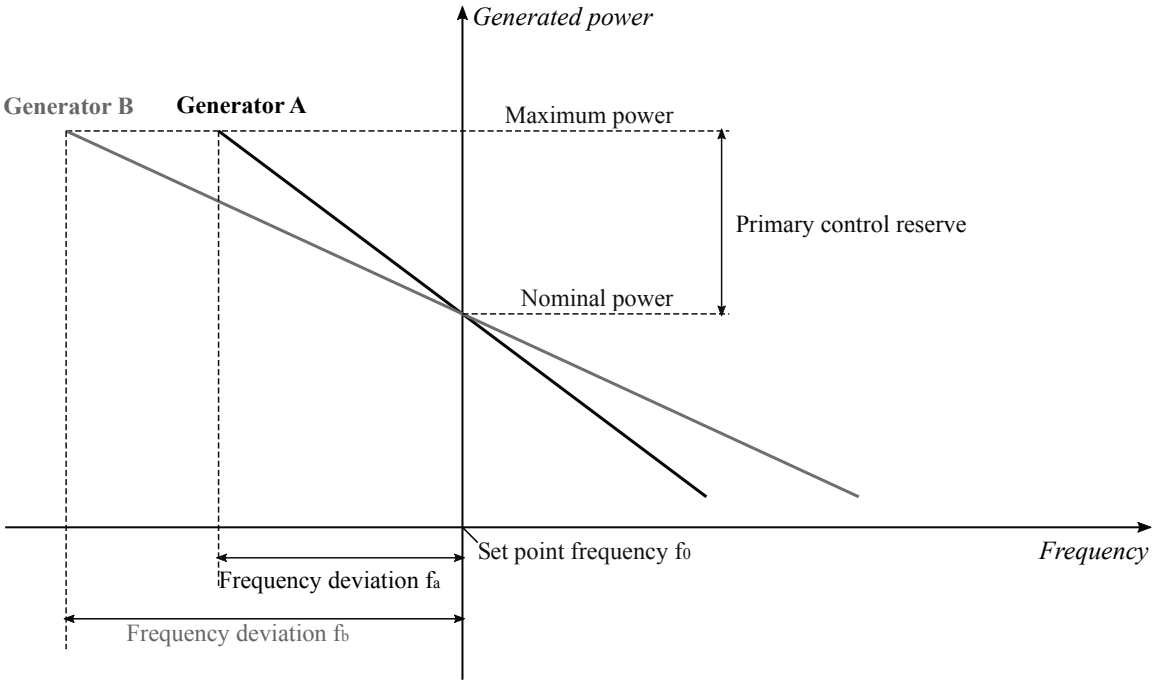

Figure 2.3: Droop characteristic of two generators A (black) and B (grey), [21]

in the following way: it shows the proportional primary control reactions of two different generators with identical control reserves to any negative frequency deviation. In the range $f_a < f < f_0$, generator **A** will provide more active power than generator **B**. When $f_b < f < f_a$, the reserve capacity of generator **A** is limited to its maximum and the output power will remain constant, while the active power provided of generator **B** will still increase. At large negative frequency deviations $f < f_b$, both generators provide the same maximum output power, corresponding to their reserve capacity, [21].

In the case of more than one generators being connected to the same electric grid, similarly to the network power characteristic, the cumulative reaction of all generators in a grid can be characterised. A common method is determining an equivalent rotating mass, which is known as central inertia approach. For this, all generating units contributing to primary control are summarized (taking into account the different rated powers) into a single equivalent machine with a total system inertia, [25][2, p.723 ff][26].
The value of system inertia is time variant, depending on the available reserve capacity connected to the grid. In networks with high shares of RES, which are usually decoupled from the grid frequency, the system inertia can vary significantly and will be in average lower than in a grid mainly powered by conventional generation units, [27].

Frequency deviations in electric distribution networks are partly compensated automatically by self-regulating effects of some loads. This stabilising behaviour, also called 'damping' effect of loads, results from frequency-dependent power consumption, for example of loads containing rotating machines. An equivalent total damping factor (damping con-

stant) can be used to describe the summarised self-regulating effect of the whole system. It is highly dependent on composition of active loads in every moment, [25][2, p.725][28, p.23].

2.3.2 Different types of load frequency control

Imbalances between generated and consumed power, and the resulting changes in system frequency, as described above, are commonly tackled by different control mechanisms. They are activated with different time lags.

- The **primary control** is the immediate compensation of *active power imbalances* between load and generation. In electricity networks based on conventional power plants, the connected turbines can restore the balance within a few seconds, based on speed change of rotating masses speed and respective governor actions. Hereafter, the system frequency will remain at a fixed value, differing from the set-point value (steady-state deviation), [28, p.20]. The re-establishment of power balance can by supported by **primary LFC** services of other electricity sources. The reserve capacities in charge will be requested to deliver active power, proportionally to the measured difference between set point and actual mains frequency, [21]. This helps stabilising the frequency deviation at its steady-state value. Primary LFC is fully activated latest after 30 s and following will be decreased to zero within 15 min.

- The purpose of **secondary control** is to eliminate the constant *frequency deviation* caused by primary control of rotating masses in conventional generators while ensuring the equilibrium between generated and consumed active power. Through contrary power action, generators in charge will steer the mains frequency back to its set point value. Secondary control is principally implemented as integral controller within the contributing generating units, [2, p.727 ff][28]. It takes over from primary frequency control after some minutes and will be inactivated after 15 min, [21].

- In case of larger or longer disturbances, **tertiary and emergency control** may be required in order to restore operating conditions after outages, [28, p.20][21]. It can be realised in manual or automatic way. In some literature sources, **tertiary control** is referred to as the most economic dispatch of generation sources according to merit order principle, [2, p.728].

2.3.3 Regulations for primary load frequency control

Continental European synchronously operated electricity transmission grid
The basic LFC mechanisms and regulations for the European synchronised grid are summarised in the documents [21] and [4], which were published by UCTE (today ENTSO-E) in 2004. The requirements and obligations for primary control actions and reserves have to be covered by third parties within the control areas. They are responsible for providing adequate organisational procedures, monitoring and contracts. The objective of primary control reserve is to react at any time to frequency deviations caused by disturbances of

the equilibrium between generated and consumed power, [21]. The target performance of summarised primary reserve capacity is defined by the following design case ("reference incident"):
The summed reserves shall be able to offset a sudden loss of 3000 MW generating capacity alone, with the resulting dynamic (maximum) frequency deviation against set point frequency not exceeding+800 mHz and the steady state deviation not exceeding 180 mHz. This design case assumes a formerly undisturbed operation with a set-point frequency of 50 Hz, a start time constant of 10 s to 12 s of generators subject to primary control, and a self-regulating (damping) effect of system loads of+1 %/Hz (load decrease of 1 % in case of 1 Hz change in frequency).
Primary control reserves are partially activated when the frequency deviation exceeds 20 mHz. This threshold value originates from the maximum permissible accuracy of the local frequency measurement (10 mHz) plus the insensitivity range of primary controllers (±10 mHz). The activated capacity increases proportionally to the measured frequency deviation, up to a quasi-steady-state deviation of 200 mHz, at which the full reserve must be activated. Regarding temporal deployment, primary control reserves should be started to be deployed immediately after an incident. The maximum deployment time depends proportionally on the required capacity. For example, in case of requested power of 1500 MW, it must be fully activated within 15 s. A disturbances corresponding to a change in power of 3000 MW must be tackled within 30 s. The secondary control will take over after 15 s to 30 s in order to eliminate the remaining quasi-steady state frequency deviation, however, primary control reserves are required by regulation to provide capability of delivery for minimum 15 minutes.

Further regulatory issues with special focus on **battery storage systems as primary control reserve** are published in [29]. The two main aspects described below are also illustrated in figure 2.4:

- **Deadband** (frequency insensitive band). Within a deadband of ±10 mHz around the set point frequency, operators of BESS are allowed to charge or discharge the batteries for reasons of optimal battery charge management. This is optional, but restricted to charge/discharge actions "in the right direction", such that they support the system frequency stabilisation.

- **Optional over fulfilment**. During primary control action, the battery storage may provide up to 20 % higher positive or negative power injection (in grid supporting direction) in order to support the battery charge management.

Enhanced Frequency Response In the interconnected transmission grid of Great Britain, the system operator National Grid Electricity Transmission (NGET) launched a first tender round for a new type of load frequency control service in 2016, [30]. The so-called "Enhanced Frequency Response" (EFR) was introduced in addition to existing primary and secondary response services, which in this grid are requested to full deliver within 10 s/30 s, and be sustained for 30 s/30 min, respectively. The main objective

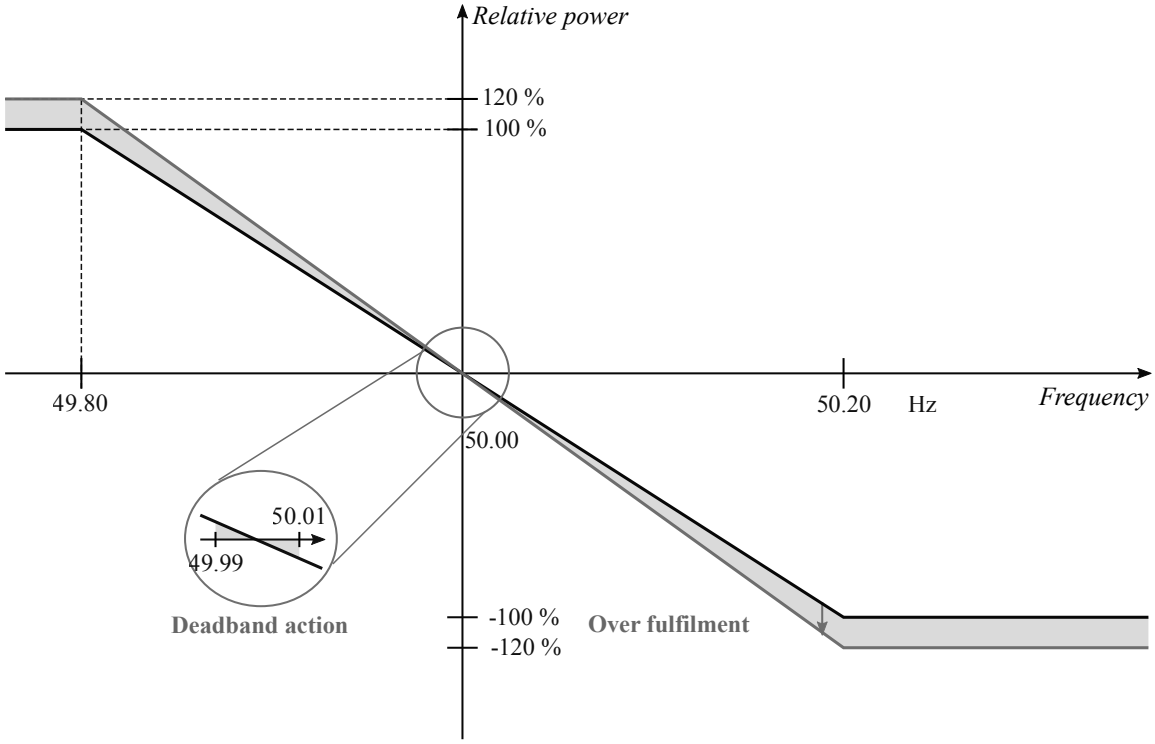

Figure 2.4: Optional over fulfilment and dead band action (shaded areas) of BESS as primary control reserves. x-axis: frequency, y-axis: power injected into grid, based on [29].

of EFR is to tackle the increasing share of renewables in the generation mix, which corresponds to a reducing level of system inertia due to the decreasing share of synchronous generation. This affects the ability of the system to manage the frequency within normal operating limits. With the help of the newly introduced type of service, the system frequency shall be maintained closer to nominal 50 Hz under normal operation conditions, acting as pre-fault frequency containment.
In order to fulfil the desired role, EFR was established as a continuously operating, sensitive LFC service with a small dead band. The assets have to be able to deliver continuous active power with a reaction time of maximum 1 s and deliver it during minimum 15 min. The active range with proportional power injection to frequency deviations specified to+50±0.5 Hz, which corresponds to maximum deviations of ±500 mHz. Two different service versions were specified, including deadbands (frequency insensitive band) of 50±0.05 Hz (±50 mHz) or 50±0.015 Hz (±15 mHz), respectively. The output power is allowed to vary between ±9 % of specified capacity. The service envelope option with a narrower dead band is referred to as being more "valuable" for the grid operator. Figures and more information can be found in [31].

2.3.4 Dynamic load frequency response model

The frequency response of a generator to a load disturbance can be modelled with simplified dynamic models. Transfer functions can be used for approximating the behaviour of a generator governor and turbine, as well as the reaction of the electric grid (composed of other rotating masses and damping loads) within the first seconds after a load change. The primary and secondary control can be represented by proportional and integral blocks in a control loop acting on the generator. The equivalent models presented in figures 2.5 and 2.6. They already include some simplifications. For example in model B proposed by [10] (figure 2.6), the governor delay time is neglected because it is assumed to be comparatively small. In this form, the presented dynamic models are only valid for isolated power systems. For modelling multi-area power networks, the interconnection of different control areas may be added, as in [28, p.25f].

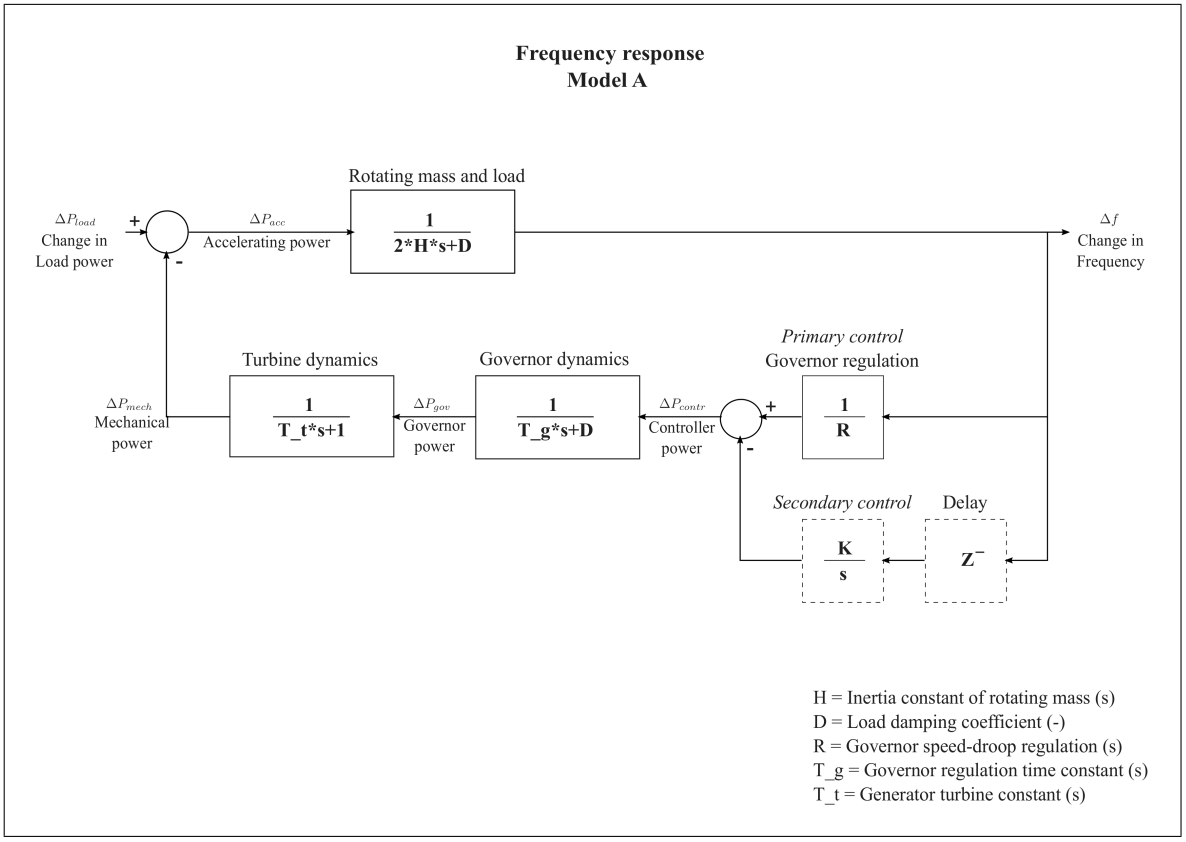

Figure 2.5: Dynamic frequency control model **A** based on transfer functions, from [28, p.26][2, p.734]. Blocks marked with dashed borders representing optional secondary control.

Based on the presented block-chart approaches, algebraic formulations of the transfer functions can be derived. The frequency response $\Delta f(s)$ to a constant step change $\Delta P(s) = \Delta P/s$ can be transformed from the frequency domain into the time domain, hence to $f(t, \Delta P)$, based on inverse Laplace transformation. This was done in [10] and [2, p.736] for the different models, leading to different algebraic functions. The formulae given

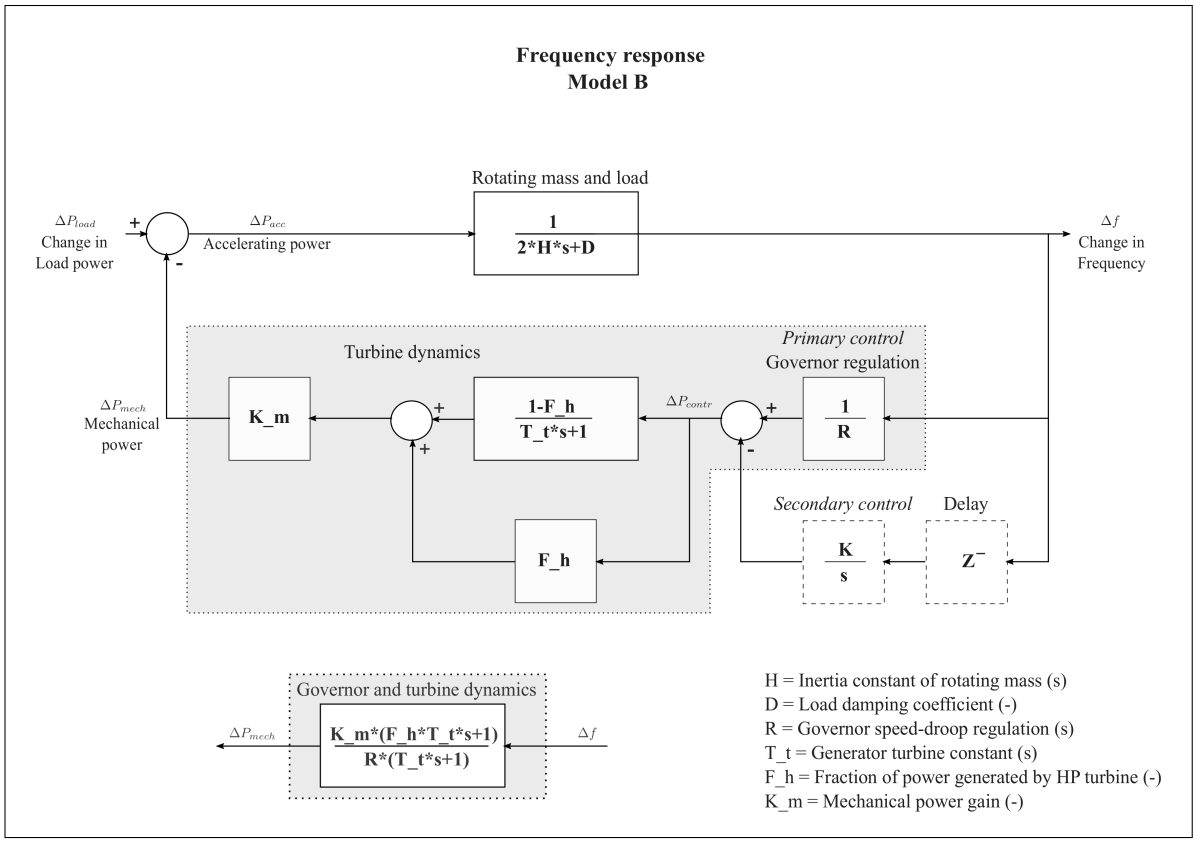

Figure 2.6: Dynamic frequency control model **B** based on transfer functions, as in [10]. The blocks representing secondary control are marked with dashed borders. In case of primary regulation only, the blocks with grey background can be replaced by the block in the bottom of the figure.

in [2, p.736] neglects both governor and turbine time constants and hence can not reflect the initial transient oscillation of frequency caused by the generator response, but only steady-state deviations. Hence it was regarded unsuitable for this thesis, in which thee focus lies on the initial large frequency deviations of transient behaviour. The algebraic function proposed by [10] can reflect the damped sinusoidal waveform of frequency deviation immediately after a step change. The relative frequency deviation $\Delta f(t)$ as function of a step change of load P_{load} and constants $k_1 \dots k_5$ can be calculated as

$$\Delta f_{rel}(t) \quad = \quad \Delta P_{load} k_1 (1 + k_2 e^{-k_3 t} \sin(k_4 t + k_5)). \tag{2.17}$$

The absolute frequency deviation in Hz can be obtained by multiplying the relative change in frequency with the system frequency, for example 50 Hz: $\Delta f(t) = \Delta f_{rel}(t) \cdot 50\text{Hz}$. The constants $k_1 \dots k_5$ are calculated from the system characteristics
H = Inertia constant of rotating mass (s),
D = Load damping coefficient (-),
R = Governor speed-droop regulation (s),
T_t = Generator turbine constant (s),
T_g = Governor turbine constant (s),

F_h = Fraction of power generated by high pressure (HP) turbine (-),
K_m = Mechanical power gain (-),
R = Governor speed-droop regulation (-)
with

$$
\begin{aligned}
k_1 &= \frac{R}{DR + K_m} \\
k_2 &= \alpha \sqrt{\frac{1 - 2T_t k_{21} k_{22} + {T_t}^2 {k_{21}}^2}{1 - {k_{22}}^2}} \\
k_3 &= k_{21} k_{22} \\
k_4 &= k_{21} \sqrt{1 - {k_{22}}^2} \\
k_5 &= \arctan\left(\frac{k_4 T_t}{1 - k_{21} k_{22} T_t}\right) - \arctan\left(\frac{k_4 T_t}{1 - k_{21} k_{22} T_t}\right) \\
k_{21} &= \sqrt{\frac{DR + K_m}{2HRT_t}} \\
k_{22} &= k_{21}\left(\frac{2HR + T_t(DR + K_m F_h)}{2(DR + K_m)}\right).
\end{aligned}
$$

The factor α was added manually for enhancing the fitting of the algebraic function to the underlying dynamic model B from the same publication [10], and also with regard to model A from [28] and [2]. The effect of model parameters on dynamic frequency response characteristics is as follows.

- The **delay times** of the turbine and governor T_t and T_g influence the strength of exponential damping on initial sinusoidal oscillation. Longer delay times result in a more damped, and also reduced maximum frequency deviation and shorter time until the steady-state deviation is reached, [10].

- Also the **HP turbine fraction** F_h has an influence on damping. The higher this value, the more damped the frequency response, [10].

- The **system inertia constant** H influences the initial slope, time and value of maximum frequency deviation. The higher the value of system inertia, the later the maximum deviation is reached, which is smaller too. Equivalent inertia values of large power systems vary over time, and are expected to decrease in future due to a higher share of RES in the grid, [27].

- The factor D represents the **damping effect** of loads, which is a change in demand power at different frequencies. It proportionally influences the frequency deviation caused by a load change. The frequency deviation is reduced by a higher damping factor value, [10].

- As expected, the **primary regulation factor** R has among the highest influence on the maximum value of frequency deviation. A higher value of R leads to a reduced maximum deviation occurring earlier in time, [10].

- The **secondary control factor** K determines how fast the steady-state frequency deviation will be reduced to zero. It is only relevant when the secondary control is included in the model. Being delayed by several seconds to minutes, secondary control usually does not influence the initial dynamic behaviour of frequency change, [28][2].

2.4 Li-ion based battery energy storage

The amount of electrical Energy Storages Systems (ESS) for different grid connected applications has been increasing significantly during the last decades. Initially being deployed in isolated grids, Battery Energy Storage Systems (BESS) are increasingly used for providing a wide range of grid-supporting services.
The need of storage solutions in the electricity grid results from both variability of demand on the consumer side, and, increasingly, of fluctuating and difficult to predict renewable energy sources on the generation side, [32]. Thus particularly in countries aiming at a transition from conventional energy sources to RES, electric storages are beginning to play a larger role in different types of services, as the decreasing amount of conventional thermal power plant results in less capacity that is able to provide frequency regulation services, [33]. Furthermore, the characteristic dynamic behaviour of systems with regard to a lower and more variable system inertia value is changed, [27]. Possible applications of BESS include energy time-shift, black-start capability and reserve power for generators, frequency regulation and other power quality services such as voltage support and enhanced integration of RES. The basic operation of a BESS in all types of services can be summarised as energy charging or discharging of different forms over a certain period of time. It results in absorption or injection of active or reactive power, [32]. Lithium-Ion (Li-ion) based BESS are particularly suitable for short-term frequency regulation services due to small response times and high cycle efficiencies compared to other types of electrical storages, [34]. Batteries of this type are also characterised by relatively small dimensions and weights, which is however of minor importance for fixed applications. High costs have been considered the main drawback of battery storage systems in the past, but are continuously decreasing.
Electrochemical storages are characterised by certain charge and discharge characteristics, caused by the underlying chemical reactions and operating conditions, such as ambient temperature. Electrochemical or electronic equivalent circuit models can represent such characteristics. Model parameters can be obtained with experiments. For example, [35] proposes a dynamic battery model, based on different mathematical descriptions during charge and discharge actions. An equivalent electric circuit model is given in [26]. For Li-ion based batteries, the extend of dynamic phenomena such as variance of voltage at different charge/discharge currents and SOC, is comparatively low. Hence, large Li-ion based BESS can be modelled as a flexible current source with a constant voltage level in less detailed simulation studies. Dependencies of the charge/discharge voltage on the instantaneous current and SOC are neglected within a certain range of operation. The nominal voltage of a BESS is defined by the number of connected single battery cells. The output voltage may be adjusted by the converter unit that couples the DC-based battery with a commonly AC-based grid. Additionally to voltage and current, also the operating

temperature of large-scale storages is assumed to be maintainable in a small range with the help of cooling systems. Naturally, all these assumptions should be validated when operating a real battery storage.

3 Model based predictive control

In this chapter, the control strategy used for the battery storage will be presented. Section 3.1 summarises the working principle of model predictive control and section 3.2 introduces a possible optimisation method for the objective function.

3.1 Model predictive control

Model Predictive Control (MPC) is an effective control strategy for linear and nonlinear systems in the presence of uncertainties, disturbances and constraints, [36]. As illustrated by the schematic structure in figure 3.1, the MPC controller consists of two main components,

- a prediction unit containing a model of the system, possibly also further aspects such as disturbance modelling,
- and a control unit, which is basically the optimisation unit.

The prediction unit's function is to forecast the future behaviour of the controlled system when a specific controller output sequence, a control signal entering the real system, would be applied. The purpose of the controller unit is, in turn, to determine the optimal control signal, among all possible sequences as specified by physical or other constraints. The desirability of any control signal is usually assessed by means of an objective function (cost function) that shall be minimised. During the optimisation process, the expected performance of different possible controller outputs is evaluated by the controller unit, [28, p.153f].

3.1.1 Working principle

The numbers in figure 3.1 indicate the following sequence of controller actions, [28, p.154]. In continuous operation, they are conducted repeatedly. The process is also illustrated in figure 3.2, including the different horizons.

1. At a sampling interval k, state(s) and/or output measurements $x(k), y(k)$ of the real system are obtained and transferred to the controller.
2. Based on real system measurements and an initial sequence of control signals over the control horizon H_u, $u(k...k+H_u|k)$, from the control unit, the prediction unit simulates the system behaviour over the prediction horizon H_p. Particularly in the presence of constraints, the initial control signal is required to be feasible.
3. The predicted output $\hat{y}(k+1...k+H_p|k)$ is transferred to the controller.
4. The optimal control sequence $u^*(k+1...k+H_u|k)$ is determined by the control unit, based on the specified optimisation method. The optimisation process may

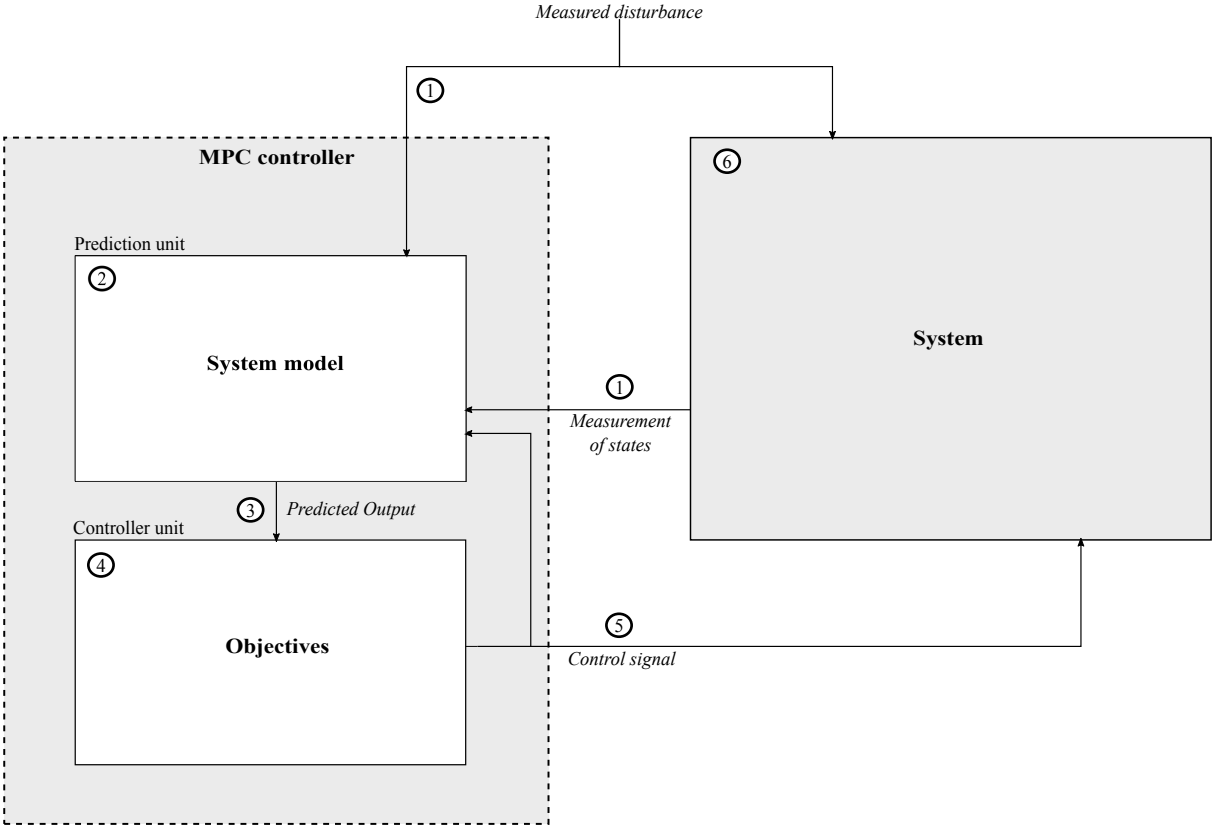

Figure 3.1: Schematic MPC controller structure and interconnection with controlled system, after [28, p.154].

include iterative computation of predicted outputs $y(k+1...\hat{k}+H_p|k)$ in the prediction unit, which result in updated values of the cost function $f(u,\hat{y})$ in the control unit. If the prediction horizon exceeds the control horizon $H_p > H_u$, the control signal is assumed to remain constant, at its last value $u(k+H_u)$.

5. When the optimal control sequence is determined, the first value of $u^*(k)$ is applied to the real system.

6. The real system reacts to the controller output and (un)measured disturbances. The sampling of states and measurable disturbances is repeated at interval $k+1$, and the control algorithm starts from step 1 again.

Figure 3.2 illustrates that a predicted output shall be reached that is as close to a desired output (reference signal) as possible by applying a suitable sequence of control signals. In the case shown, the prediction horizon exceeds the control horizon and the control signal is kept constant after the end of the control horizon.

Various different MPC strategies exist, varying among others with respect to the system model formulation, objective function and optimisation method. Furthermore, different ways of implementing measured or unmeasured disturbances, as well as soft or hard constraints, are possible. The MPC controller may also store previous disturbance and mea-

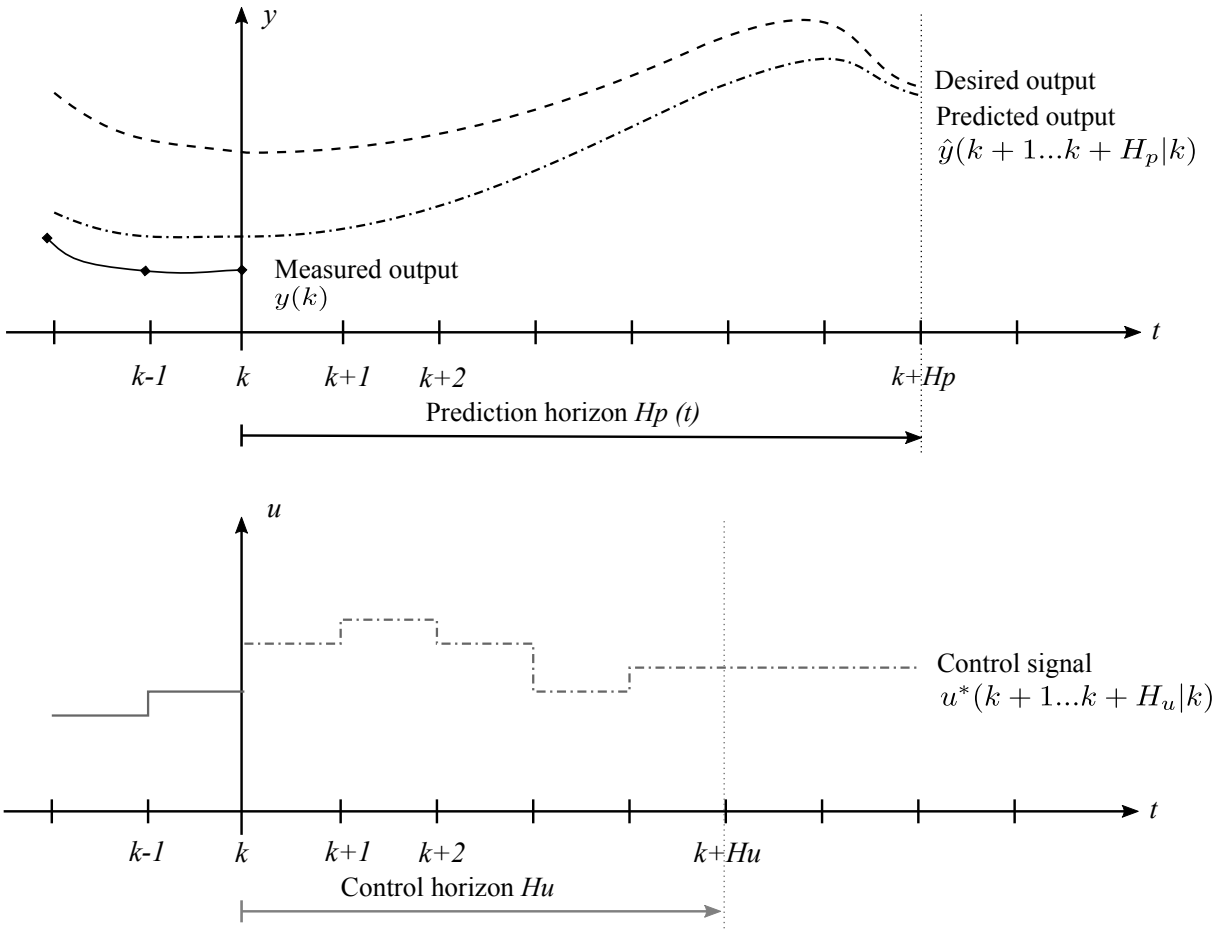

Figure 3.2: Schematic MPC controller concept with output prediction and control input horizon, desired and predicted future output, and past real behaviour of the controlled system, after [28, p.155]

surement values and use them as additional input for modelling future system behaviour in the prediction unit.

3.1.2 Optimisation of the objective function

As described in the previous section, each iteration of MPC algorithm includes determining the most preferable control signal, which is the input sequence for the controlled object. In the presented case, the controller shall compute the optimal future values of power fed into the grid or absorbed by the battery storage. This can be realised using a nonlinear optimisation algorithm that minimises a given cost function.

The objective or cost function $f(x)$ is a measure of undesirability of a particular vector of variables x. The set of variables x^* which returns the lowest cost $f(x^*)$ is regarded as solution vector of the optimisation problem. The objective function can be formulated in

different ways, for example as summed k weighted optimisation criteria $f_i(x), i = 1, ..., k$

$$f(x) \quad = \sum_{i=1}^{k} w_i f_i(x), \tag{3.1}$$

with weigths $w \in \Re^k$, or as weighted norms of optimisation criteria, for example absolute values

$$f(x) \quad = \sum_{i=1}^{k} w_i |f_i(x)|. \tag{3.2}$$

Other expressions and norms such as quadratic terms or maxima (infinite norm), and combinations are possible. The cost function for a specific optimisation problem is formulated with regard to applicable objectives and their importance, taking into account the selected optimisation algorithm and convergence properties.

The purpose of a minimisation algorithm is to solve an unconstrained optimisation problem. This can be applied to the minimisation of an objective function $f(x) : \Re^n \mapsto \Re$,

$$\text{minimise} \quad f(x), \tag{3.3}$$

with regard to the arguments (optimisation variables) $x = (x_1, ..., x_n)$, [37, p.1]. This corresponds to finding the optimal vector x^*, for which the objective function f has its smallest value among all possible vectors x: for any x, $f(x) \geq f(x*)$. The optimization problem is called linear, if the objective function f is linear, otherwise it is nonlinear.

3.2 Nelder-Mead simplex optimisation

The numeric Nelder-Mead simplex method was applied in the form of a Matlab function, `fminsearch`. The principle for multidimensional unconstrained minimization was first published in [38] and described in [39]. It is also known as downhill simplex method. As direct search method, the algorithm has the advantage of being derivative-free and easy to implement on the one hand. On the other hand, it is basically heuristic and not guaranteed to converge to a local or even global minimum, [40][39]. The following sections will further explain the optimisation method.

3.2.1 Nelder-Mead simplex algorithm

In Nelder-Mead algorithm, the optimisation of n variables, which corresponds to finding the minimum of the objective function in an n-dimensional space $\Re^n$, is performed by using an n-dimensional simplex. This simplex is a type of polyhedra formed by $n + 1$ different points (vertices). For example in 1-dimensional space the simplex will be a line defined by two points; a two-dimensional simplex is a triangle, including its interior; and a 3-dimensional simplex would be a tetrahedron with 4 vertices [37]. During the minimisation process, an initial simplex is moving and adapting itself to the local landscape (of the objective function), and finally contracts onto a minimum [39].

In each iteration, based on the calculated values of the objective function $f(x_i)$ at several surrounding points x_i, the NelderMead simplex can change in the five different ways: Reflection, Expansion, Outside contraction, Inside contraction or Shrink.
In all cases but shrinking, the vertex with the "worst" (highest) value of the objective functionis replaced by a new point in $\Re^n$, [40], moving the simplex in the direction of the smallest calculated cost function value. The downhill simplex method is a direct search method, which means it does not require analytical or numerical determination of derivatives. It is only necessary to determine a number of specific values of the objective function f in each iteration, at least one for each vertex. This may be computationally expensive, but makes the algorithm suitable for computer-based minimisation of complex nonlinear real-world problems, [40]. However, depending on the surface of the objective function, problems of false and premature convergence of downhill simplex algorithm have been reported by several sources, as in [41].

3.2.2 Optimisation with inequality constraints

The Nelder-Mead simplex was originally proposed for minimisation of unconstrained objective functions, [40]. However, real-world problems usually contain some form of physical constraints, e.g. the operating range of generators or other machines. It is possible to expand the optimisation method by including m equality or inequality constraints, set by the constraint functions $c_i : \Re^n \longmapsto \Re, i = 1...m$ with constant limits (bounds) $b_1, ..., b_m$, [37, p.1], leading to

$$\text{minimise} \quad f(x) \tag{3.4}$$

$$\text{subject to} \quad c_i(x) \leq b_i, \quad i = 1...m. \tag{3.5}$$

The solution vector $x*$ shall be determined as the vector that has the smallest objective value among all vectors that satisfy the given constraints.
Constrained optimisation problems can be approximated with unconstrained methods combined with **penalty functions**, [42]. In accordance with such penalty functions, additional terms are added to the cost function if any constraints are violated. This penalty term implies a significant increase in costs, which makes the algorithm unlikely to converge beyond the constraint boundaries. Using penalty functions enables an optimisation process only inside the feasible region, hence finding a feasible initial starting point is essential for applying this strategy. In [43], it is proposed to extend the Matlab-function `fminsearch` based Nelder-Mead optimisation by inequality constraints using infinite barriers as penalty functions.

Barrier function terms may be included in the cost function in order to implicitly represent constraints. Using such terms, feasible points are favoured that are further away from the specified boundaries compared to those which are closer to the constraints. The value of a barrier function increases if the vector of optimisation variables x approaches the specific boundary, becoming very high (infinite) at the constraint value, similar to penalty functions. However, barrier functions are only applied inside the feasible region. The most common barrier function is the logarithmic function

$$\Phi_i(x) \quad = \tfrac{1}{t} \log(-c_i(x)), \tag{3.6}$$

for any of the m constraint functions $c_i(x), i = 1, ..., m$ with the parameter t, [37, p.562f]. The function goes towards infinity for values close to zero. As t increases, so does the slope of the barrier function $\Phi_i(x)$ close to the boundary, which for this function is zero. This corresponds to an increasing accuracy of approximation to the indicator function $I_-(u)$ which is zero for all positive values of u and zero, and infinite for all values below zero:

$$I_-(u) = \left\{ \begin{array}{ccc} 0 & \text{for} & u \geq 0 \\ \infty & \text{for} & u < 0 \end{array} \right\}$$

3.3 Golden section search optimisation

When evaluating the performance of the controller, as described in chapter 5, it was observed that the first element of the optimised control signal has the largest influence on the controller behaviour. Furthermore, the determined sequences did not always show the desired positive effect on the system in continuous operation. Thus, it was considered to apply a more simple and faster optimisation algorithm.
It was decided to use golden the section search method. The derivative-free algorithm very efficient for determining extrema of an objective functions in one dimension, [44]. It aims at solving an unconstrained minimisation problem within a specified interval $[x_{low}, x_{up}]$, which is assumed to contain one single minimum. This is related to monotonic increase and decrease of the objective function herein, [45]. In each iteration, the objective function values of two points inside the interval are computed. The points are determined based on their distance to the lower and upper bounds

$$(\Phi - 1)(x_{up} - x_{low}) \quad = \quad \frac{\sqrt{5} - 1}{2}(x_{up} - x_{low}) \approx 0.6180(x_{up} - x_{low}),$$

applying the "golden ratio" $\Phi = \frac{\sqrt{5}+1}{2} \approx 1.6180$. Out of the two points

$$\begin{aligned} x_1 &= x_{low} + (\Phi - 1)(x_{up} - x_{low}) \text{and} \\ x_2 &= x_{up} - (\Phi - 1)(x_{up} - x_{low}), \end{aligned}$$

the one with the lower cost function value is selected for replacing one of the interval bounds (the bound it is closer to) in the next iteration's interval. The algorithm is stopped at a small difference between the calculated two points' cost function values or when a very small interval size is reached.

4 Modelling and control algorithm

This chapter will present the detailed structure and working principle of the proposed controller. After introducing the basic steps performed by the control algorithm in 4.1, the modelling approaches of the single components are presented in 4.2. Section 4.3 contains a summary of the selection and analysis of demand data used in the simulation case studies. The terms of the applied objective function are introduced in 4.4.

4.1 Controller structure and algorithm

Figure 4.1 shows a schematic overview of the proposed controller's components. On the left hand side, the MPC controller is illustrated with its prediction unit containing a simplified system model, and a controller unit including the objectives in forms of a cost function. The controller is connected to the "real world" electricity network on the right hand side, which in this case is represented by a larger, more complex model.

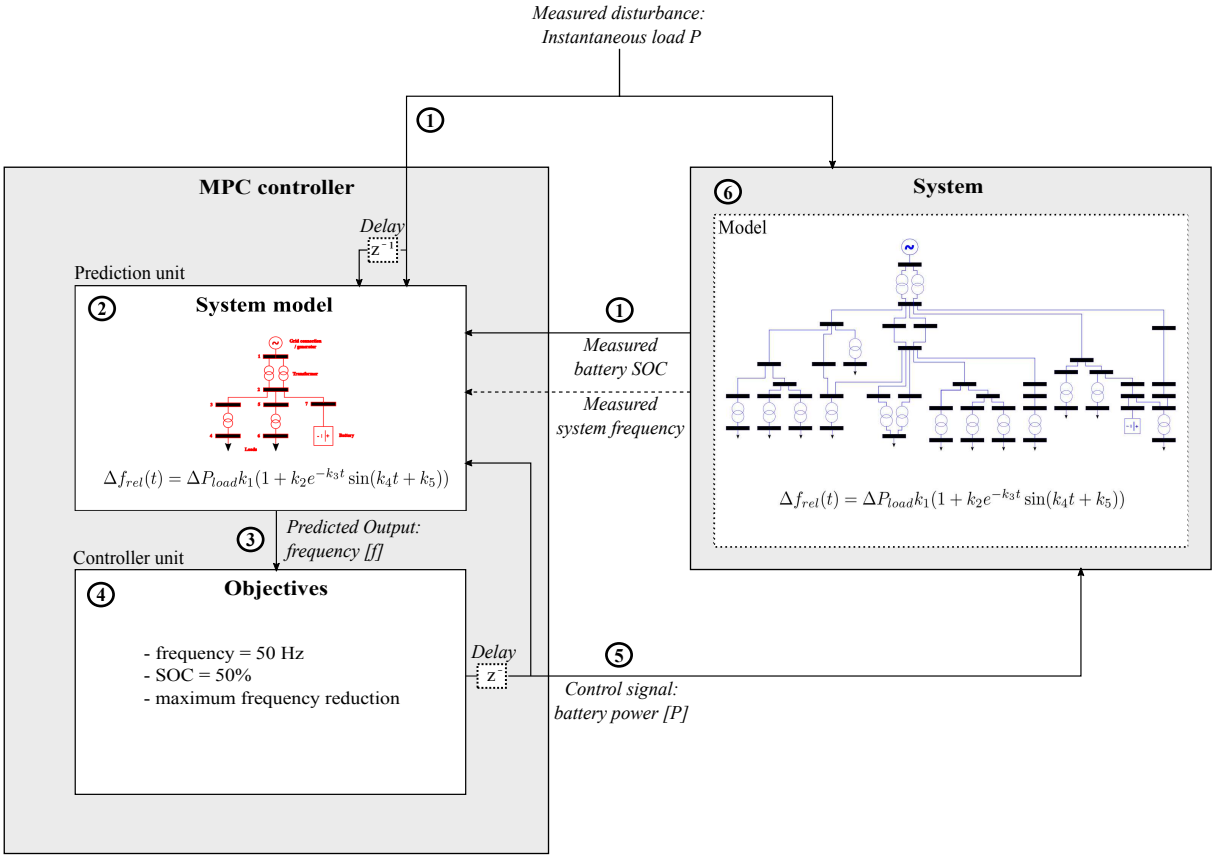

Figure 4.1: Schematic controller structure including modelling approaches (left) and interconnection with (modelled) electric distribution network (right).

The following signals are processed by the control algorithm, similarly to the MPC principle presented in chapter 3.

1. The main **input** to both the MPC controller and the electric distribution network (system) is the changing demand power. It corresponds to a measured disturbance. The second input to the controller is a measurement of actual battery SOC, entering the MPC controller as state input. For enhanced controller performance, a measurement of current or past system frequency is transferred to the controller as second state input. All inputs are transferred to the controller at constant sampling intervals.

2. The **prediction unit** receives the current state and disturbance inputs, possibly also stored former values, and an initial battery control sequence. Based on these inputs, the future system behaviour is predicted over the simulation horizon.

3. The **estimated system behaviour**, in this case most importantly the predicted future frequency deviation, is given to the controller unit.

4. The purpose of the **controller unit** is to determine a future sequence of battery active power injections into the electricity grid, which leads to a minimum value of a pre-specified cost function. In this case, an optimisation method is used that iteratively transfers updated control signals to the prediction unit. Following, it computes the corresponding cost function values from the returned estimated system behaviour.

5. Finally, the **control sequence** is transferred to the battery storage and the first element is applied. A certain delay time elapses between the entrance of inputs to the controller and power injection of the battery storage. It is expected to be caused by MPC computation time and physical delays of measurements and electrical battery components. At the next sampling interval, the control algorithm will start again from step 1 with updated inputs.

The proposed controller principle is based on certain assumptions. For example, it is based on measured sums of system loads. An alternative approach would be approximating such measurements with suitable estimation techniques if they are not available. The control approach origins from the assumption that active power measurements can be performed faster than frequency measurement. Within the prediction unit, a simplified model of the network is assumed to simulate with satisfying accuracy the stepwise adjustment of power delivered by a conventional generator in order to meet changing summarised network loads. From this, a future frequency deviation results, which is predicted with an algebraic model.

Figure 4.2 illustrates the principle of the MPC controller in continuous operation with regard to timing. After each sampling interval T, the continuous system states and measured disturbance P_{demand} are retrieved. As proposed in literature (Bakken et al in 2005, [18]), it was assumed that the generator's power is adjusted only stepwise to the continuously changing power of system loads. Between the samplings, the generator power was assumed to be constant. The sampling interval in simulation studies was $T = 1$ s.
The battery power is changed after periods of the same length as sampling interval T and hold constant in between. However, the change of battery power can only be adjusted

after a small delay time T_{bat}, which varied in the range of 0 s $< T_{bat} \leq T$, that is smaller or equal to the sampling interval. A delay time of $T_{bat} = T$ would mean the battery storage power changes at the same point in time as the next change in load and generator power. As the generator was assumed to be only adjusted to the changing demand at sampling intervals T, this would be the most consistent controller setting. The delay time of the battery storage was unknown in this thesis. The influence of different delay times was assessed during simulation studies by setting it to different values.

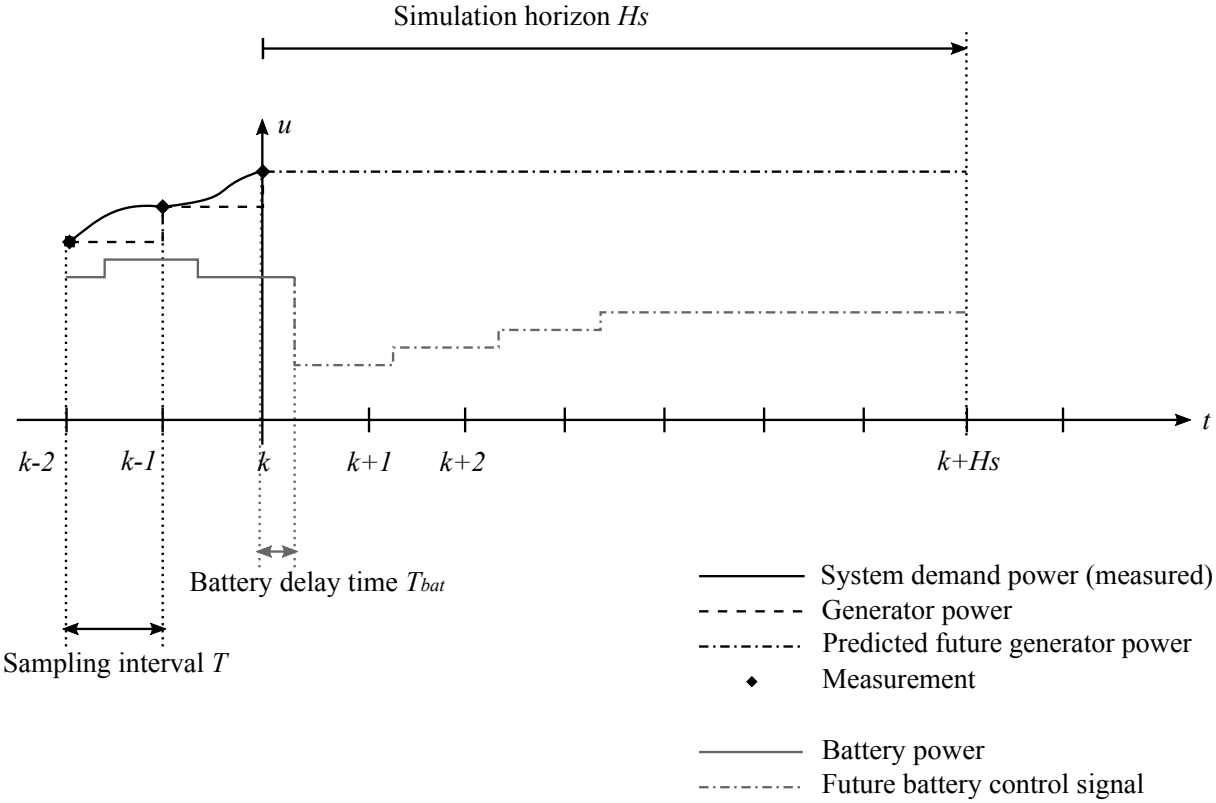

Figure 4.2: Principle of stepwise power flow [18], sampling intervals and battery delay time.

Based on measured system states and disturbance, after each sampling a simulation is conducted for predicting the future system behaviour during the simulation horizon H_s. In order to reflect transient frequency response characteristics, this is done with a higher resolution. It was chosen as 10 calculated values per second, as trade-off between accuracy and computation time. Battery delay times were always set to multiples of this simulation resolution.

4.2 Network modelling

Both simplified and large network models consist of two main components:

- A **static single-line load flow** model with constant PQ-load buses, variable gen-

erator slack buses, and line data representing network transmission lines and transformers.

- And a **dynamic frequency deviation model**, forecasting future values of system frequency caused by a step change in generator power.

The two models are presented in the following sections, followed by the modelling approach for the battery storage.

4.2.1 Static electricity network model

The main objective of applying load flow models of the electricity grid is to provide a realistic estimation of active and reactive power losses in the network. These can be considerably high. Additionally, operating limits of one or several connected generator(s) and voltage magnitudes and angles at all buses could be included in the load flow algorithm, if such values were known.

For representation of a real-world distribution grid, a modified version of the "EHV1" test feeder was used that have been presented in section 2.2.3. As the original test feeder shows stability issues, but a stable network model was required, the problematic part of the test feeder was removed. Furthermore, a connection to another network was removed and the battery storage was connected at the same bus instead. By this, the number of connected "conventional" generators was reduced to one, which shall represent a single connection of a distribution grid to the transmission network. This corresponds to creating a kind of island network, as the complex interaction mechanisms with the rest of the grid are simplified and replaced with one synchronous generator. The reduced network consisted of 46 buses, of which 14 were PQ-loads. Most of the loads were connected via one or two of totally 16 transformers. The battery storage was treated either as PQ-load or generator, depending on the purpose of the respective calculation step. In order to reflect different sizes of loads in the large network model, new demand data values were shared among the load buses based on the initial shares of loads in the original test feeder. Inside the controller, a very simplified network representation was used in order to increase simulation speed. It was constructed with the smallest number of buses representing the basic components of the large test feeder. These include a generator (connection to the transmission grid), coupled to medium voltage level via two transformers, two loads at low voltage level, each connected via another transformer, and the battery storage connected at medium voltage level. The adjusted "large" network model is depicted in figure 4.3, together with the simplified model. The line characteristics of the simplified model were heuristically determined with respect to similar active and reactive power losses within the complete operating range of the network models. The diagram in figure 4.4 illustrates that the calculated losses in both network models are in well accordance.

4.2.2 Dynamic frequency deviation model

A suitable dynamic model for frequency response to load changes was selected based on comparison of the different approaches presented in section 2.3.2. These were two dynamic

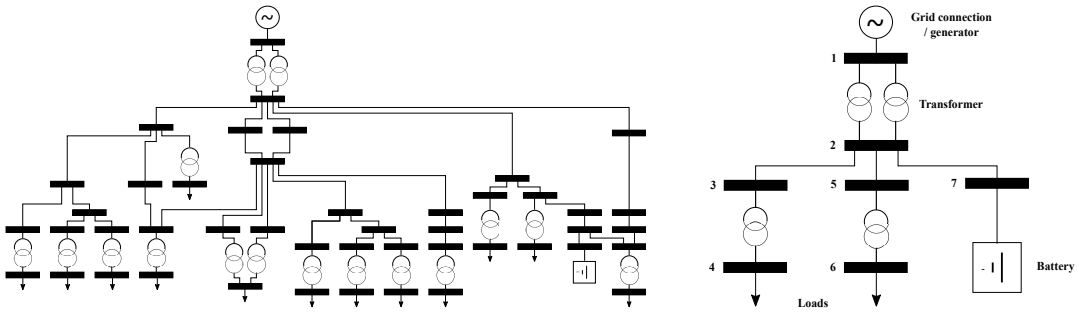

(a) Large network model (modified UK "EHV1" distribution test feeder, [14]).

(b) Simplified network model.

Figure 4.3: Comparison large and small network model.

block-based models A and B realised in Matlab Simulink (figure 2.5, 2.6) and an algebraic equation 2.17 derived from Model B. The estimated responses of the different models to a single and a double step change are illustrated in figures 4.5 and 4.6. Using the algebraic equation, the total frequency deviation was calculated as sum of future deviation vectors resulting from single step changes. This is illustrated in figure 4.7. For example, in the case of double step change, two frequency responses were calculated from the respective relative changes in power. Following, they were added, including the same shift in time as the load changes they arose from.
The generator specifications applied in the simulations are summarised in table 2.

Parameter	Symbol	Value	Unit	Source
Equivalent system inertia	H	4.0	s	[10], [27]
Load damping factor	D	1.0	1/Hz	[10]
Turbine (reheat) time constant	T_t	0.40	s	[28], [2]
Governor time constant	T_g	0.08	s	[28]
Governor regulation (primary control)	R	0.05	Hz	[10]
Secondary control factor	K	-0.50	-	[28]
Mechanical power gain factor	K_m	0.99	-	[10], adjusted
Fraction of high pressure turbine	F_h	≈ 0	-	[10], adjusted

Table 2: Generator and power system specifications used for estimation of dynamic frequency response

The following observations can be made in the figures.

- The frequency deviation is significantly reduced in the double step change case compared to a single step change in load power for all models. This illustrates the positive effect of battery action.
- By including secondary control in the models, the long-term frequency deviation decreases and will asymptotically approach zero. However, in reality secondary

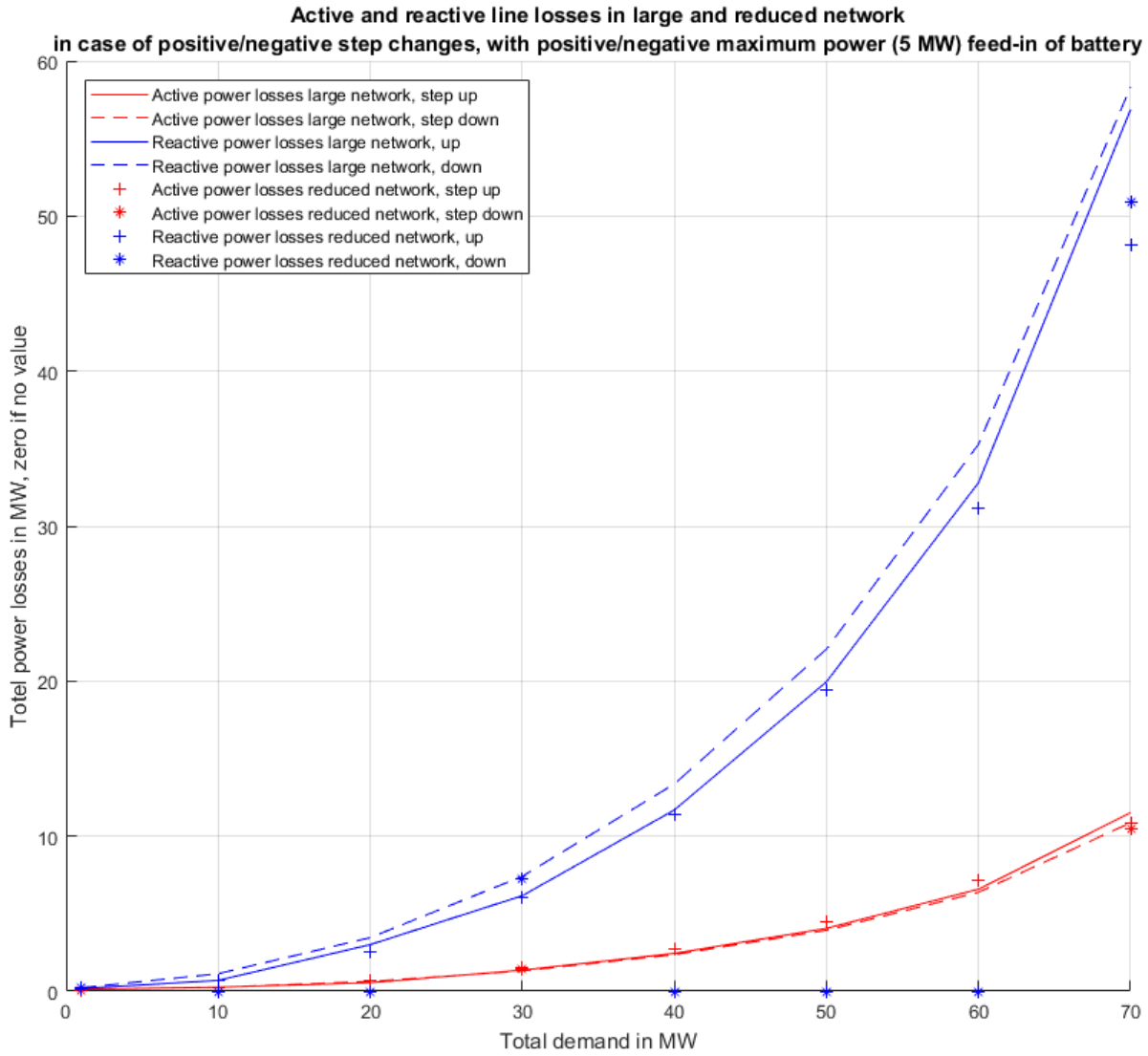

Figure 4.4: Calculated active and reactive power losses in large and simplified electricity network models.

control is activated after several dozens of seconds to minutes. In the models shown, a delay of only two seconds was applied in order to demonstrate the influence of secondary load frequency control.

- Comparing the different models, the steady-state frequency deviations estimated by models only including primary control is very similar. However, the initial maximum frequency deviation estimated by model A is larger than by model B. The parameters of the algebraic equation were slightly tuned such that the estimated frequency response is as close to both models A and B for both single and double step changes as possible.

A significant advantage of the algebraic equation is the computation time, which was found

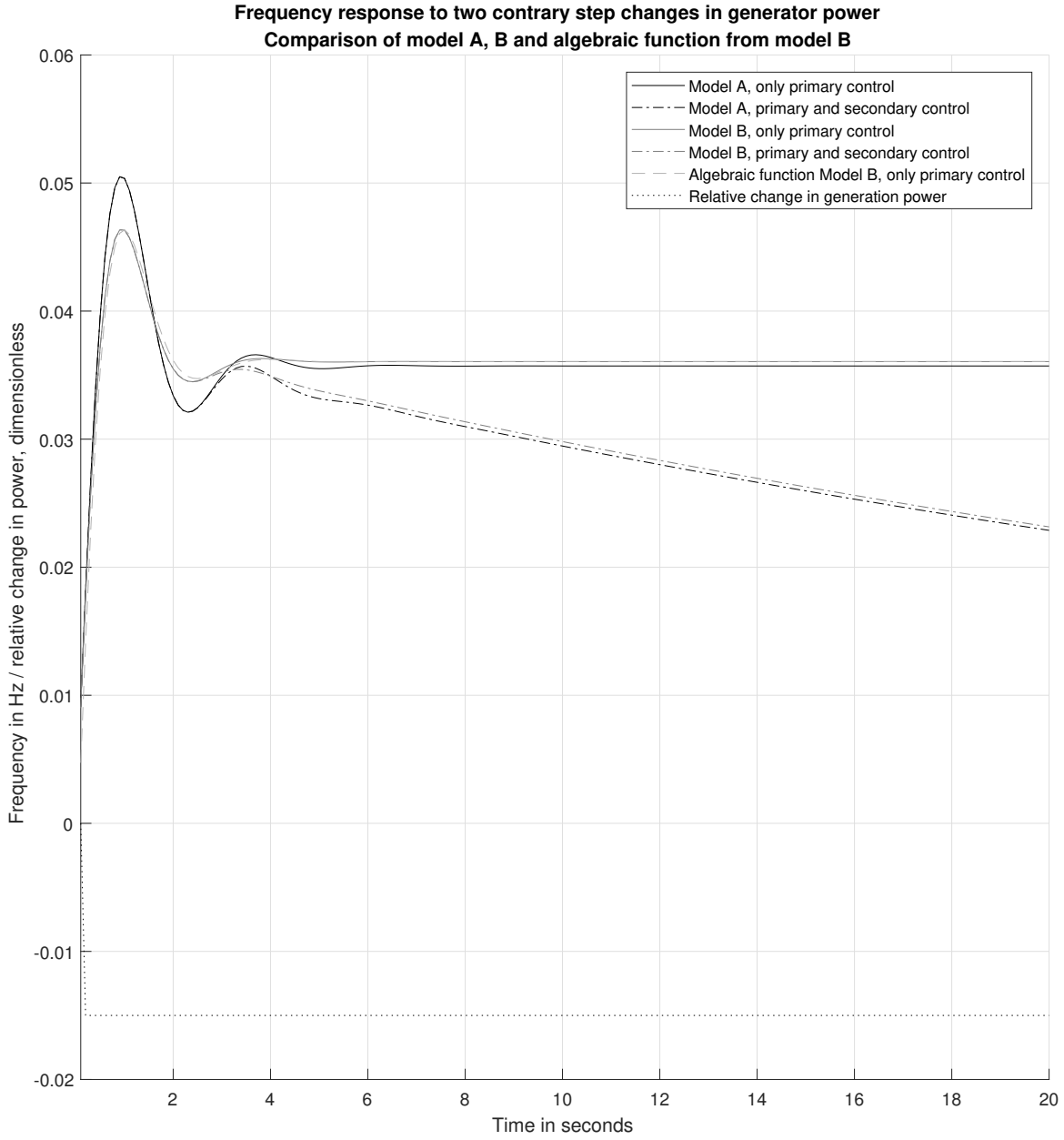

Figure 4.5: Frequency response (deviation from nominal mains frequency in Hz) of different models to single step change (decrease) in load power.

to be significantly lower compared to the block-based models implemented in Simulink. This may result from the latter being called again for each prediction. A time saving factor of 50 to 100 was observed, see table 3. For the algebraic equation, based on the assumption that system specifications variables will remain during all simulated states of the power system, it is possible to calculate the needed constants only once. This enables further increase of simulation speed.
The point in time at which secondary control action is usually started is minimum 15 sec-

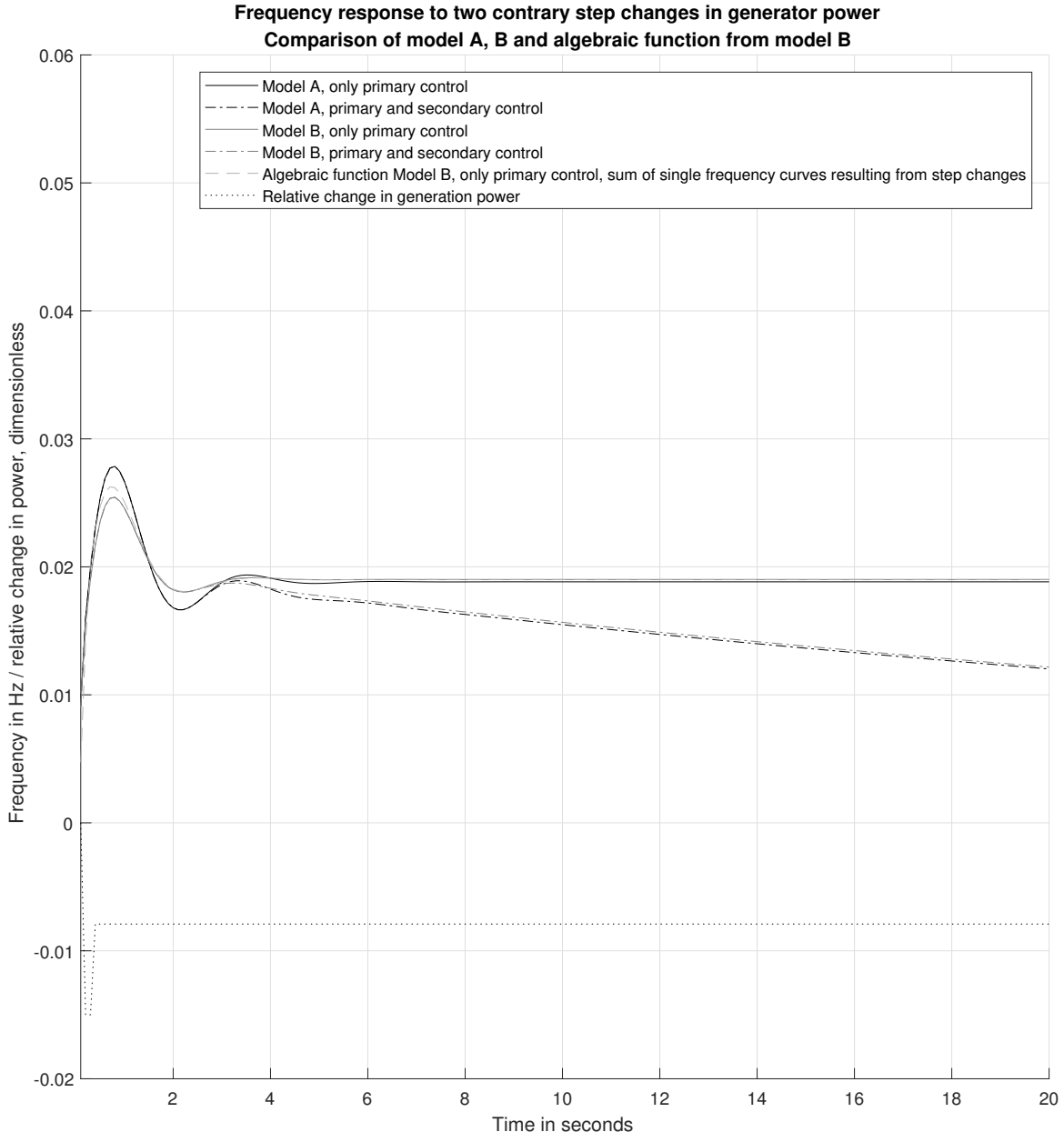

Figure 4.6: Frequency response (deviation from nominal mains frequency in Hz) of different models to negative step change in load power, followed by an increase in power due to battery action.

onds after a load change, based on measured frequency deviations integrated over time. As this is beyond a suitable prediction horizon for the battery controller, it was decided to imply a frequency response model without secondary control.
Due to the good performance compared to the other models and the higher computational speed, the algebraic equation with generator parameters as of table 2 was chosen as model for frequency prediction. The frequency response characteristics were calculated with a

resolution of 0.1 s, which corresponds to 10 values per second and was assumed to reflect expected changes in frequency properly. Only primary, but not secondary control action was included in the model, which is acceptable as discussed above.

Desired effect of battery storage

Each recorded variation of system loads causes, in the simulations stepwise, change in the generator active power. This results in a frequency deviation characteristic that can be estimated with the selected model.
The intended role of the battery storage connected to the electric network was to act as an additional, flexible and controllable load. By suitable battery action, thus change of actual active power injected into the grid, generator changes should be triggered that cause frequency deviations in the opposite direction to the former dynamic frequency response. This principle is illustrated in figure 4.7. The first dynamic frequency response is changed by a change in generator power in order to meet a variable demand. Following, the battery power is changed. By this, a new value of total system loads is achieved that have to be delivered by the generator. This second change in generator power will lead to another frequency deviation, which preferable should be in opposite direction to the initial one, such that the total deviation (sum of single dynamic responses) is minimised. The battery storage action that causes another change in generator power is delayed by some small time period. Hence, the amount of battery power needed to minimise the total frequency deviation was expected to be slightly different from the initial system load change. Additionally, the battery storage is the connection to the electric grid at a single point, in contrast to the distributed system loads. Thus any battery action was expected to result in changing line losses, that would have to be compensated by the generator as well and could be taken into account with suitable network models.

Applying suitable battery power vectors can lead to the following two main possible effects.

- a reduction of maximum predicted frequency deviation, and
- a delayed time of occurrence of maximum frequency deviation.

The first effect is the main objective of the battery storage. The second effect is small, but still considered to be positive because it "buffers" the frequency deviation resulting from a change in load, meaning it offers the possibility to other load frequency control reserves with a longer reaction time to become active.

4.2.3 Battery storage model

In section 2.4, the approximate representation of a large Li-ion based BESS as an ideal current source at constant output voltage was introduced. For the battery model in this thesis, this assumption was further expanded: the storage was regarded as an ideal power source that could deliver any required active (or reactive) power at the nominal grid

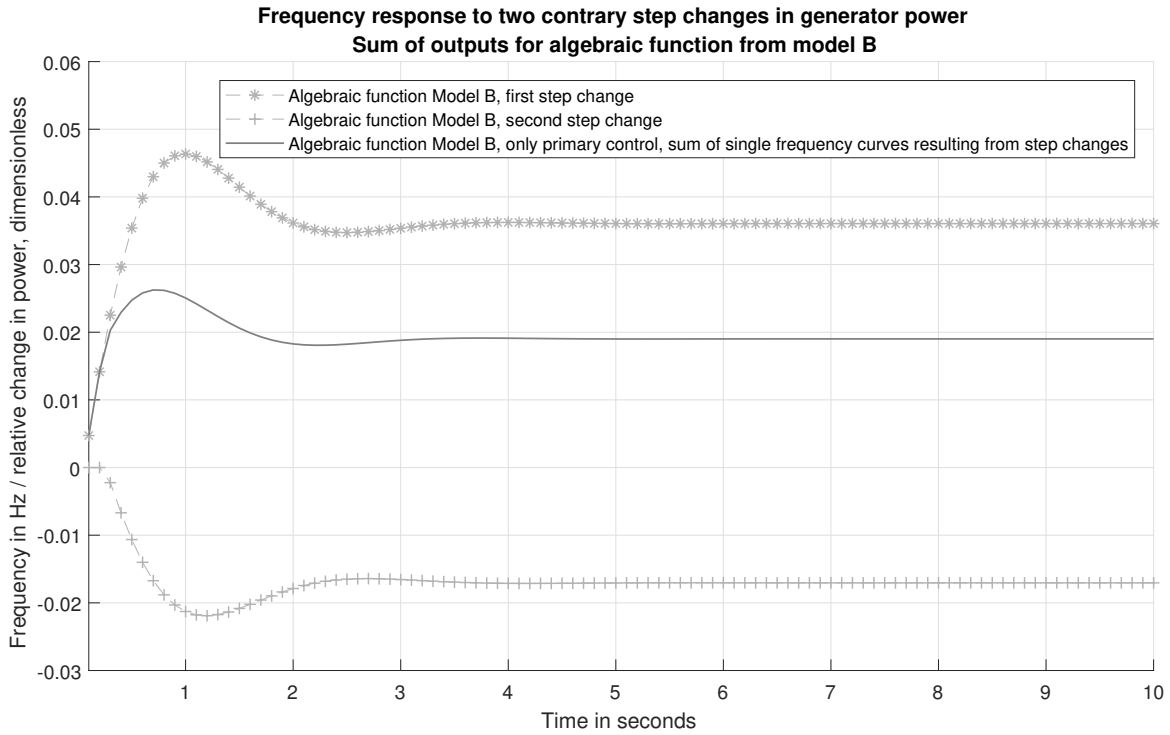

Figure 4.7: Frequency response (deviation from nominal mains frequency in Hz) of algebraic function as sum of responses to two subsequent step changes.

Model	Simulation time 1 step	Simulation time 2 steps	Unit
Block-based model A	< 0.05	< 0.05	s
Block-based model B	< 0.05	< 0.05	s
Algebraic function (from B)	< 0.001	< 0.001	s

Table 3: Approximate computation time needed for simulation of single and double steps with different dynamic frequency response models. The exact values vary in each call, depending not only on the programme (e.g. if Simulink was already started), but also on hardware and potential use by other processes.

voltage level. However, the battery action is limited to a certain range of operation that among others is formed by the following physical constraints.

- Limited capacity (energy content). The actually stored energy can be expressed as SOC, which is the actual energy stored as percentage of nameplate capacity.
- Minimum and maximum battery power.
- Reaction time for power delivery.

The latter parameter was created as artificial parameter combining computation time of the controller unit, transfer time of the control signal to the battery storage and physical

delay time until power delivery at grid connection point.As minimum and maximum SOC, 10% and 90% were chosen. These values correspond to the typical range of constant output voltage of Li-ion batteries. Furthermore any possible deep discharge effects and system stresses are prevented, which increases the lifetime of the storage. For flexible operation of the battery storage, a medium state of charge should be maintained, from which battery action in both positive and negative power range are possible.
Injecting energy into the grid at maximum power is possible, but should be avoided during longer periods of time. On the one hand, it may cause thermal stress on electric components, and on the other hand, it will effect the battery SOC.

Regarding combinations of battery maximum power/nameplate capacity, feasible values were retrieved from a data sheet of the real market product "Y.Cube 500/1.5" of "Younicos" Inc., [46]. As the storage product is scalable by combining single units, different battery storage sizes were simulated as multiples of one storage unit, with the specifications as in table 4. The storage is assumed to be suitable for the proposed application, as the same manufacturer had installed a large battery plant based on Li-ion technology (lithium-manganese-oxide) that provides frequency regulation services, [33]. The 5 MW/5 MWh battery power plant of 2013/14, which was expanded to totally 15 MW/15 MWh in 2016, is operated by WEMAG AG. It is located close to Schwerin, Germany, hence in a region highly penetrated with renewable energy sources, mainly wind power and can be seen as a reference case for the future application of the proposed controller. A reactions time of this storage systems of 200 ms was reported in [47].

Parameter	Value	Unit
Maximum power	±500	kVA
Nameplate capacity (energy)	887	kWh
Minimum state of charge (SOC)	10	%
Maximum state of charge (SOC)	90	%

Table 4: Battery model specifications, from Y.Cube 500/1.5, [46].

4.3 Demand data

A set of synthetic data of one year active and reactive demand power with a resolution of 1 second was retrieved from [48] for evaluating the performance of the battery controller. The data set had been generated from two sets of real residential measurements and hence was assumed to be representative for domestic loads in distribution networks and scalable to electric system of desired sizes. The three phase power consumption measurements were summed for applying them in the single phase load flow algorithm. Furthermore, after analysing the relationship of active and reactive power (see section 4.3.1), only active power values were used and reactive power was estimated proportionally.

4.3.1 Analysis of single phases and relationship of reactive to active power

In single line load flow calculation, all phases are assumed to be equally loaded and thus can be replaced by one phase. This assumption was validated for the given demand data set by means of a visual analysis. Figure 4.8 illustrates the phase-wise and total active and reactive power over one day. It can be concluded from the plots that

- Active power is approximately equally distributed among the three phases. Peak loads in single do occur seldom and randomly. Hence, the single phase active power values can be represented by their sum.
- A daily pattern is visible for active power consumption, with times of high load in the morning and evening hours, and low consumption during the night.
- Reactive power in different phases varies more than active power. The sum of reactive power consumption is mostly significantly lower than for active power (in diagram: pay attention to different scales). There is no clear continuous daily demand profile as for active power, only a phase of low reactive power consumption during night time.
- Active power consumption is purely positive, which indicates absence of any generating sources, such as distributed PV installations. Those would result in negative loads when more energy would be generated than consumed. Thus, the flow of energy within the grid is mono directional from the generator to the load(s).
- Reactive power consumption is mainly positive, which represents inductive loads (such as motors), but can be partly negative, indicating capacitive consumers.

Reactive and active power

For simplified controller design and implementation, it was examined if instantaneous reactive power values could be estimated in a simple manner from active powers. A visual analysis of the demand data set, shown in figure 4.9, revealed that the ratio of reactive to active power ratio Q/P is approximately normally distributed around a mean value of $\overline{Q/P} = 0.11$ (see lower subplot), though with a relatively large standard deviation of $\sigma(Q/P) = 0.051$. A correlation analysis resulted in a relatively low correlation coefficient (as measure of linear dependence between two variables) between active and reactive power of $\rho(P, Q) = 0.77$, which is in accordance with the large variance value. The values of $\overline{Q/P}$, $\sigma(Q/P)$ and $\rho(P, Q)$ were calculated with the complete data set of one year.

The middle subplot of 4.9 does not indicate any clear dependency between Q/P ratio and the time of the day. Though, this was further evaluated with a scatter plot, see figure 4.10. In the plot, different typical Q/P values during certain periods of the day can be observed. However, a correlation coefficient of $\rho(Q/P, t) = 0.24$ indicates that there is no simple linear relationship between the two variables.
It was decided to approximate the Q/P ratio as a constant proportion of 0.10 in the

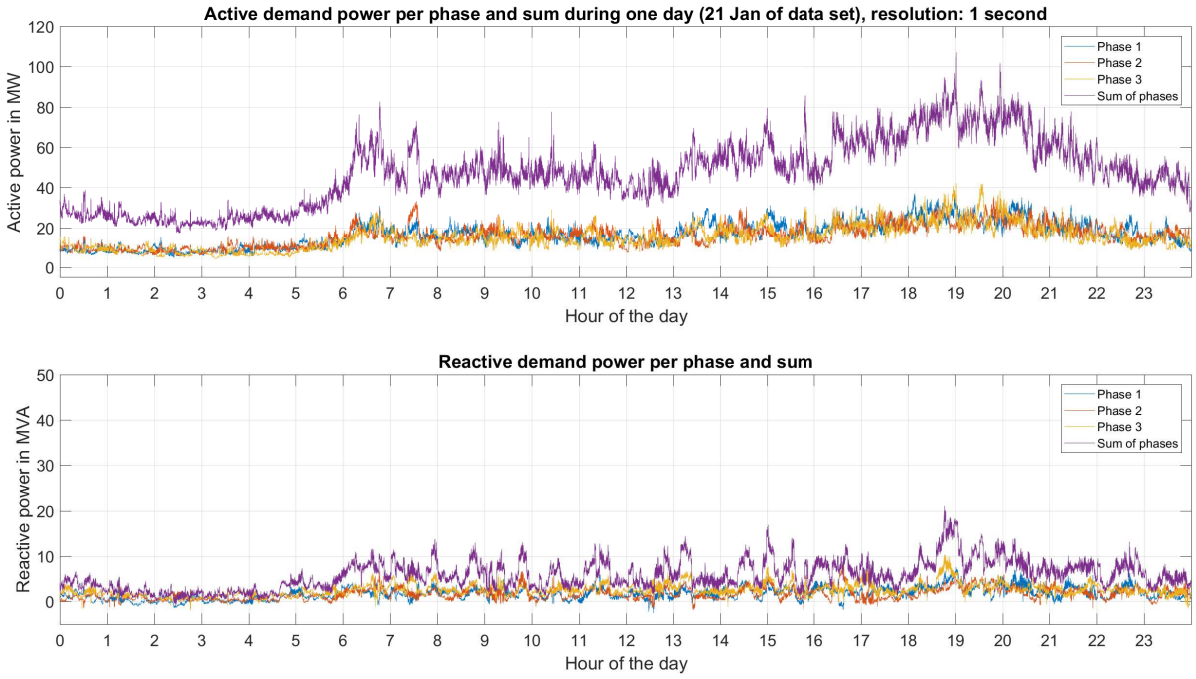

Figure 4.8: Demand data plots of one day (a Wednesday in January), showing single phase active and reactive power and sum, data from [48].

controller algorithm and network simulations. This line together and the least square regression line are also plotted in 4.10.

4.3.2 Demand power analysis and prediction approaches

With the help of the demand data set, different short-term prediction approaches for demand power changes were evaluated. First, it was examined if correct predictions of demand power would improve the frequency prediction performance. As illustrated in figure 4.11, this is the case. The mean average prediction error (MAPE) can be reduced linearly to the number of correctly predicted future values of demand power. After the specified number of correctly changing future demand powers, a constant power value was assumed. The values in the figure are based on the complete data set of one year, calculated as mean average of single results obtained with a sliding window. Following, several different prediction strategies for demand power were applied and evaluated.

Moving average

In the prediction approach based on the moving average principle, the next value of demand power was estimated by an average of a specified number of former demand power values. Afterwards, the new value was hold constant until the end of the simulation horizon. For continuous operation, the moving average was computed using a sliding

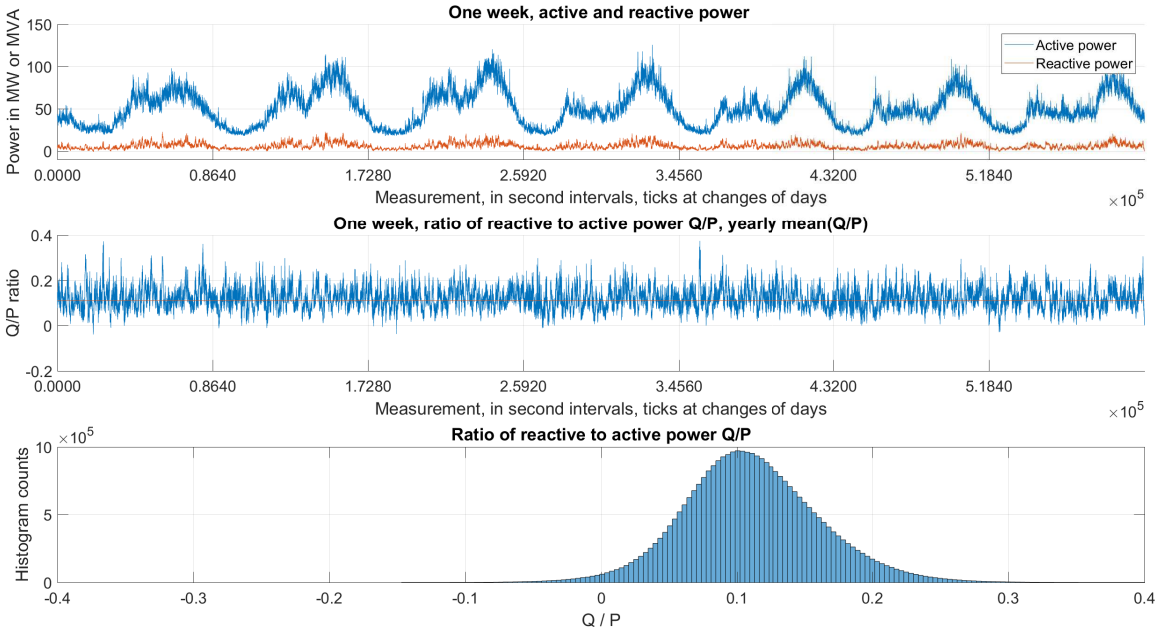

Figure 4.9: Summed active and reactive demand power, ratio Q/P with mean line, and histogram, first week (January) of data from [48].

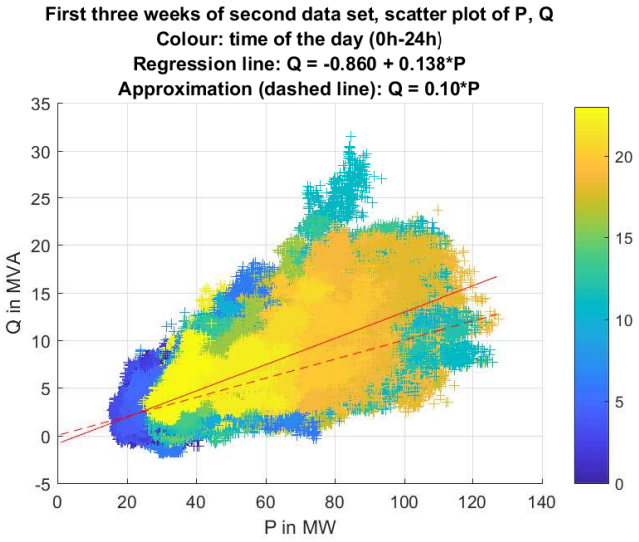

Figure 4.10: Summed demand active and reactive power values and linear approximation lines, one day (21 January) of data from [48].

window. The number of elements included in the sliding window was varied from 0 s to 1 h. The performance of this approach was evaluated with a simulation horizon of 9 s (including current value: 10 s). From the results summarised in table 5, it was concluded that this estimation method is not suitable for predicting future demand data. The "best"

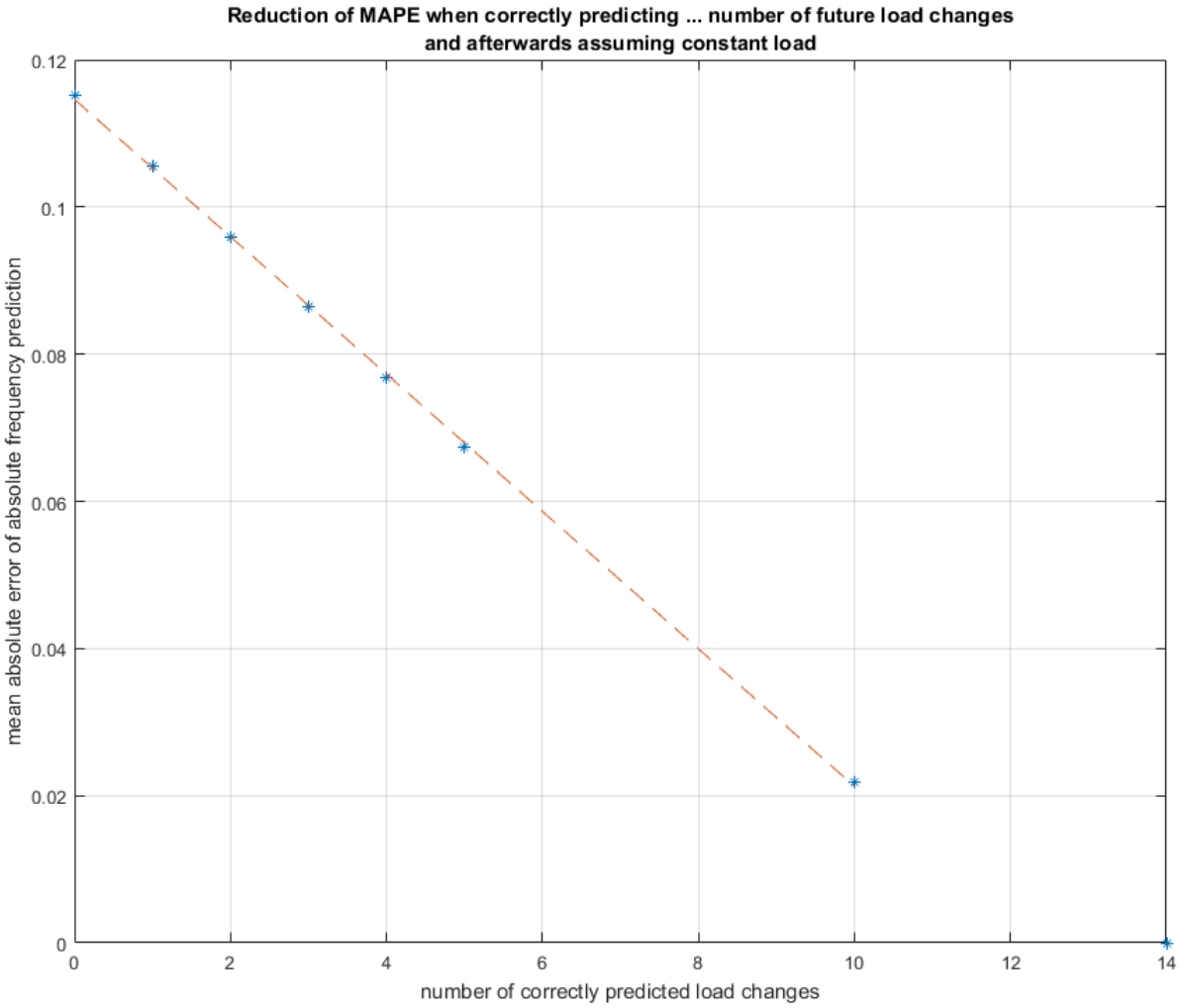

Figure 4.11: Prediction performance of future frequency deviation at correct estimation of varying number of future demand data values. Recoreded as mean average prediction error (MAPE). Simulation horizon: 14 s. If all future demand power values are correctly predicted, MAPE=0 by definition, data from [48].

prediction of next instantaneous demand powers was recorded for assuming that all future power values equal the currently measured power (no average).

Relationship subsequent power changes

It was further evaluated if relative changes in demand power correlate with the current power value or with former relative change. The corresponding histograms are shown in figure 4.12. High peaks around zero in both histograms indicate no linear relationships of this kind within the given data set. Regarding the relationship of two subsequent changes (right subplot), as small irregularity of histogram shape at -1 indicates that an change in power is slightly more likely to be followed by a change in opposite direction.

Number of past demand power values	MAPE
60*60 (1 hour) -1	4.52
30*60 (30 minutes) -1	3.74
10*60 (10 minutes) -1	3.09
1*60 (1 minute) -1	1.82
30 (seconds) -1	1.57
10 (seconds) -1	1.31
0 (current value)	1.07

Table 5: Mean average prediction error (MAPE) compared to real power values. Future demand power values during simulation horizon of 10 s were estimated as constant value, calculated as moving average of varying number of former demand power values. Figures based on first 100 000 summed demand power values from data from [48]

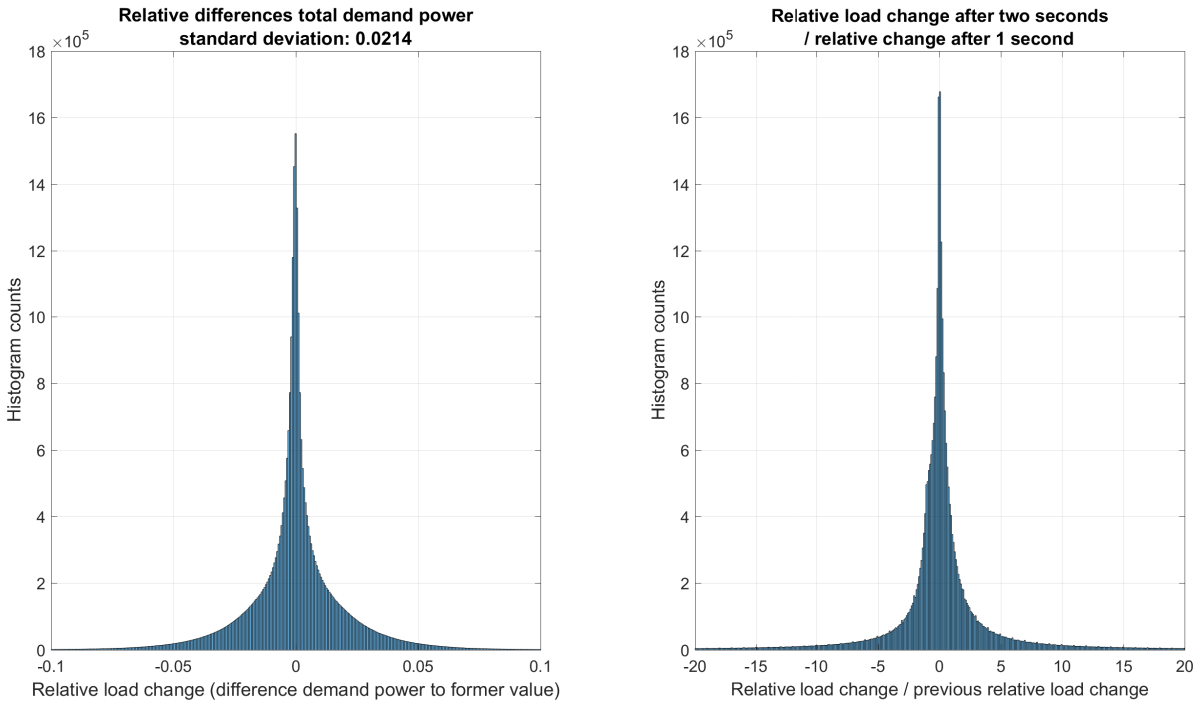

Figure 4.12: Relative change in demand power compared to current power value (left), and ratio of two subsequent relative changes (right) with base values: power before each change, data from [48].

Harmonic analysis

It was evaluated if demand power could be short-term predicted applying dynamic harmonic regression methods, as for example in [49]. First, a Fourier analysis was conducted using Matlab Fast Fourier Analysis (function `fft`). This was expected to help identifying periodic patterns in the demand power data, together with their typical lengths. The

results of the Fourier analysis are displayed in figure 4.13. The plot also shows summed demand powers over the entire year (upper subplot) and amplitude spectrums (middle and lower subplot). Particularly in the lower subplot, it can be clearly seen that the highest peaks of the amplitude spectrum coincide with frequencies of diurnal periodic patterns and harmonics (red lines correspond to recursive signal periods of months, weeks, days, half days, hours and minutes). Also some weekly periodic behaviour can be identified. In the range of minutes, which is of interest for short-term load prediction as usable in the controller, no significant peaks can be observed. In this range, the amplitude magnitudes are approximately uniformly and randomly distributed, and very small compared to longer periods' peaks, hence they can be considered as noise.

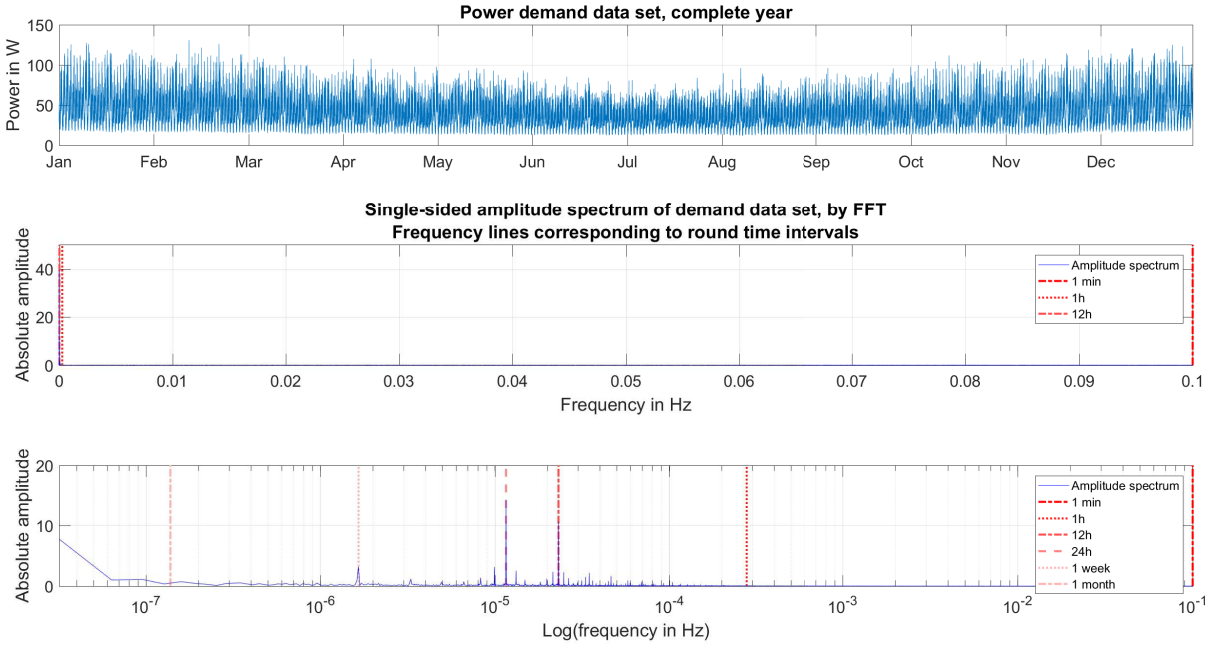

Figure 4.13: Fourier analysis. Upper subplot: Illustration of demand data over 24 h to show high variability. Middle plot: Single-sided amplitude spectrum including also high frequencies (repeating patterns with small periods). Better visibility of high absolute magnitude values at low frequencies in lower subplot through logarithmic x-axis. Vertical lines indicating round values (legend entries top down correspond to red lines from right to left), data from [48].

It can be concluded from the Fourier analysis that at the desired time scale, harmonic regression is not a promising approach for predicting future demand power values due to the lack of corresponding periodic behaviour of data. Hence, no further investigations in this direction were performed.

Finally, it was decided to estimate the load power over the complete simulation horizon as constant value, which equals the current available measurement. This approach is assumed to be a simple method and in well accordance with the histograms of relative and subsequent load changes of figure 4.12.

4.4 Objective function

The controller unit of the MPC seeks to find a control signal x^* resulting in a minimum value of the objective function $f(x)$ (cost function) with the help of a suitable optimisation method. In direct search algorithms, the cost function value is iteratively determined for each different control signal x. In this case, the control signal is a vector of future battery power values, $\vec{P}_{battery}$. The objective function was formulated as linear combination of three weighted terms $f_i(x)$

$$f(x) \quad = \sum_{i=1}^{3} w_i f_i(x).$$

The single terms were defined such that smaller values are more desirable, hence a minimisation algorithm could be applied. The first two terms represent the desired effect of battery action.

1. The expected **absolute maximum future frequency deviation from the set point frequency** that is predicted to occur at the next sampling time shall be minimised. The difference in frequency to f_n after 1 s resulting from the measured change in generator power ΔP_{load} and battery action according to the control signal $[P_{battery}]$ can be expressed as

$$f_1(\vec{P}_{battery}) = w_1 \cdot \left| \hat{f}((\vec{P}_{battery}|f, \Delta P_{load})(1\text{ s}) - f_n \right|,$$

   based on the estimated frequency deviation $\hat{f}((\vec{P}_{battery}|f, \Delta P_{load})(1\text{ s})$. The absolute frequency deviation also depends on the current system frequency f at the sampling time. The set point frequency were always assumed to be the nominal grid frequency of 50 Hz.
   Throughout simulations, typical frequency deviations in the range of ±...100 mHz were observed, leading to cost function term values of around $0 \ldots 0.1$. The term was weighted with $w_1 = 100$, as it was considered the most important one, directly reflecting the intention of the battery controller.

2. Independently from the total deviation to set point frequency, the expected **relative reduction of maximum frequency deviation**, compared to inactive battery storage ($\vec{P}_{battery} = 0$) should be minimised. In case of desirable effect of battery action, this term

$$\Delta\hat{f}_{rel}(\vec{P}_{battery}) = \frac{max\left(\Delta\vec{\hat{f}}(\vec{P}_{battery}|\Delta P_{load})\right) - max\left(\Delta\vec{\hat{f}}(\vec{P}_{battery} = 0|\Delta P_{load})\right)}{max\left(\Delta\vec{\hat{f}}(\vec{P}_{battery} = 0|\Delta P_{load})\right)}$$

   is < 0 and larger negative values are more preferable. The maximum future frequency deviations of active and inactive battery storage were determined independently from their time of occurrence. The weighting factor was set to $w_2 = 1$. For this term, often values in the range of $0.1 \ldots 1$ were observed.

The third term of the cost function was formulated as a barrier function with the intention of preventing deep discharge.

3. The logarithmic **barrier function for battery state of charge** at the end of simulation horizon H_{sim},was formulated as

$$\begin{aligned} f_3(\vec{P}_{battery}) &= -w_3 \log\left(SOC(\vec{P}_{battery})(H_{sim}) - 10\ \%\right) \\ &\quad -w_3 \log\left(-SOC(\vec{P}_{battery})(H_{sim}) + 90\ \%\right), \end{aligned}$$

based on the logarithmic barrier function presented in equation 3.6. It contains a positive term added to the objective function when the predicted SOC at the end of the simulation horizon is close to the minimum SOC value of 10 % (lower bound) and a second term with similar effect for the upper bound of 90 %. The weighting factor was set to $w_3 = 1$. An exemplary barrier function's graph is depicted in figure 4.14.

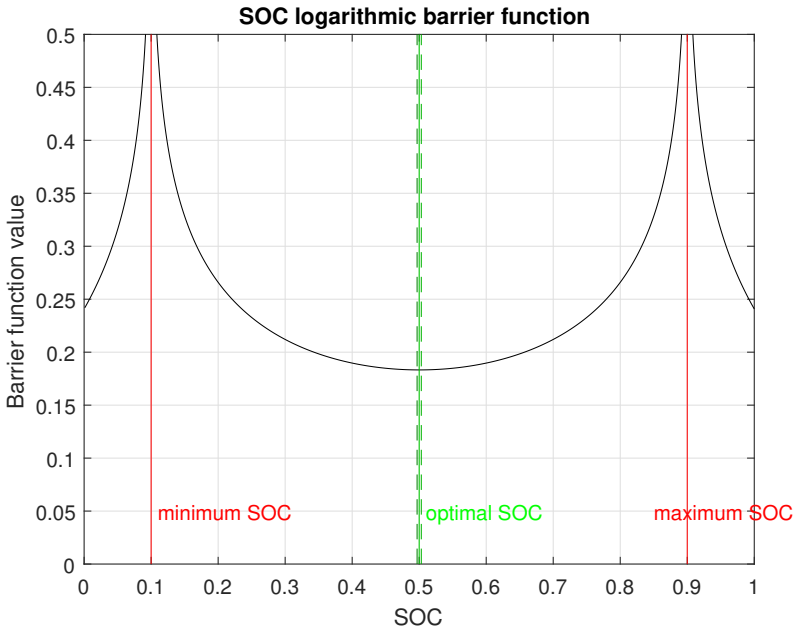

Figure 4.14: SOC barrier function with specified parameters and weights. Dashed lines indicating changes of SOC within one second when operated at maximum power (±0.31 %).

As can be seen from the simulation study results presented in chapter 5, the third cost function term did not show the desired effect in continuous battery operation. This may result from the very small influence of battery power action during small periods of time (such as simulation horizons of few seconds) on SOC of a large battery storage. For example, when operated at full power, the change in SOC of one battery module (0.5 MVA/0.887 MWh) over 20 s with maximum active power injection into the grid would be only $\Delta SOC = 0.500\ \text{MW} * 20\ \text{s}/3600\ \text{s/h}/0.887\ \text{MWh} = 0.0031 = 0.31\ \%$. Furthermore, the slope of the barrier function is relatively small for most values of SOC,

except extreme values, leading to small influence on the cost function.
As an alternative approach, it could be considered to limit the SOC to the operating range with a penalty function. In order to prevent constant charge or discharge action, a suitable additional barrier function could be applied that penalises constant operation of battery at high power in one direction over long periods of time.

Any **hard constraints** on the optimisation problem were realised as infinite penalty function terms added to the objective function in case of specified barriers being exceeded. However, in this application, all physical constraints were included directly in the calculation of battery power vectors, in order to ensure they would be never exceeded. By doing so, the possible problem of infeasible starting points in the optimisation algorithm was avoided, which can arise when imposing constraints directly on the optimisation method.

5 Simulation studies

This chapter presents a simulation study, which was conducted with the aim of evaluating the controller performance in continuous operation and for comparing different operating modes, controller and battery designs. A vector of demand power from the same period of time was used in all different variants. All simulations were conducted with both optimisation algorithms presented in chapter 3: Nelder-Mead simplex optimisation and golden section search method.

5.1 Comparison of operating modes

The performance of the MPC control algorithm should be compared to other operating modes of the battery storage. The computed modes were inactive battery, LFC-similar operation and the proposed MPC controller, as described below.

(I.) In **inactive battery** storage ("no battery") mode, the values of active and reactive power injected into the grid were zero at all times. Mode (I) should represent simulations of original power system's behaviour without BESS.

(II.) In **load frequency control** (LFC) mode, the battery was requested to feed in active power proportionally to the currently measured frequency deviation, in accordance with regulations in the Continental European interconnected synchronous area (as described in section 2.3.3). It was assumed that system frequency was sampled at the same point in time as the demand power values, hence at intervals of 1 second. The frequency deviations caused at that moment were not yet included in the frequency measurement, meaning it actually represents the last sampling's frequency. The battery power was determined proportionally to frequency deviation, up to its maximum power. Deadband action was included in the range of small deviations from set point system frequency. It was only activated when having positive effect on battery SOC, driving it closer to 50 %. Over fulfilment was not included in the algorithm. The calculated change of battery power was applied after the specified battery delay time. Afterwards, the battery power was held constant until the next change.

(III.) In the third operating mode, the battery storage's reacted to measured changes in total system load, based on the **model predictive control** (MPC) algorithm presented in the former chapter.

The simulation of "real" power system only included primary control action, which is part of the frequency deviation model recursively computed after each sampling time. It was a larger, more complex version of the system model inside the MPC controller, which clearly focussed on short-term calculations. Not including secondary or tertiary control action limits the feasible time ranges for evaluation of controller performance to small periods, as load-following over longer periods ($> 15 \ldots 30$ s) is the main task of these control services. Dismissing them, the model won't be able to represent slow adaption of the power system

to a new load-generation power equilibrium. Furthermore, in real interconnected power grids, also interchange of energy with other control areas helps stabilising the system. The used algorithm did not contain these processes. Hence, results of simulations over short periods of time were expected to be more realistic and reliable compared to simulating longer periods of time.

5.2 Load data

For evaluating the performance of the proposed control algorithm in continuous operation, it should be applied during in a simulation of a representative period of time. After each sampling, a battery control signal would be computed by MPC controller and returned to the "real" system model, in which the system behaviour including battery storage action is simulated. The computed system frequency and battery SOC would be then used as controller input at the next sampling instance, together with the next value of the demand power vector.

It was considered to simulate periods of weeks or days from different seasons of the year in order to evaluate different load patterns and magnitudes. However, due to the algorithm limitations to short periods of time, it was not feasible to compute whole days or even weeks. Thus, and also due to low computational speed, it was decided to select periods of maximum half an hour. The selected period of time was during morning hours (6 h-7 h) with intervals of mainly rising, but also and falling demand power values. The selected time of 20 min is illustrated in figure 5.1.

When used for simulations, the selected vector of power values were scaled such that it was in the middle of the used load flow simulation network's feasible range (also see figure 4.4 in section 4.2). The original load power of the test feeder was 38 MW active power, and maximum applicable total power the modified network was found to be around 60 MW to 70 MW, with any exceedance leading to non convergence of the load flow algorithm.

5.3 Parameter variation

In simulation studies, different system and controller parameters were varied in order to evaluate the proposed LFC control algorithm and compare it to the other operational modes presented in section 5.1. The same sequence of demand data, selected according to section 5.2, was used in all simulations. Each simulation run consisted of an initialisation, in which system states were reset to their nominal values, a simulation phase, in which all time values of the demand vector were simulated and the battery storage reacted according to the respective operating mode. The system states and outputs of interest were stored for each time step. After fully simulating one variant case, some pre-specified performance criteria were determined from the stored values. The following different battery parameters were varied.

- **Battery size** by means of nominal capacity/maximum power. This parameter was varied with the aim of evaluating the influence of battery size on the controller's

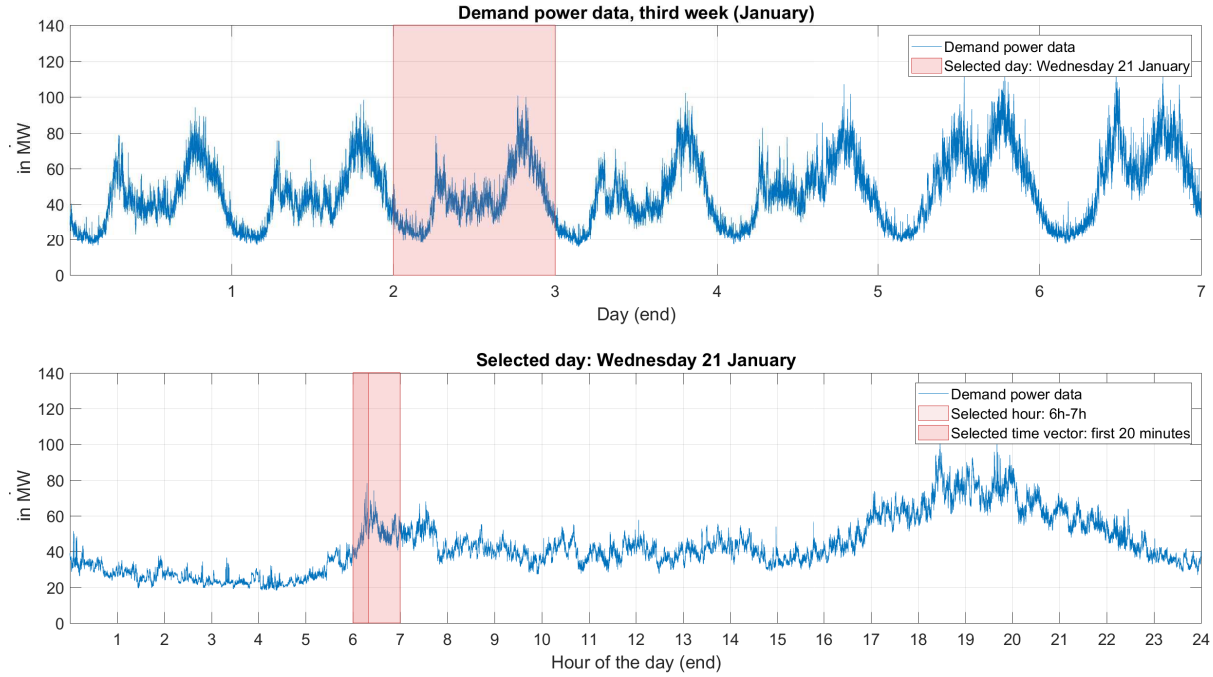

Figure 5.1: Selcted demand data for evaluation of controller performance in continuous operation, data from [48].

performance and to possibly optimising the storage size. The different simulated battery sizes were multiples of the base battery storage (500 kVA/887 kWh, see section 4.2.3).

- **Battery delay time** T_{delay}. As the real delay time of the later implemented battery storage, controller and grid connection is unknown, different values were evaluated that were assumed to be feasible.

- **Simulation horizon**. The simulation horizon is expected to influence the computational effort within the controller for prediction of system behaviour. It should be evaluated, if also the controller performance is affected by simulation horizons of different lengths. The simulated values of H_{sim} were chosen according to the modelling approaches that showed highest frequency deviations in time spans of 1 s to 3 s after a step change in generator power (see diagrams 4.5, 4.6).

Parameter	Values	Unit
Battery size	1.0, 3.0, 5.0	MVA
Battery delay time	100, 500, 1000	ms
Simulation horizon	2, 6, 10	s

Table 6: Parameters varied in simulation studies

All possible combinations of the parameters in table 6 were computed ($3 \cdot 3 \cdot 2 = 18$ variants), using the different operating modes and optimisation approaches.

5.4 Performance evaluation

In order to compare the controller performance in the different variants, in each simulation the following variables were recorded:

- Vector of battery power P_{bat}.
- Vector of battery SOC.
- Vector of system frequency f_{sys}.
- Vector of expected relative reduction of predicted maximum frequency deviation.
- Vector of expected relative reduction of area under predicted frequency deviation over the simulation horizon.
- Total time needed for simulation of the variant in each mode.

These result values were used to compute some **performance measures** for each simulated variant, operating mode, and optimisation method:

- Mean **average of system frequency** $\overline{f}_{sys}$. The closer this value is to the nominal grid frequency, the better the average performance of the controller.
- **Standard deviation of system frequency** $\sigma(f_{sys})$, representing the variability of system frequency. As large frequency deviations are undesirable, a value close to zero is preferable.
- **State of charg**e at the end of the simulation period. The final SOC after a certain period of operation is an indirect measure of overall energy injected into or absorbed from the grid. If total sum of positive and negative powers are equal, this variable would be zero. Being calculated relative to the storage capacity, SOC values are independent from the battery size and hence suitable for comparison of different design cases.
- **Variability of battery power**, by means of the sum of absolute differences in power injected into or absorbed from the grid by the battery storage. Many large changes in power will lead to a higher value. Because this figure correlates with the battery size (larger battery designs allow larger maximum power values), it is scaled by the nominal power of the storage. A small value of variability is preferable, as it is assumed that many, especially large changes in power injection stress all electrical components and thus lead to earlier ageing effects and higher costs of maintenance and replacement.

5.5 Results and analysis

This section presents the simulation study results, analysis and interpretation. It includes the comparison of the two proposed optimisation algorithms. All referenced result plots can be found in section 5.5.6.

5.5.1 System frequency without battery action

The diagrams in section 5.5.6, for example figure 5.2, illustrate the values of several system parameters of interest computed in continuous simulation over 20 min. The subplots on the left hand side present results of the operating mode II (load frequency control) and the right ones of operating mode III (MPC). In both plots, the calculated system frequency is plotted in blue, and the system frequency modelled without battery storage (mode I) in light blue. The demand power data, as selected in the previous section, is plotted in grey. A moving average line in black illustrates the overall increase of demand power during the simulated period.
In operating mode I (inactive battery storage), two main observations can be made with regard to the observed **system frequency**, see for example figure 5.2.

- The system frequency tends to decrease over time due to the increasing summed system loads. In real power systems, secondary control services would be activated to compensate the long long-term distortions of active power balance.
- The frequency deviations computed with the current settings of frequency response characteristic model are comparatively large. It is assumed that a realistic parametrisation would lead to much smaller variations in the power system frequency.

5.5.2 Observed issues with different operating modes and optimisation algorithms

The calculated battery power is indicated with a red line in the plots. In all computed variants, the same undesirable behaviour of the battery storage after a certain time can be observed: the **battery system "hangs"**, meaning it keeps almost constantly feeding in energy at maximum power. Through this, the energy stored in the battery is reduced without having any positive effect on the frequency of the connected power system.
In case of operating mode II (LFC), the effect is assumed to result from large measured frequency deviations, to which the battery reacts with proportional power, as requested by the regulations. Measured large system frequency deviations are partly caused by the changing demand power and the very sensitive frequency response model, as discussed above. However, also the extreme reaction of the battery storage itself can cause large frequency deviations, sometimes leading to short periods of oscillation. The effect is more likely to occur at larger battery sizes, as the requested battery power is proportional to the storage size. At small battery sizes and fast reaction (small battery delay times), the desired stabilising effect of the battery storage on the system frequency can be observed, for example in figure 5.2, at least in the initial period of the demand vector. The system frequency throughout the remaining simulated time depends on the frequency value at the time when the undesirable battery behaviour begins.
In operating mode III (MPC), the effect of hanging battery storage was observed too, particularly at small battery storage sizes and long delay times. The reasons for hanging are suspected to lay mostly with the used optimisation methods and the form of the cost function.

It can be observed that the compensation of frequency deviations by the battery storage is similar to load following. However, long periods of frequency directions in one direction can cause problems to both optimisation algorithms, in a similar way to storages of different size, as illustrated in figures 5.3 and 5.5. When working constantly at maximum power, the controller's task would be to detect the instances when a deviating battery power would have a positive effect due to the changed state of the power system. This expected behaviour could not be observer for either of the two optimisation algorithms. The golden section search method resulted in almost constant maximum power injections, see figures 5.2 and 5.3. The MPC with Nelder-Mead simplex optimisation returned even battery control signals that lead to larger system frequency deviations compared to an inctive battery storage, as it is visible in figures 5.4 and 5.5. Some further issues related to the used Nelder-Mead simplex algorithm were detected when analysing the optimisation process. For example, often initial changes of the simplex in an undesirable direction were observed, but they could not be influenced in an efficient way. Furthermore, unsuitable initial step sizes of simplex changes were detected, leading to ignorance of more suitable battery power values. The initial step size could not be directly controlled either in the chosen algorithm. Hence the golden section optimisation algorithm should be preferred.

5.5.3 Varying battery storage size

The effect of battery storage size on the controller performance have been partly described in the previous section. When comparing the system frequency with an MPC-battery to the system frequency in operating mode I (no battery action), it can be concluded that large battery storages can lead to a good stabilisation of frequency. In figures 5.2, 5.3, 5.4 and 5.5 it can be seen that the plotted graphs of larger batteries are closer to the set point frequency of 50 Hz, at least as long as the battery storage acts in the intended way. With regard to operating mode II (LFC), smaller storages show more desirable performance. This is related to frequency deviations caused by large storage power values, as discussed above.

The effect of different battery storage sizes on the frequency stabilisation performance is summarised in figure 5.6 for the golden section search and in figure 5.7 for the Nelder-Mead simplex optimisation. The influence of other varied parameters is discussed in the following sections. The diagrams show that the average system frequency deviates more from the set point frequency when applying the proposed methods, than without battery storage. In operating mode II (middle subplot), the performance clearly decreases with increasing battery size. Only for large battery storages with Nelder-Mead simplex optimisation (figure 5.7, right subplot), a small reduction of mean frequency deviation can be observed.

As further performance measurement, the standard deviation of the computed system frequency vector was computed. It can be seen in figure 5.8 that the system frequency can be stabilised when applying an MPC with golden section search methods, with improving performance at larger battery sizes. The performance of the simplex optimisation-based MPC varies (figure 5.9). The implemented LFC algorithm did not show any stabilising effect.

5.5.4 Varying simulation horizon

It could have been expected that for the multi-dimensional Nelder-Mead simplex optimisation, an increasing simulation horizon improves the controller performance, because an optimal future battery power with an increased number of elements is determined. In the golden section search optimisation, which is one-dimensional, only a constant battery power vector was computed, hence the simulation horizon should not have any influence on the controller performance regarding frequency stabilisation. For both optimisation algorithms, it is expected that a longer simulation horizon leads to an increased computation time.

Figures 5.10 and 5.11 illustrate the controller behaviour with a simulation horizons of 5 s. In comparison to figures 5.3 and 5.5 ($H_{sim} = 2$ s), no difference can be detected for the MPC applying the golden section search minimisation method. Using simplex optimising MPCs even reduced the system performance, as larger changes in battery power resulted in increasing deviations of the system frequency from the set point value.

This is also reflected in the results of the performance measure power variability in the charts 5.12 and 5.13. The summed changes of battery power are significantly higher when applying an MPC with Nelder-Mead simplex optimisation (figure 5.13), particularly with longer simulation horizons, illustrated by lines with markers in the form of triangles. The calculates relative power changes are larger at smaller battery storage sizes. The SOC at the end of the simulation horizon is influenced by larger deviations of the battery power from a constant maximum value in a slightly positive way. This is displayed in figure 5.15: the final SOC is closer to the desired value of 50 %.

The observed behaviour of the Nelder-Mead simplex optimisation controller at long simulation horizons is undesirable with regard to the frequency stabilisation, as it is reflected in figures 5.7 and 5.9. It results in larger mean deviations and a higher variability of the system frequency. It is suspected that the poor optimisation performance results from the default value of zero power injection in the simplex algorithm. This setting should allow the optimisation algorithm to evaluate power changes in both directions.
In case of a longer simulation horizon, more input signal steps are computed by the multi-dimensional optimisation method. However, the effect of any change in the injection power of the battery storage on the power system is short-term. Furthermore, all but the first elements of the control signal vector will be discarded anyway. Hence, in higher dimensions, the optimisation algorithm aims at determining a signal that has little positive (as observed even negative) influence on the controller performance, but it significantly increases the computation time.

The increased simulation time of the Nelder-Mead simplex algorithm compared to the golden section search method can be seen in figures 5.16 and 5.17. The latter plot also illustrates the negative effect of an increasing simulation horizon. Both MPC versions showed significantly higher computation times than the LFC operating mode (pay attention to different scales of subplots). But the measured simulation times per sampling interval are still below one second, which allows real time implementation. The variation of the elapsed time in the other operating modes is very small. It may have been caused by varying simulation horizons that were also applied when simulating the large “real” net-

work, and from varying number of calls of internal loops and if-cases. Also other software running on the simulation computer at the same time may have had some influence.

5.5.5 Varying battery delay time

As further parameter, the battery delay time that elapsed between sampling and change of active power injected or absorbed by the battery storage was varied in the simulation studies. In all performance plots, it can be seen that longer delay times lead to worse controller performance, except the standard deviation of system frequency and simplex optimisation (figure5.9), and the computation times (figures 5.16 and 5.17). In the time plots in figures 5.18 and 5.19, the formerly observed positive effects of battery storages with shorter delay times are not visible any more. In MPC operation, the computed battery power remains at its minimum or maximum value for most of the time. As mentioned in section 4.1, a battery delay time equal to the sample time would actually be the most consistent controller design, but unfortunately revealed the least desirable performance.

5.5.6 Result figures

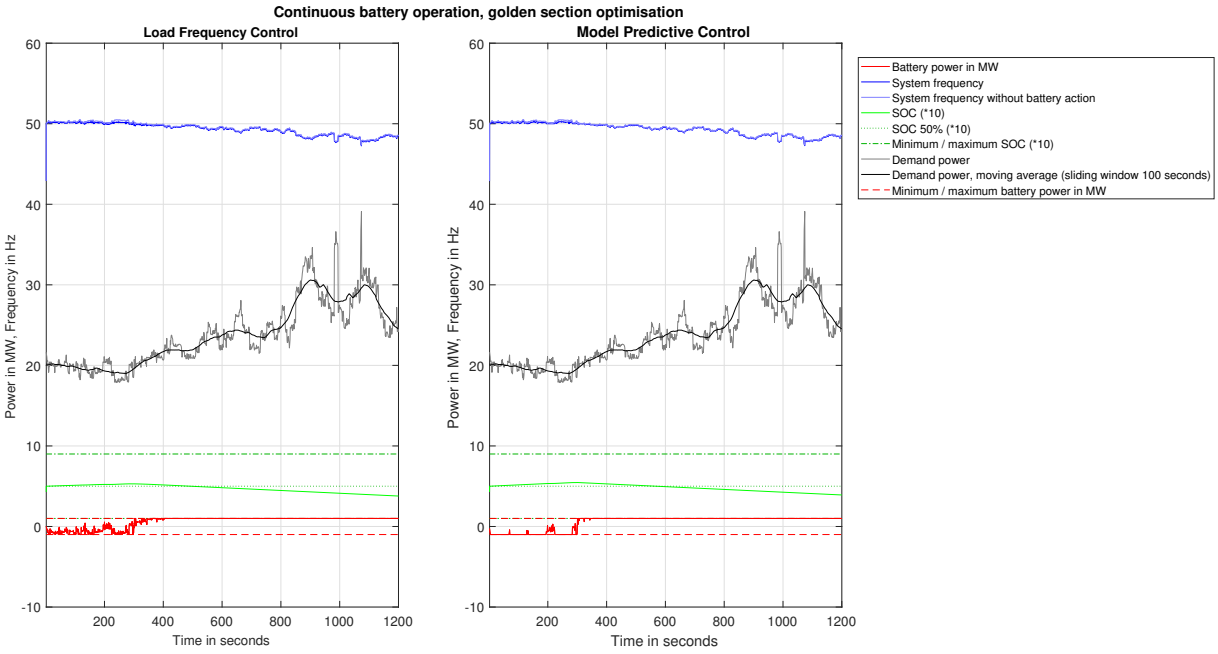

Figure 5.2: Continuous operation of battery storage, MPC with golden section search optimisation, **1 MVA**, $T_{delay} = 100$ ms, $H_{sim} = 2$ s.

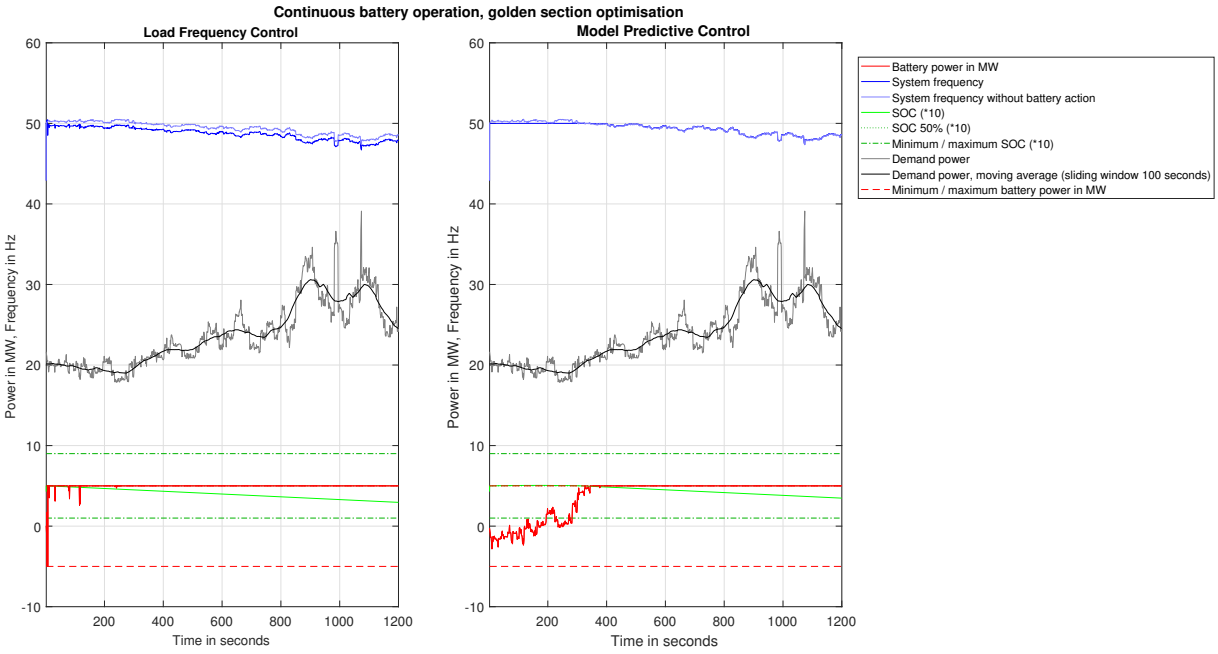

Figure 5.3: Continuous operation of battery storage, MPC with golden section search optimisation, **5 MVA**, $T_{delay} = 100$ ms, $H_{sim} = 2$ s.

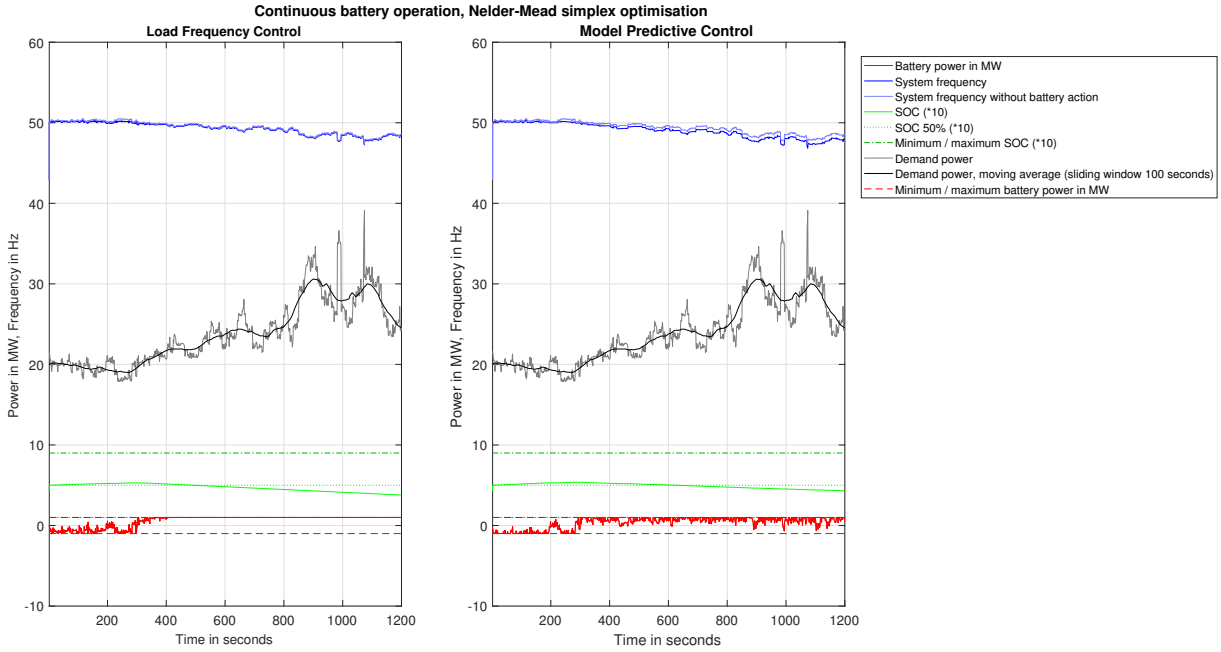

Figure 5.4: Continuous operation of battery storage, MPC with Nelder-Mead simplex optimisation, **1 MVA**, $T_{delay} = 100$ ms, $H_{sim} = 2$ s.

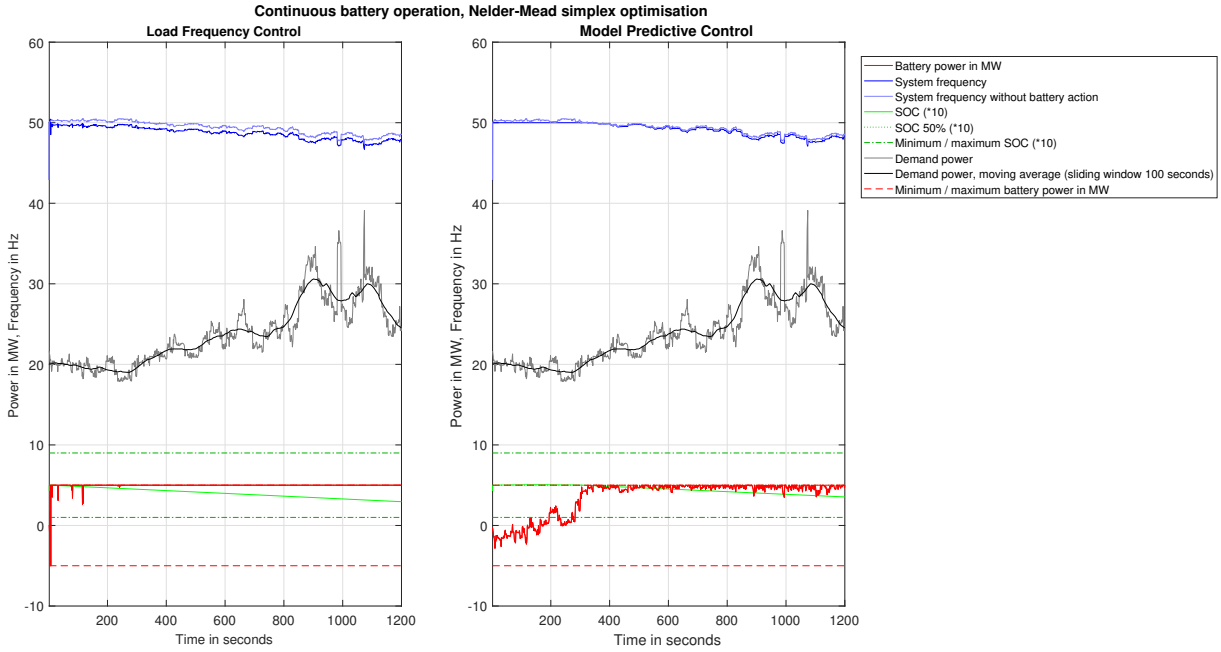

Figure 5.5: Continuous operation of battery storage, MPC with Nelder-Mead simplex optimisation, **5 MVA**, $T_{delay} = 100$ ms, $H_{sim} = 2$ s.

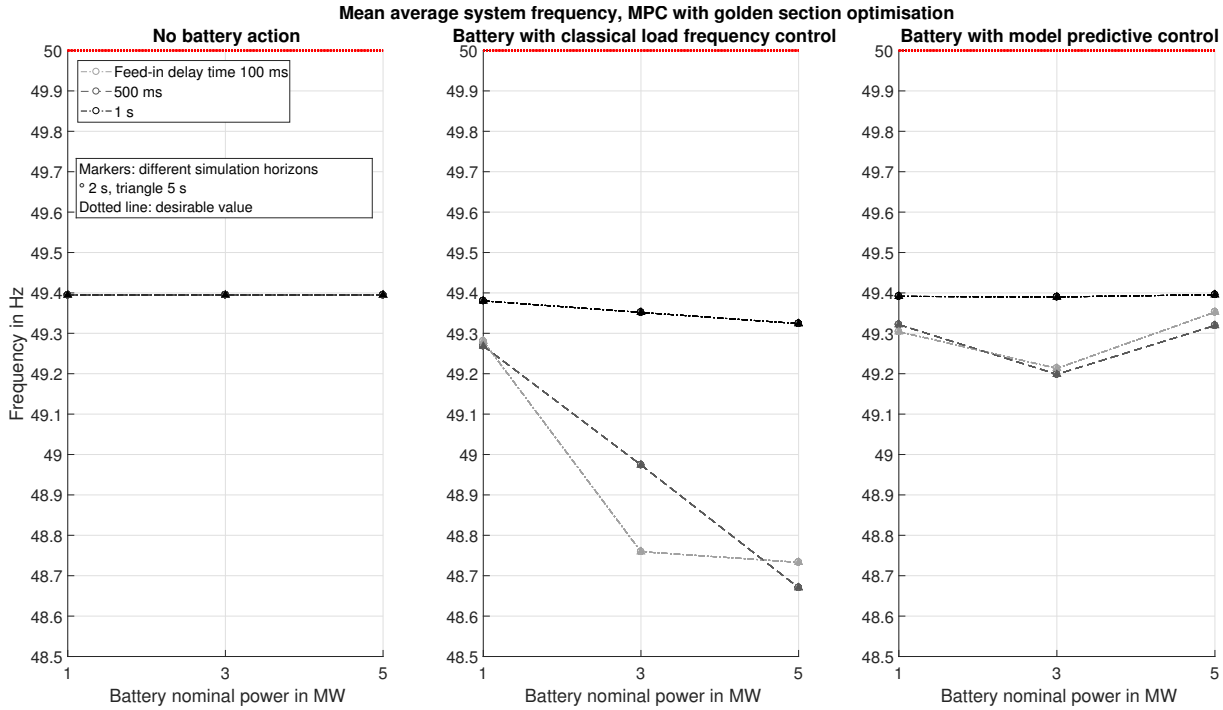

Figure 5.6: Comparison of mean average system frequencies, MPC with golden section search optimisation.

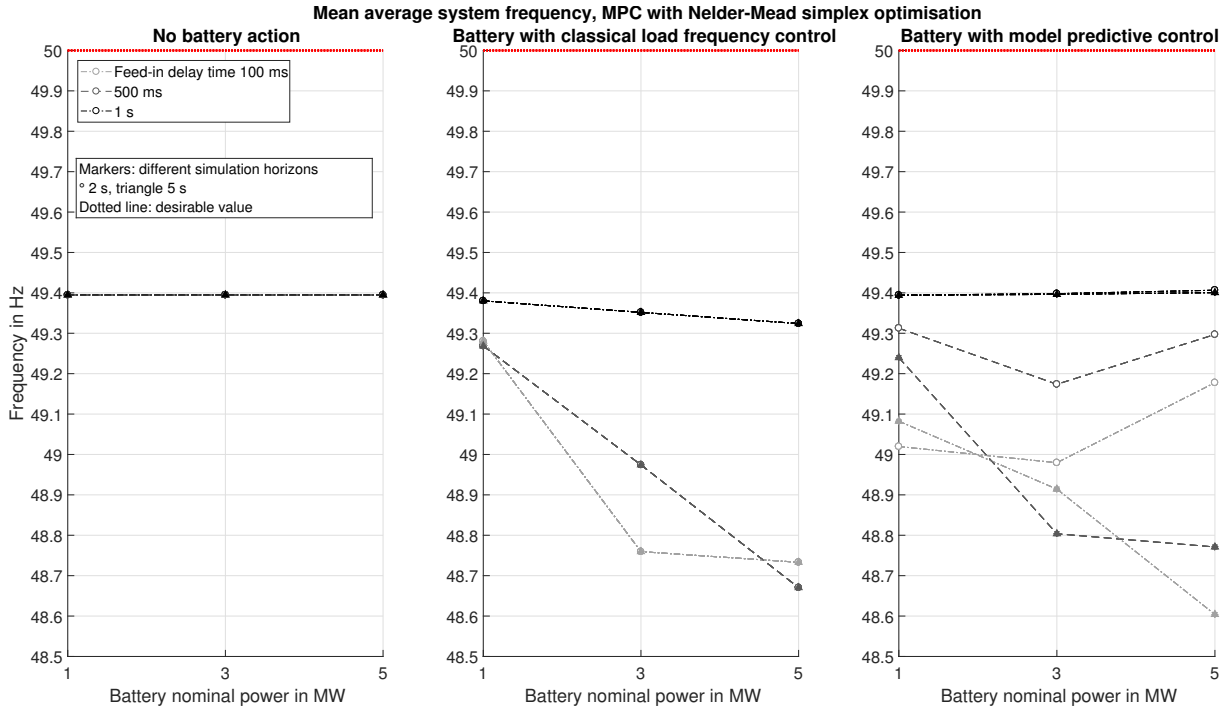

Figure 5.7: Comparison of mean average system frequencies, MPC with Nelder-Mead simplex optimisation.

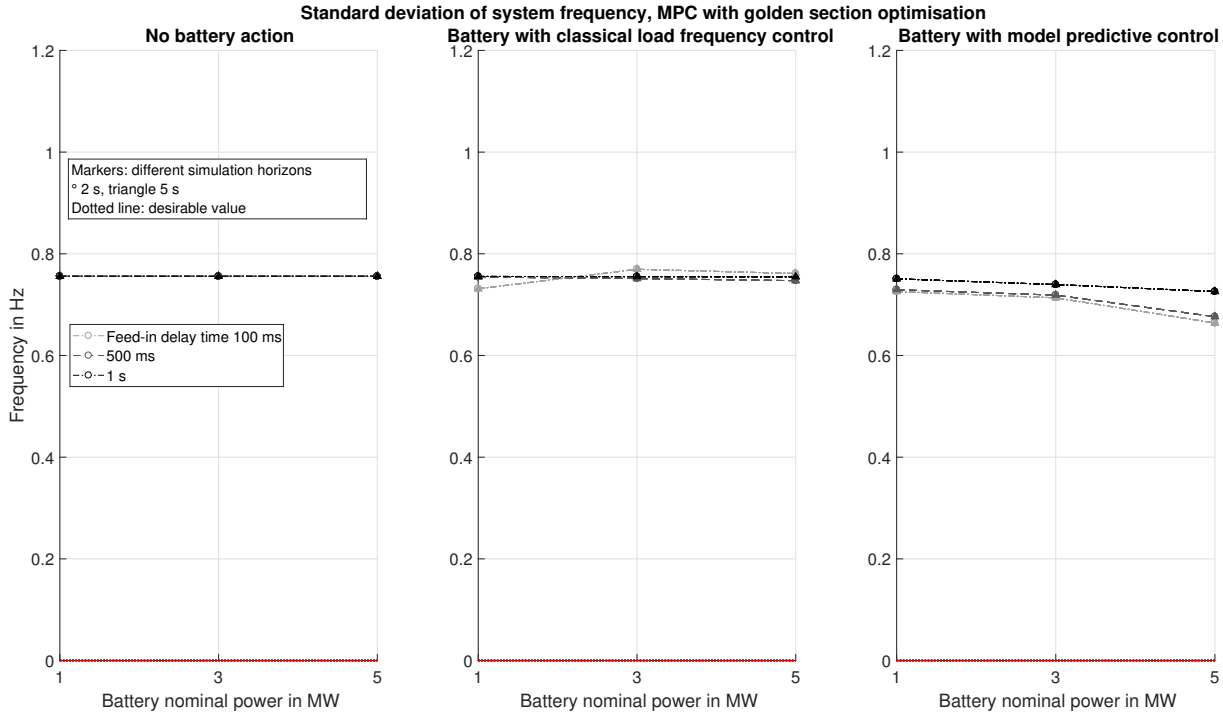

Figure 5.8: Comparison of system frequency standard deviation, MPC with golden section search optimisation.

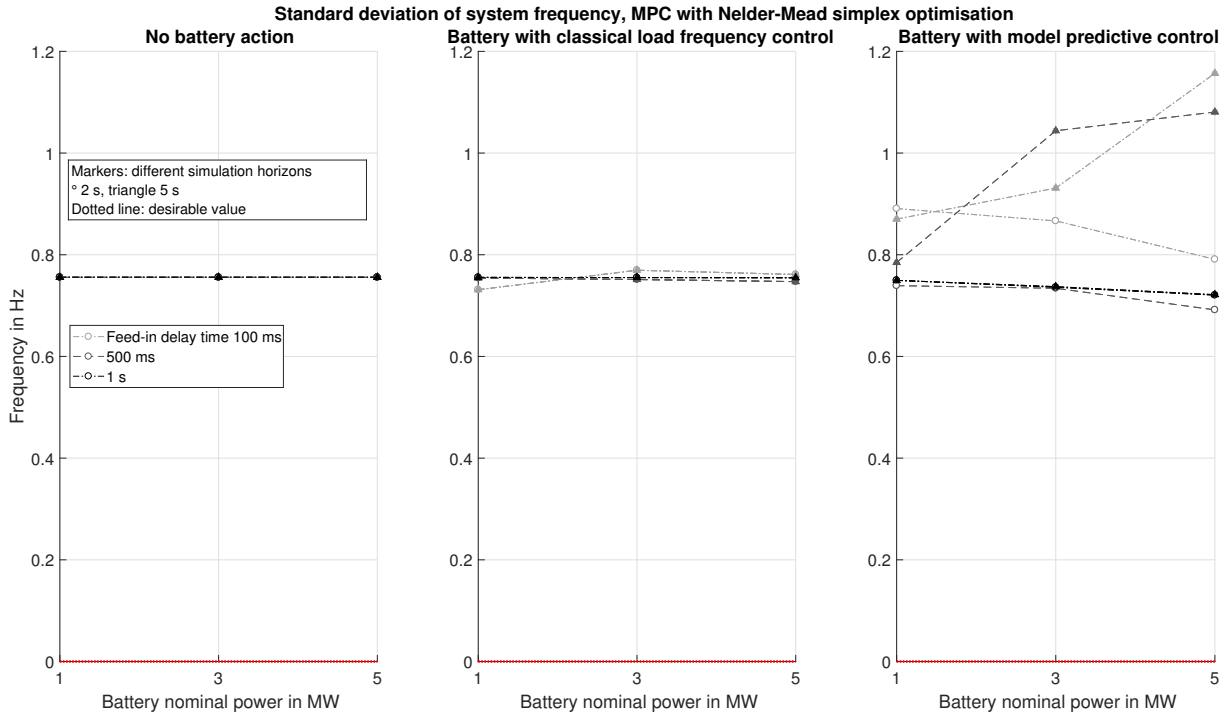

Figure 5.9: Comparison of system frequency standard deviation, MPC with Nelder-Mead simplex optimisation.

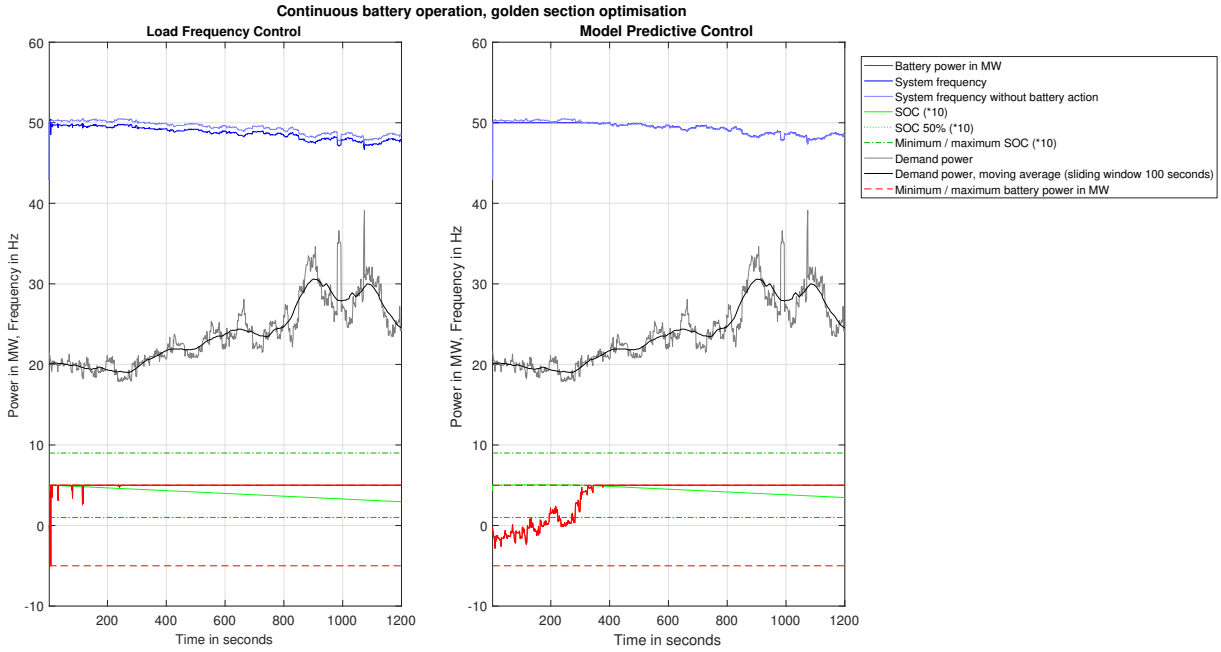

Figure 5.10: Continuous operation of battery storage, MPC with golden section search optimisation, **5 MVA**, $T_{delay} = 100$ ms, $H_{sim} = 5$ s.

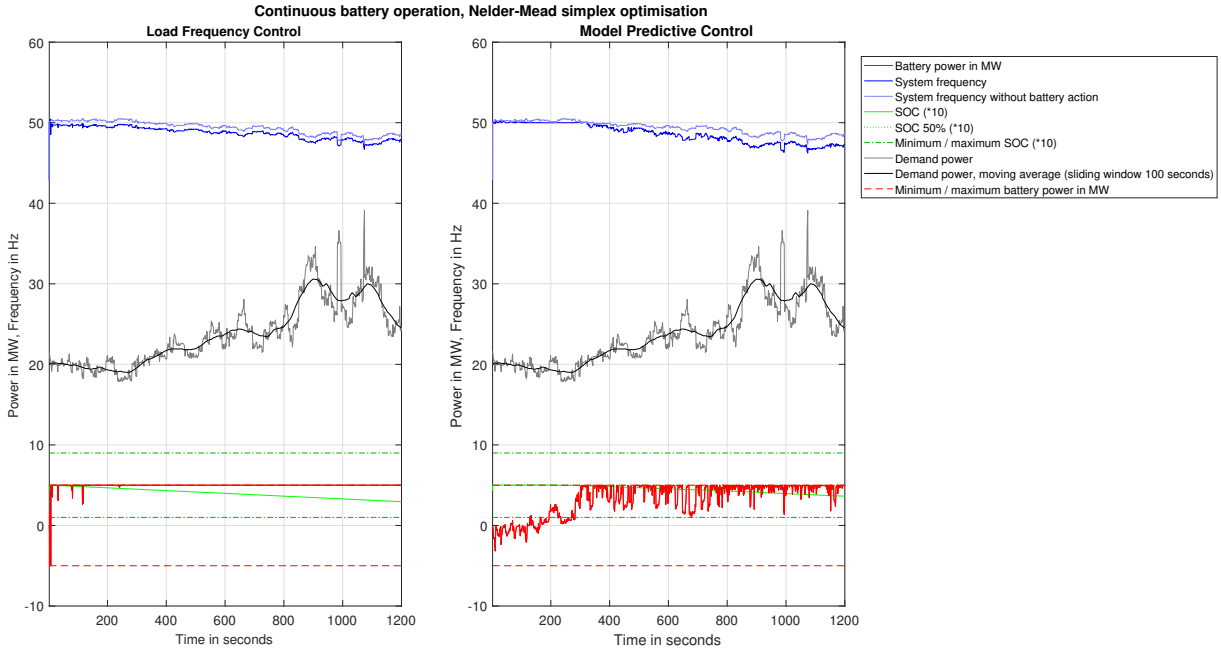

Figure 5.11: Continuous operation of battery storage, MPC with Nelder-Mead simplex optimisation, **5 MVA**, $T_{delay} = 100$ ms, $H_{sim} = 5$ s.

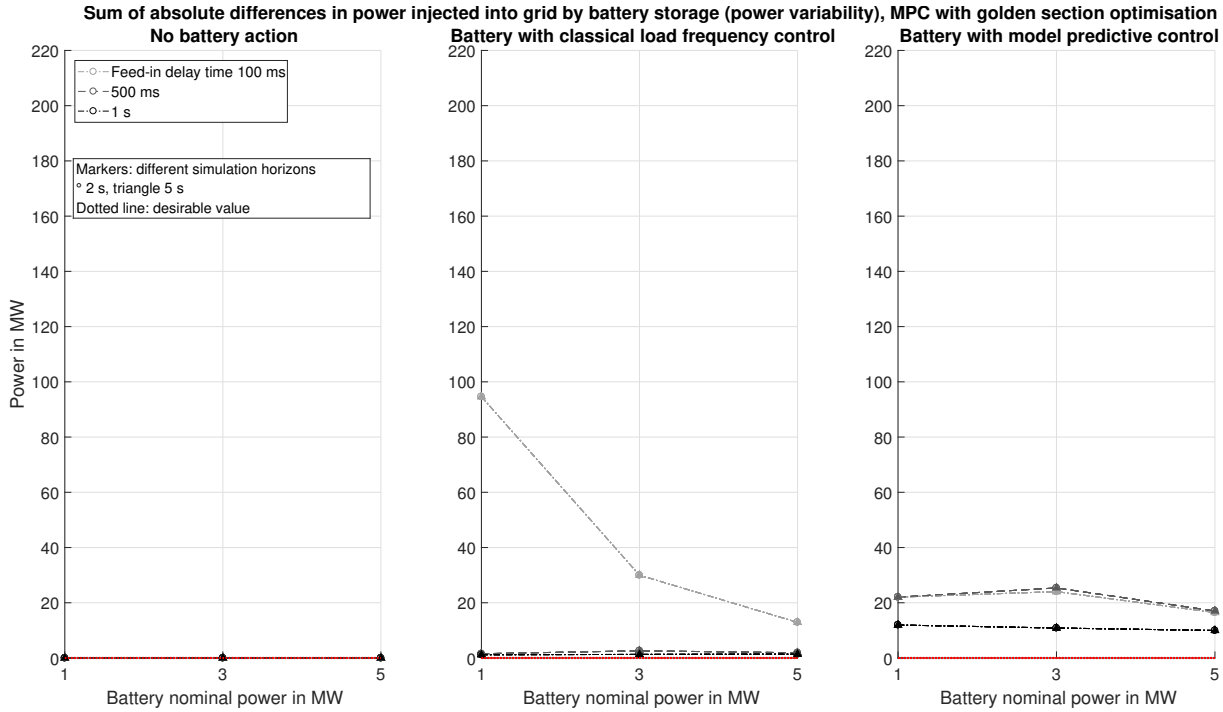

Figure 5.12: Comparison of sums of absolute differences in power injected into grid by battery storage, scaled by battery size, MPC with golden section search optimisation.

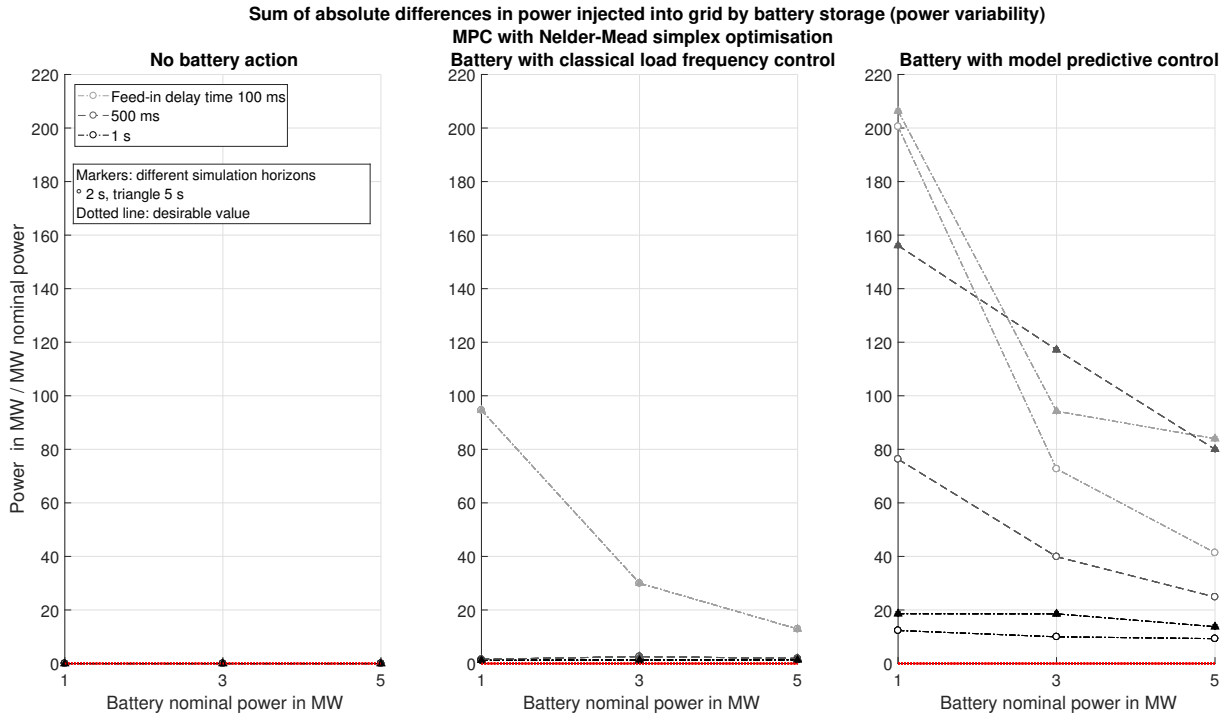

Figure 5.13: Comparison of sums of absolute differences in power injected into grid by battery storage, scaled by battery size, MPC with Nelder-Mead simplex optimisation.

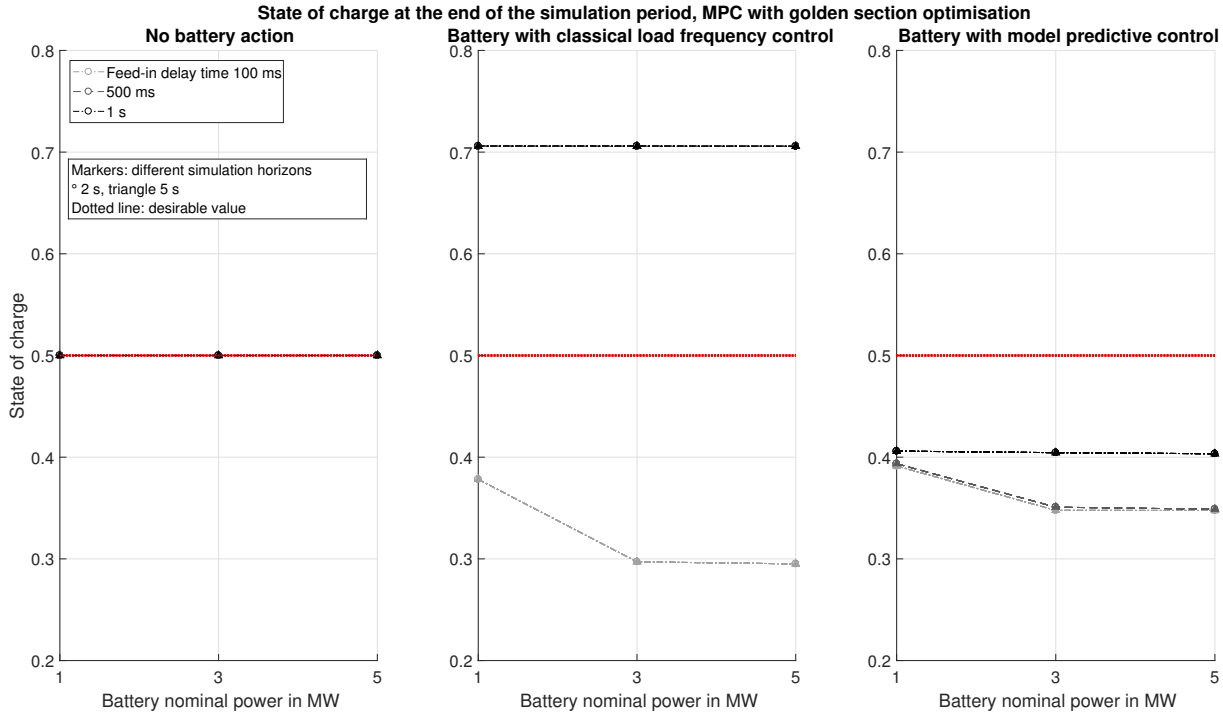

Figure 5.14: Comparison of SOC at the end of simulated demand vector, MPC with golden section search optimisation.

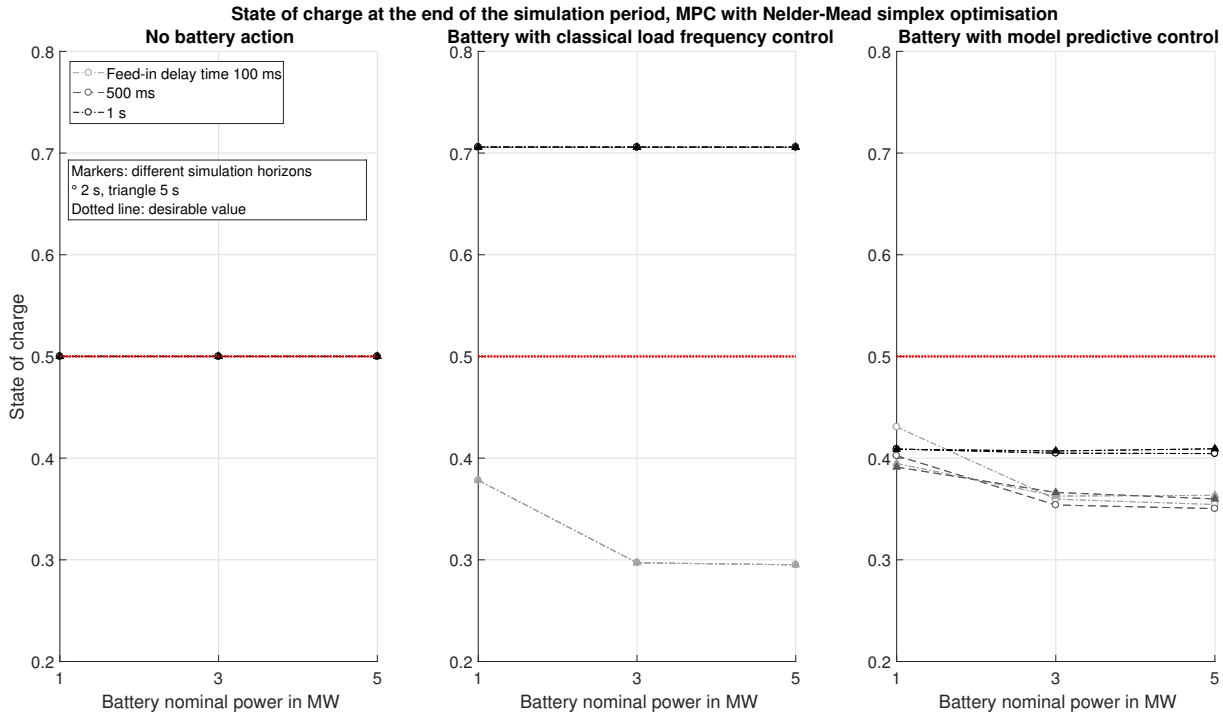

Figure 5.15: Comparison of SOC at the end of simulated demand vector, MPC with Nelder-Mead simplex optimisation.

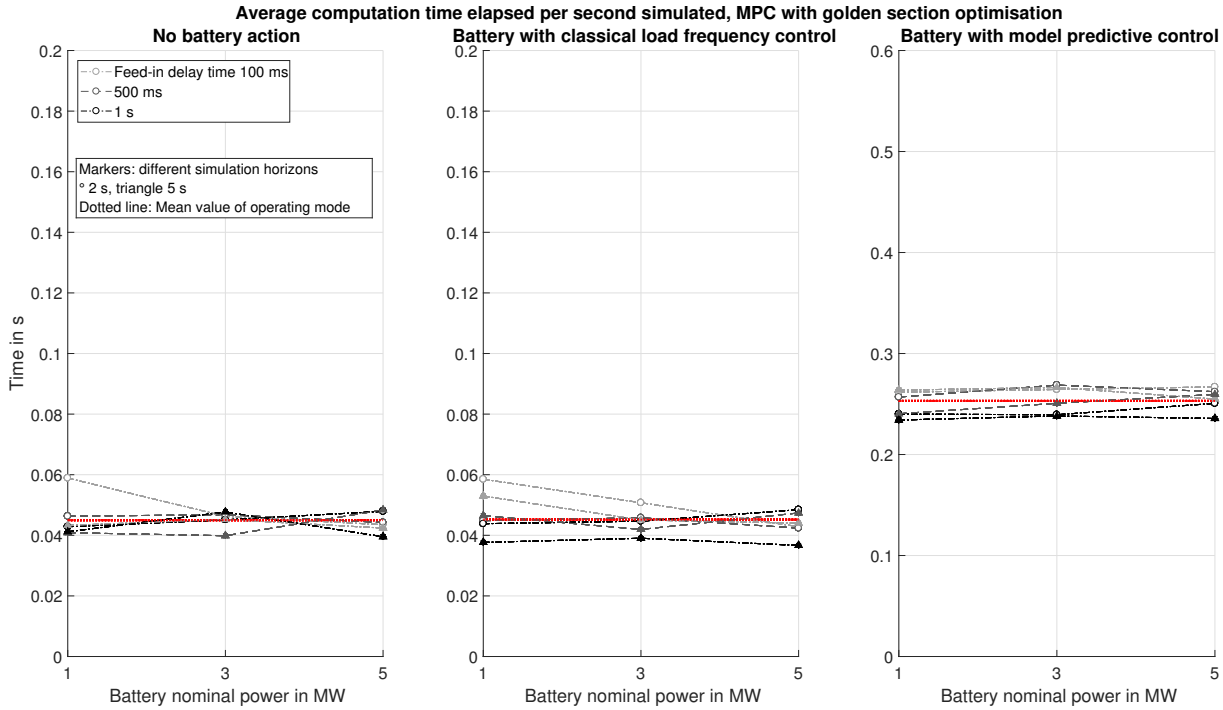

Figure 5.16: Comparison of computation time, MPC with golden section search optimisation.

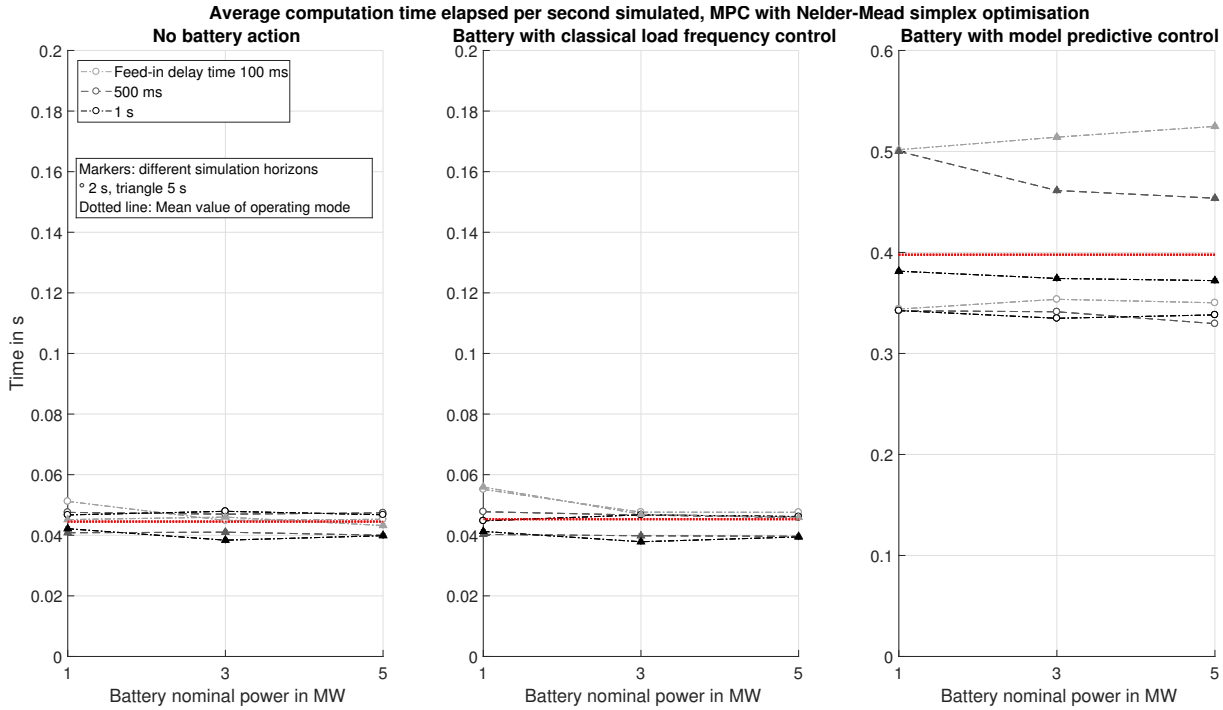

Figure 5.17: Comparison of computation time, MPC with Nelder-Mead simplex optimisation.

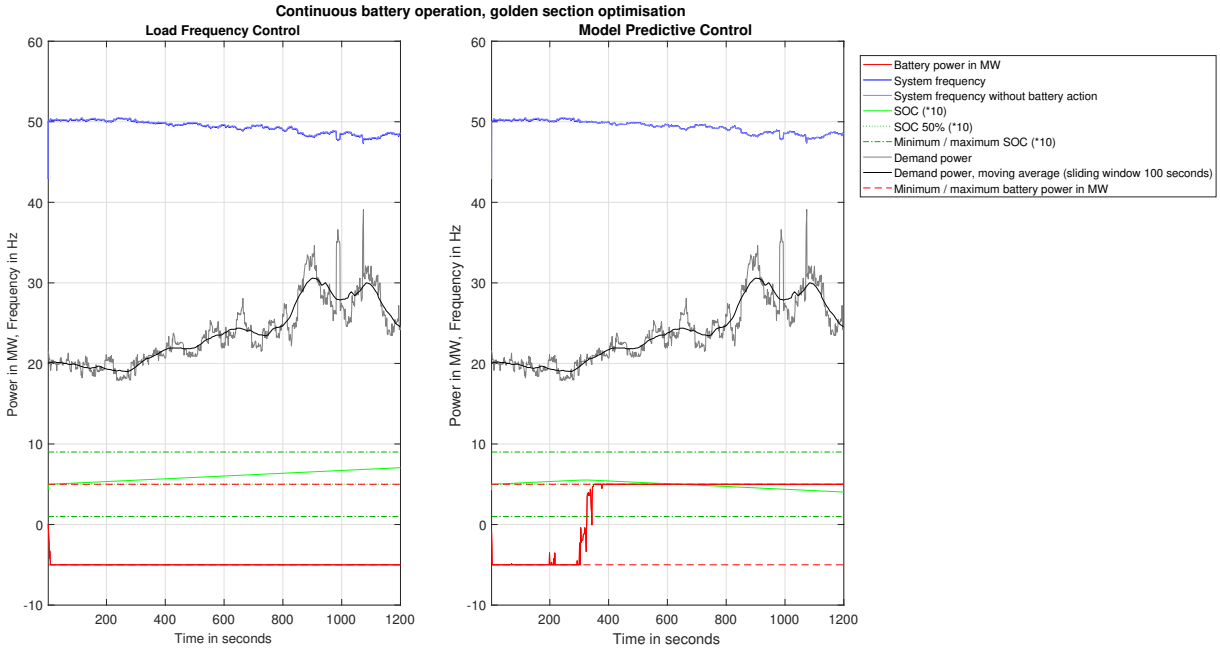

Figure 5.18: Continuous operation of battery storage, MPC with golden section search optimisation, **5 MVA**, $T_{delay} = 1$ s, $H_{sim} = 2$ s.

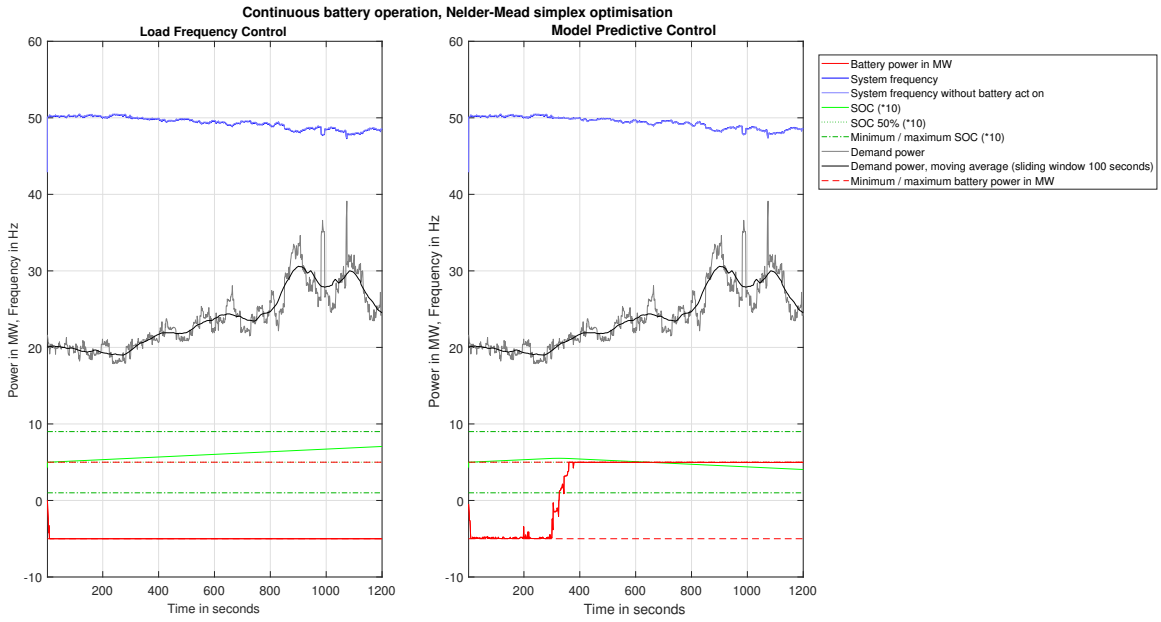

Figure 5.19: Continuous operation of battery storage, MPC with Nelder-Mead simplex optimisation, **5 MVA**, $T_{delay} = 1$ s, $H_{sim} = 2$ s.

6 Conclusion and Outlook

In this chapter, the main conclusion from the simulation study are summarised and the limitations of the proposed methods are discussed together with proposals for future work.

6.1 Conclusion

The presented model-based predictive controller for the battery storage based on load flow computations shows potential of performance improvement compared to the principle of conventional proportional primary load frequency control. The computation times that have been recorded in a simulation study are promising with regard to real time implementation.

The modelling approach and performance evaluation were based on various assumptions and revealed certain limitations with regard to implementation and performance. For example, the algebraic dynamic frequency response model was based on simplified theoretic concepts. Literature values were used for parametrisation. In the simulation study, it was found that the frequency deviations computed with the current settings are comparatively large. Realistic values may lead to smaller variations in power system frequency. Also further controller and simulation parameters, such as the reactance time of the battery storage, result from thumb values, literature values and assumptions.
In the simulation study, both simplified and "real-world" simulations were based on the same model, only with different complexity. Hence, the reliability of the evaluation results should be regarded as limited. It was not possible to conduct simulations over a longer period of time with satisfying accuracy and realistic results. This is due to the focus of this work on short-term simulations.

With regard to the working principle of the proposed model predictive controller, some assumptions made in section 4.1 can be regarded as contradictory. Concerning the point in time of changing generator power, on the one hand, a stepwise generation change at each sampling interval was assumed. On the other hand, also a change in generator power was modelled that occurred immediately after any battery storage action. Simulations with a battery delay time that equalled the sampling interval showed reduced performance compared to shorter delay times.
Two different optimisation algorithms were evaluated. The simpler, one-dimensional golden section search method showed improved performance compared to the multi-dimensional constrained Nelder-Mead simplex algorithm. However, the expected controller behaviour and performance was not reached with any of the two optimisation methods.

6.2 Outlook

The following set of proposals for future work can be given. It is recommended to consult further expertise on synchronous generating power sources, with regard to several characteristics. Gathering further information on realistic frequency response actions and

parameters would enable more accurate modelling approaches. Additionally, more information on common practice and intervals of power changes in order to compensate recorded load changes would be helpful for adjusting the system and frequency response models.
It should be considered to calculate frequency deviations caused by battery action only at the next sampling time, corresponding to a battery delay times that equals the sampling interval. For improved modelling of the battery storage, it would be interesting to include feasible values for battery reaction time, sampling interval, possible intervals of battery power changes.

With regard to performance evaluation of the control algorithm, the reliability of results could be improved by applying a more sophisticated, realistic model of the power system. Including secondary and optionally tertiary LFC, as well as interaction with neighbouring control areas, may allow evaluations over longer periods of time.
The computational speed of the controller and hence the controller performance may be further enhanced by suitable technical solutions.

References

[1] U. EURELECTRIC, "Power distribution in europe, facts & figures," EURELECTRIC,Union of the Electricity Industry, Tech. Rep., 2013. [Online]. Available: http://www.eurelectric.org/media/113155/dso_report-web_final-2013-030-0764-01-e.pdf

[2] A. J. Schwab, *Elektroenergiesysteme*, A. J. Schwab, Ed. Springer-Verlag GmbH, 2017. [Online]. Available: http://www.ebook.de/de/product/24473479/adolf_j_schwab_elektroenergiesysteme.html

[3] B. Elia, "Electricity market players," 2017. [Online]. Available: http://www.elia.be/en/about-elia/electricity-market-players

[4] E. N. o. T. S. O. ENTSO-E, "Ucte oh policy 1: Load-frequency control," March 2009. [Online]. Available: https://www.entsoe.eu/disclaimer/Pages/default.aspx

[5] ——, "Transmission system map," 2015. [Online]. Available: https://www.entsoe.eu/map/Pages/default.aspx

[6] J. Arrillaga and C. P. Arnold, *Computer Analysis of Power Systems*. JOHN WILEY & SONS INC, 1991. [Online]. Available: http://www.ebook.de/de/product/3055885/jos_arrillaga_c_p_arnold_computer_analysis_of_power_systems.html

[7] G. Andersson, "Modelling and analysis of electric power systems," *ETH Zurich*, September 2008.

[8] Z. Kremens and M. Labuzek, "Load flow analysis incorporating frequency as a state vector variable," in *Harmonics and Quality of Power, 2000. Proceedings. Ninth International Conference on*, vol. 2. IEEE, 2000, pp. 526–530.

[9] Praviraj, "Newton-raphson loadflow," 2009. [Online]. Available: https://de.mathworks.com/matlabcentral/fileexchange/21059-newton-raphson-loadflow

[10] P. M. Anderson and M. Mirheydar, "A low-order system frequency response model," *IEEE Transactions on Power Systems*, vol. 5, no. 3, pp. 720–729, 1990.

[11] W. H. Kersting, "Ieee distribution planning working group report," *IEEE Trans. Power Syst*, vol. 6, no. 3, pp. 975–985, 1991.

[12] IEEE, "Ieee pes distribution system analysis subcommittee's distribution test feeder working group," 1991. [Online]. Available: http://ewh.ieee.org/soc/pes/dsacom/testfeeders/index.html

[13] U. UWEE, "Power systems test case archive," University of Washington, Tech. Rep., 1993. [Online]. Available: http://www.ee.washington.edu/research/pstca/pf14/pg_tca14bus.htm

[14] C. SEDG, "United kingdom generic distribution system (ukgds)," Github, 2005. [Online]. Available: https://github.com/sedg/ukgds

[15] M. Okamura, Y. O-ura, S. Hayashi, K. Uemura, and F. Ishiguro, "A new power flow model and solution methodincluding load and generator characteristics and effects of system control devices," *IEEE transactions on power apparatus and systems*, vol. 94, no. 3, pp. 1042–1050, 1975.

[16] R. Ramírez-Betancour, V. Gutierrez-Martinez, and C. R. Fuerte-Esquivel, "Static simulation of voltage instability considering effects of governor characteristics and voltage and frequency dependence of loads," in *North American Power Symposium (NAPS), 2010*. IEEE, 2010, pp. 1–7.

[17] L. M. Castro, C. R. Fuerte-Esquivel, and J. H. Tovar-Hernández, "Solution of power flow with automatic load-frequency control devices including wind farms," *IEEE Transactions on Power Systems*, vol. 27, no. 4, pp. 2186–2195, 2012.

[18] B. H. Bakken, A. Petterteig, E. Haugan, and B. Walther, "Stepwise power flowa new tool to analyse capacity shortage and reserve requirements," in *15th Power Systems Computation Conference*, 2005.

[19] P. E. Sørensen, A. D. Hansen, P. Christensen, M. Mieritz, J. Bech, B. Bak-Jensen, and H. Nielsen, "Simulation and verification of transient events in large wind power installations," Risø National Laboratory,, Tech. Rep., 2003.

[20] A. F. Stephanie Hay, "A review of power system modelling platforms and capabilities," The Institution of Engineering and Technology (IET), Tech. Rep., March 2015.

[21] E. N. o. T. S. O. ENTSO-E, "Appendix 1: Load-frequency control and performance," June 2004. [Online]. Available: https://www.entsoe.eu/disclaimer/Pages/default.aspx

[22] [Online]. Available: http://www.mainsfrequency.com/frequ_info_en.htm

[23] T. Weißbach and E. Welfonder, "High frequency deviations within the european power system: Origins and proposals for improvement," in *Power Systems Conference and Exposition, 2009. PSCE'09. IEEE/PES*. IEEE, 2009, pp. 1–6.

[24] T. Gobmaier, Ed., *Netzfrequenz als Indikator für die Stabilität des Verbundnetzes*. 10. Internationale Energiewirtschaftstagung (IEWT) an der TU Wien, 2017.

[25] I. Egido, F. Fernandez-Bernal, P. Centeno, and L. Rouco, "Maximum frequency deviation calculation in small isolated power systems," *IEEE Transactions on Power Systems*, vol. 24, no. 4, pp. 1731–1738, 2009.

[26] P. Mercier, R. Cherkaoui, and A. Oudalov, "Optimizing a battery energy storage system for frequency control application in an isolated power system," *IEEE Transactions on Power Systems*, vol. 24, no. 3, pp. 1469–1477, 2009.

[27] P. Dubucq and G. Ackermann, "Frequency control in coupled energy systems with high penetration of renewable energies," in *Clean Electrical Power (ICCEP), 2015 International Conference on*. IEEE, 2015, pp. 326–332.

[28] H. Bevrani, *Robust power system frequency control*. Springer, 2014, vol. 85.

[29] Deutsche ÜNB, "Eckpunkte und Freiheitsgrade bei Erbringung von Primärregelleistung," April 2014.

[30] nationalgrid, "Enhanced frequency response invitation to tender for pre-qualified parties v2.2," July 2016. [Online]. Available: http://www2.nationalgrid.com/Enhanced-Frequency-Response.aspx

[31] ——, "Enhanced frequency response seminar," Presentation Slides, June 2016. [Online]. Available: http://www2.nationalgrid.com/Enhanced-Frequency-Response.aspx

[32] N. Günter and A. Marinopoulos, "Energy storage for grid services and applications: Classification, market review, metrics, and methodology for evaluation of deployment cases," *Journal of Energy Storage*, vol. 8, pp. 226–234, 2016.

[33] Younicos AG, "Schwerin battery park," 2016.

[34] X. Luo, J. Wang, M. Dooner, and J. Clarke, "Overview of current development in electrical energy storage technologies and the application potential in power system operation," *Applied Energy*, vol. 137, pp. 511–536, 2015.

[35] O. Tremblay and L.-A. Dessaint, "Experimental validation of a battery dynamic model for ev applications," *World Electric Vehicle Journal*, vol. 3, no. 1, pp. 1–10, 2009.

[36] J. M. Maciejowski, *Predictive control: with constraints*. Pearson education, 2002.

[37] S. Boyd and L. Vandenberghe, *Convex optimization*. Cambridge university press, 2004.

[38] J. A. Nelder and R. Mead, "A simplex method for function minimization," *The computer journal*, vol. 7, no. 4, pp. 308–313, 1965.

[39] J. C. Lagarias, J. A. Reeds, M. H. Wright, and P. E. Wright, "Convergence properties of the nelder–mead simplex method in low dimensions," *SIAM Journal on optimization*, vol. 9, no. 1, pp. 112–147, 1998.

[40] M. H. Wright, "Nelder, mead, and the other simplex method," *Documenta Mathematica*, vol. 7, pp. 271–276, 2010.

[41] R. R. Barton and J. S. Ivey Jr, "Modifications of the nelder-mead simplex method for stochastic simulation response optimization," in *Proceedings of the 23rd conference on Winter simulation*. IEEE Computer Society, 1991, pp. 945–953.

[42] P. A. Jensen and J. F. Bard, *Operations research models and methods*. John Wiley & Sons Incorporated, 2003, vol. 1.

[43] J. DErrico, "fminsearchbnd, fminsearchconfile exchangematlab central," 2012. [Online]. Available: https://uk.mathworks.com/matlabcentral/fileexchange/8277-fminsearchbnd--fminsearchcon

[44] Y.-C. Chang, "N-dimension golden section search: Its variants and limitations," in *Biomedical Engineering and Informatics, 2009. BMEI'09. 2nd International Conference on*. IEEE, 2009, pp. 1–6.

[45] W. Y. Yang, W. Cao, T.-S. Chung, and J. Morris, *Applied numerical methods using MATLAB*. John Wiley & Sons, 2005.

[46] Younicos AG, "Y.cube factsheet," 2017. [Online]. Available: https://www.younicos.com/de/produkte/y-cube/

[47] B. BVES, "Anwendungsbeispiel speichertechnologien lithium-ionen grospeichersystem zur bereitstellung von primrregelleistung sowie weiteren systemdienstleistungen," Juli 2016.

[48] T. Tjaden, J. Bergner, J. Weniger, and V. Quaschning, "Representative electrical load profiles of residential buildings in germany with a temporal resolution of one second," 2015. [Online]. Available: https://pvspeicher.htw-berlin.de/veroeffentlichungen/daten/lastprofile/

[49] D. J. Pedregal and J. R. Trapero, "Electricity prices forecasting by automatic dynamic harmonic regression models," *Energy Conversion and Management*, vol. 48, no. 5, pp. 1710–1719, 2007.